A STUDY OF THE INTERACTION OF STRONG ELECTROMAGNETIC WAVES AND ANISOTROPIC ION BEAMS WITH A BACKGROUND PLASMA

A Thesis presented to the

Department of Physics

University of Durban Westville

In partial fulfilment

of the requirements for the Degree

Master of Science

by

PRAVIN SINGH

FEBRUARY, 1989

TO SURESH

ACKNOWLEDGEMENTS

I wish to sincerely thank the following persons who have contributed to this thesis in various ways.

Professor R. Bharuthram, my supervisor, for his expert guidance, interest and assistance.

Professor M.A. Hellberg, for many helpful discussions and suggestions.

Dr. P.K. Shukla, Ruhr–Universitat Bochum, West Germany, for having suggested the problem analysed in chapter five.

Professor R.G. Ori for his understanding and patience.

Mr. S. Baboolal for his assistance.

My parents, for their support over the many years.

ABSTRACT

The interaction of an anisotropic (in velocity space) ion beam with an isotropic background hydrogen plasma is theoretically investigated. The length and time scales are such that both the ions and electrons are magnetized. Using linear theory, the electrostatic dispersion relation is derived, and solved fully, using no approximations. It is shown that the anisotropy can significantly enhance the instability growth rates as compared to the isotropic case. The importance of ion magnetization is illustrated. Comparisons are made with unmagnetized plasma results.

The modulational instability of an arbitrarily–large–amplitude electron cyclotron wave along the external magnetic field is investigated, taking into account the relativistic electron quiver velocity and the relativistic ponderomotive force. Three types of plasma slow responses, the forced–Raman, quasistatic and forced–quasistatic, are considered and a parameter study of the instability growth rates is carried out.

CONTENTS

LIST OF SYMBOLS

SYMBOL	DESCRIPTION
$\vec{A}$	vector potential
a	$(T_e/T_i)(n_{io}/n_{eo})$
b	$(T_e/T_\perp)(n_{bo}/n_{eo})$
$\vec{B}_o$	magnetic field
c	speed of light
$C_\perp$	$(T_\perp/m_i)^{1/2}$
$C_\parallel$	$(T_\parallel/m_i)^{1/2}$
C_s	ion sound speed = $(T_e/m_i)^{1/2}$
$d^3\vec{V}$	$dV_x\, dV_y\, dV_z$
$\vec{E}$	electric field
e	electronic charge
f_j	distribution function of particles of type j
f_{jo}	equilibrium distribution function of particles of type j
i	$\sqrt{-1}$
I_p	modified Bessel function of order p
I	intensity
$\vec{J}$	current density
J_p	Bessel function of order p
$\vec{k}$	wave propagation vector = $[k_x, k_y, k_x]$
k_o, K	wavenumber
$k_\perp$	component of $\vec{k}$ perpendicular to $\vec{B}_o = B_o\hat{z}$ = $(k_x^2 + k_y^2)^{1/2}$
m_j	mass of particles of type j
m_{jo}	rest mass of particles of type j

SYMBOL	DESCRIPTION
n_o	plasma density
n_j	density of particles of type j
n_{jo}	equilibrium density of particles of type j
$\vec{p}_j$	relativistic momentum of particles of type j
p_o	pump wave amplitude
t	time co–ordinate
T	plasma temperature
T_e	Boltzmann's constant × electron temperature
T_i	Boltzmann's constant × ion temperature
$T_\perp$	beam ion temperature perpendicular to $\vec{B}_o$
$T_\parallel$	beam ion temperature parallel to $\vec{B}_o$
$\vec{V}$	velocity vector
$V_\perp$	component of $\vec{V}$ in the x – y plane = $(V_x^2 + V_y^2)^{1/2}$
$\vec{V}_o$	drift velocity
V_A	Alfven speed
V_e	electron thermal speed = $(T_e/m_e)^{1/2}$
V_i	ion thermal speed = $(T_i/m_i)^{1/2}$
V_ϕ	wave phase speed
$\hat{x}, \hat{y}, \hat{z}$	unit vector in x, y, z – directions respectively
$Z(\lambda)$	plasma dispersion function with argument λ
$Z'(\lambda)$	$\frac{d}{d\lambda} Z(\lambda)$
a	Ω_{eo}/ω_o
a_b	$k_\perp^2 C_\perp^2/\Omega_i^2$
a_j	$k_\perp^2 V_j^2/\Omega_j^2$
β	ratio of plasma pressure to magnetic pressure (chapter two)

SYMBOL	DESCRIPTION
β	$1-\delta$
β	$m_{eo}c^2/T_e$ (chapter five)
β_b	$\sigma\,\beta$
β_Q	$\beta\sigma/(1+\sigma)$
Γ_{pj}	$e^{-a_j}\, I_p(a_j) \quad j = i,e,b$
Γ	$(1+p^2)^{-1/2}$
γ	imaginary part of complex ω
Δ	$(\omega_o^2 - k_o c^2)/\omega_{peo}^2$
δ	$T_\perp/T_\parallel$
δ	non–linear frequency shift (chapter five)
ϵ	$(m_{eo}/m_i)^{1/2}\,\omega_o/\omega_{peo}$
λ_{dj}	Debye length of particles of type j = $(T_j/4\pi n_{jo}e^2)^{1/2}$
λ_{db}	Debye length characterized by beam ions = $(T_\perp/4\pi n_{bo}e^2)^{1/2}$
ρ_s	ion gyroradius at electron temperature = (C_s/Ω_i)
ρ_i	ion gyroradius = (V_i/Ω_i)
η	$1 + a(1+p^2)^{-1/2}$
θ	angle between wave– vector $\vec{k}$ and beam velocity $\vec{V}_o$
θ	azimuthal angle
ψ	angle between k_x and $k_\perp$
ϕ	electrostatic potential
σ	T_e/T_i
ω	complex frequency
$\bar{\omega}$	Doppler shifted frequency = $\omega - \vec{k}\cdot\vec{V}_o$
ω_r	real part of ω
ω_{peo}	electron plasma frequency = $(4\pi n_{eo}e^2/m_{eo})^{1/2}$

SYMBOL	DESCRIPTION
ω_{pe}	electron plasma frequency = $(4\pi n_{eo} e^2/m_e)^{1/2}$
ω_{pi}	ion plasma frequency = $(4\pi n_{io} e^2/m_i)^{1/2}$
Ω_{eo}	electron gyrofrequency = $(eB_o/m_{eo}c)$
Ω_e	electron gyrofrequency = $(eB_o/m_e c)$
Ω_i	ion gyrofrequency = $(eB_o/m_i c)$
∇	differential operator = $\frac{\partial}{\partial x}\hat{x} + \frac{\partial}{\partial y}\hat{y} + \frac{\partial}{\partial z}\hat{z}$

CHAPTER ONE

INTRODUCTION

Of the many fields of research associated with plasma phenomena, the quest for the ideal plasma conditions for the realization of a successful fusion reactor has recently received the most attention. This requires plasma densities $n \sim 10^{15} cm^{-3}$ and plasma temperatures $T \sim 10$ keV. Ohmic heating is not suitable for reaching such high temperatures since the plasma resistivity ($\propto T^{-3/2}$) decreases with temperature. Thus other heating mechanisms are essential. Of these, wave heating and heating by injection of particle beams are popular schemes. In the former case coupling between the incident wave and plasma particles is responsible for energy transport from the wave to the particles, while in the latter case this is achieved by collisional effects between the beam and plasma particles. However, it is well known that the above interactions are inherently accompanied by instabilities, both linear and nonlinear, excited by the available free energy. Such instabilities lead to anomalous particle and energy transfer across the confining magnetic field, thereby hindering plasma confinement.

In this thesis we examine linear instabilities associated with (incident) particle–particle interactions, and a nonlinear instability associated with (incident) wave–particle interaction. The model for the former case considers the effect of the anisotropy in velocity distribution of an incident ion beam drifting through a background magnetized plasma of isotropic electrons and ions on low frequency electrostatic instabilities. Drift speeds perpendicular and parallel to the external magnetic field are separately considered. Such beams are not only possible in laboratory plasmas, but have also been observed in space plasmas, e.g in the foreshock region of the earth's bowshock interacting with the solar wind.

After a survey of the relevant literature in chapter two, the kinetic dispersion relation for electrostatic instabilities associated with our ion beam–plasma system, with magnetized ions and electrons, is derived in chapter three. In chapter four we present detailed numerical solutions of the dispersion relation for low frequency modes.

The use of intense electromagnetic waves is important for plasma heating experiments as well as laser–plasma interactions, e.g inertial fusion and beat–wave particle accelerators. In addition, they are employed in modification experiments of the lower part of the earth's atmosphere. In chapter five we consider the modulational instability of a large amplitude electromagnetic wave arising from an interaction with the plasma slow response. Three types of slow responses, the forced–Raman, quasistatic and forced–quasistatic are modelled. The corresponding instability growth rates are analytically derived and graphically compared.

Finally in chapter six we present a summary of all our results, conclusions are drawn and extensions discussed.

CHAPTER TWO

REVIEW OF LITERATURE

Gresillon et al. [1] investigated the turbulence excited by an ion beam in an unmagnetized plasma. They used an argon plasma ($m_i/m_e = 40$) with temperature $T_e = 5T_i$. Using linear theory they showed that for small ion beam drift speeds ($V_0/C_s \sim 0.7$), which corresponds to the ion–ion streaming instability with phase velocity close to C_s, the instability propagates essentially parallel to the beam direction. As V_0 was increased ($V_0/C_s \geq 1.4$) propagation was more oblique and for relatively high velocities ($V_0/C_s \sim 2.5$) they identified both the ion–ion streaming and ion acoustic instabilities. They measured the spatial structure of the turbulence in an experiment and found that it displayed characteristics similar to that of the ion–ion streaming instability.

Lemons et al. [2] showed that the threshold velocity for the ion–ion streaming instability is much lower than that for the ion acoustic waves. Fuselier and Gurnett [3] have shown that ion acoustic–like waves in the foreshock generally propagate obliquely to the magnetic field. Similar obliquely propagating ion acoustic–like waves have been observed by Gallagher [4] in the magnetosheath.

Akimoto and Winske [5] studied the general properties of the ion beam instability. They used this to account for the ion acoustic–like waves detected at the ramp of the earth's bow shock. They considered unmagnetized electrons and ions and obtained a necessary condition $V_0 \cos\theta \leq C_s$ for the instability to propagate. Here V_0 is the beam speed and θ is the angle between the beam direction and wave–vector. They used the above condition to explain oblique propagation (to the beam) at large beam speeds. They also found the following:

(1) Increasing the ion beam temperature (T_b/T_e) causes the waves to propagate less obliquely (to the beam).

(2) The effect of a temperature anisotropy in the beam ($T_\perp/T_\parallel > 1$) is to increase the total beam temperature $T_b = (2T_\perp+T_\parallel)/3$ and thus cause propagation to be less oblique. They kept $T_\parallel = T_i$ fixed and increased $T_\perp$ and used typical anisotropies ($T_\perp/T_\parallel = 2.5$).

Using a flat topped electron distribution (FTED) they showed that an anisotropy in the background ions enhances the instability for slow ion beams.

Akimoto and Omidi [6] did a theoretical survey of the ion beam instability in order to explain the generation of broadband electrostatic noise (BEN) in the earth's magnetotail. For their parameters they showed that electron magnetization had little effect on the ion beam instability. They showed for the first time that both the ion–ion streaming and ion acoustic instabilities could operate simultaneously in the magnetotail in the presence of one ion beam. They also found the following:

(1) The ion–ion streaming instability can dominate the ion acoustic instability for beam densities satisfying $0.1 \leq n_{bo}/n_e \leq 0.9$.

(2) Increasing the ion beam temperature T_b/T_i causes the ion acoustic instability to damp and detracts the ion–ion streaming instability.

(3) The ion acoustic instability propagates essentially parallel to the ion beam while the ion–ion streaming instability propagates obliquely for large beam speeds.

They accounted for the broadband nature of the electrostatic noise by attributing it to both the ion acoustic and ion–ion streaming instabilities.

Gary and Omidi [7] studied the ion–ion streaming instability in detail. They considered a homogeneous plasma with two counter–streaming ion components, a less dense beam and a more dense core with relative drift speed V_0. They considered both an

unmagnetized plasma and a plasma with a uniform magnetic field $B_0\hat{z}$. In the latter case they considered electron magnetization but treated the ions as unmagnetized. They used typical plasma parameters $T_e = 10\ T_i$, $n_{bo} = 0.1\ n_e$ and a hydrogen plasma with $m_i/m_e = 1836$. Their results are summarized below.

(1) The ion–ion streaming mode can be driven unstable by the ion beam in an unmagnetized plasma.

(2) At relatively large drift speeds ($V_0 > C_s$) the instability grows only at angles strongly oblique to the beam.

(3) At $T_b/T_c < 1$ (ratio of beam temperature to ion core temperature) the instability is fluid like but becomes a beam resonant kinetic instability as $T_b/T_c \rightarrow 1$.

(4) At $T_b/T_c \geq 1$, increasing T_b/T_c reduces the growth rate.

(5) The threshold drift speed for the ion–ion streaming instability lies well below that for the ion acoustic instability for a wide range of plasma parameters.

(6) A temperature anisotropy ($T_{\perp e}/T_{\parallel e} > 1$) in the background electrons enhances the growth rate at oblique propagation to the beam.

(7) Electron magnetization can enhance or detract the instability at sufficiently large drift speeds.

Fuselier et al. [8] considered the generation of enhanced ion acoustic waves by field aligned ion beams upstream from the earth's bow shock. They used the model of Gary and Omidi [7]. They showed that stability properties of the wave depended on details of the beam distribution, in particular that the growth of the ion–ion streaming instability is determined by the slope of the beam distribution function at angles oblique to the magnetic field.

Papadopoulos et al. [9] considered the case of two equi–density counter–streaming ion beams with velocity $\pm \vec{V}_0$, perpendicular to a magnetic field $\vec{B}_0$. Their model was rather

restricted in that the modified two–stream instability was confined to perpendicular propagation ($\vec{k} \perp \vec{B}_0$). In addition, the ions were unmagnetized. They found a zero frequency mode ($\omega_r = 0$) and maximum growth rate $\gamma_{max} = \omega_{lh}/2\sqrt{2}$. Here $\omega_{lh} = \omega_{pi}/[1+(\omega_{pe}/\Omega_e)^2]^{1/2}$ is the lower hybrid frequency and ω_{pi} and ω_{pe} are the total ion and electron plasma frequencies. At maximum growth they found that $\vec{k}.\vec{V}_0 = \sqrt{3/8}\ \omega_{lh}$ is constant.

McBride et al. [10] studied the modified two–stream instability using a crossfield (perpendicular to magnetic field $\vec{B}_0$) electron–ion streaming model. The ions were unmagnetized. They considered the electrostatic as well as electromagnetic cases and used both linear and nonlinear theory. They considered the case $k_z/k \approx (m_e/m_i)^{1/2}$ corresponding to angles slightly off the perpendicular (to $\vec{B}_0$) and showed that in the fluid limit maximum growth $\gamma_{max} = \omega_{lh}/2$ occurs at $k = \sqrt{3}\ \omega_{lh}/V_0$ and $\omega_r = \sqrt{3}/2\ \omega_{lh}$. Here V_0 is the electron–ion relative drift speed. They found that the instability is an important turbulent heating mechanism, that heats both the ions and electrons comparably.

Wu et al. [11] in their study of kinetic crossfield instabilities considered unmagnetized ions streaming through magnetized electrons, with relative drift $\vec{V}_0$, perpendicular to a magnetic field $\vec{B}_0$. They showed the existence of an instability when $V_0 > V_A$ (Alfven speed). The unstable waves contained both electrostatic and electromagnetic contributions. For the case of high beta (β) (ratio of plasma pressure to magnetic pressure) plasmas, say $\beta = 1$, they found the instability to be highly kinetic. In the limit $\theta \leq 90^\circ$ (θ is the angle between $\vec{B}_0$ and the wave–vector) and $\beta \ll 1$, they identified the usual modified two–stream instability. In this limit they showed that the instability could be suppressed by electromagnetic effects when $V_0 > V_A$. They concluded that electromagnetic effects are unimportant for low beta cases if $V_0 < V_A$.

In their study of the modified two–stream instability, Bharuthram and Johnstone [12] considered counter–streaming, equi–density (50%), ion beams perpendicular to a magnetic field. They allowed for an anisotropic velocity distribution in the ion beams and considered magnetized ions. They also obtained $\omega_r = 0$ and found that the maximum growth rate was independent of the drift speed V_0. In particular they found that $\gamma_{max} = 3\sqrt{2}/32\ \omega_{lh}$ and that $\vec{k}.\vec{V}_0 = 3\sqrt{2}/8\ \omega_{lh}$ is constant at maximum growth. The effect of the anisotropy was to reduce the growth rate due to and increase in total beam temperature.

CHAPTER THREE

DERIVATION OF THE KINETIC DISPERSION RELATION

In deriving the linear dispersion relation we follow the method of Gary and Sanderson [13] and Bharuthram [14]. We consider a homogeneous collisionless plasma with stationary isotropic electrons and two ion components, an anisotropic beam and an isotropic background ion population. A uniform magnetic field $\vec{B}_0$ is present in the $\hat{z}$ – direction. The electrostatic approximation is used. Thus the electric field $\vec{E}_1$ can be written as $\vec{E}_1 = -\nabla\phi_1$ where ϕ_1 is a scalar potential. Therefore by Maxwell's equation

$$\nabla \times \vec{E} = -\frac{\partial \vec{B}}{\partial t}$$

perturbations in the magnetic field are neglected. In our model both the ions and the electrons are assumed to be magnetized. This allows low wave frequencies ω with $|\omega| \sim \Omega_i$, where Ω_i is the ion gyrofrequency.

3.1 ION BEAM TERM

The ion beam is treated as an anisotropic drifting Maxwellian with temperature $T_\perp$ ($T_\parallel$) perpendicular (parallel) to the magnetic field. The beam is allowed to have an externally excited drift with velocity $\vec{V}_{oy}$ perpendicular to $\vec{B}_0$ and $\vec{V}_{oz}$ along $\vec{B}_0$. The analysis is carried out in the background electron\ion rest frame. The beam and background ions are assumed to have equal masses m_i. The configuration is illustrated in fig 3.1.1.

FIG 3.1.1

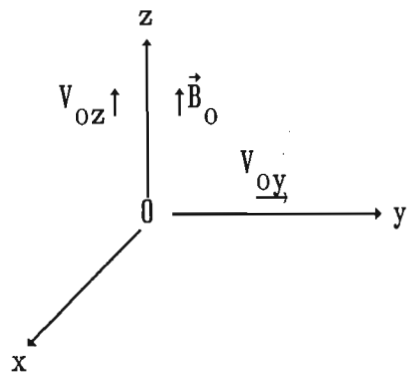

The equilibrium beam–ion velocity distribution is chosen to be

$$f_{bo} = \frac{n_{bo}}{(2\pi C_\perp^2)(2\pi C_\parallel^2)^{1/2}} \exp\{-[V_x^2 + (V_y - V_{oy})^2]/2C_\perp^2\} \times \exp[-(V_z - V_{oz})^2/2C_\parallel^2] \qquad 3.1.1$$

where $C_\perp = (T_\perp/m_i)^{1/2}$, $C_\parallel = (T_\parallel/m_i)^{1/2}$ are the perpendicular and parallel velocities of the beam ions and n_{bo} is the beam density. We consider small perturbations about the equilibrium quantities:

$$f_b = f_{bo}(V) + f_{b1} ,$$
$$\vec{E} = \vec{E}_o + \vec{E}_1, \ (\vec{E}_o = 0)$$
$$\vec{B} = \vec{B}_o + \vec{B}_1 ,$$

in the linearization of the Vlasov equation

$$\frac{\partial f_b}{\partial t} + \vec{V}\cdot\nabla f_b + \frac{d\vec{V}}{dt}\cdot\frac{\partial f_b}{\partial \vec{V}} = 0 .$$

Using the ion equations of motion

$$\frac{d\vec{V}}{dt} = \frac{e}{m_i}\left[\vec{E}_0 + \vec{E}_1 + \frac{\vec{V}\times\vec{B}_0}{c} + \frac{\vec{V}\times\vec{B}_1}{c}\right], \qquad 3.1.2$$

the Vlasov equation for the ion beam becomes

$$\frac{\partial f_{b1}}{\partial t} + \vec{V}\cdot\nabla f_{b1} + \frac{e}{m_i}\left[\vec{E}_0 + \frac{\vec{V}\times\vec{B}_0}{c}\right]\cdot\frac{\partial f_{b1}}{\partial \vec{V}} = -\frac{e}{m_i}\left[\vec{E}_1 + \frac{\vec{V}\times\vec{B}_1}{c}\right]\cdot\frac{\partial f_{bo}}{\partial \vec{V}}. \qquad 3.1.3$$

For the electrostatic approximation $\vec{E}_1 = -\nabla\phi_1$ ($\vec{B}_1 = 0$) and for $\vec{E}_0 = 0$, since there is no equilibrium electric field, (3.1.3) can be written as

$$\frac{df_{b1}}{dt} = \frac{e}{m_i}\nabla\phi_1\cdot\frac{\partial f_{bo}}{\partial \vec{V}},$$

where the operator $\frac{d}{dt}$ is defined as the rate of change following an unperturbed orbit in phase space [13]. Integrating along the unperturbed orbits we obtain

$$f_{b1}(\vec{r},\vec{V},t) = \frac{e}{m_i}\int_{-\infty}^{t}\nabla\phi_1(\vec{r}',t')\cdot\frac{\partial f_{bo}(\vec{V}')}{\partial \vec{V}'}\,dt', \qquad 3.1.4$$

where $\vec{V}' = \frac{d\vec{r}'}{dt'}$, $\frac{d\vec{V}'}{dt'} = \frac{e}{m_i}\left[\vec{E}_0 + \frac{\vec{V}'\times\vec{B}_0}{c}\right]$, $\vec{r}'(0) = \vec{r}$, $\vec{V}'(0) = \vec{V}$.

In the above equation we have assumed that the plasma is undisturbed at $t' = -\infty$. From (3.1.1)

$$\frac{\partial f_{bo}}{\partial \vec{V}'} = -\left[\frac{V_x'}{C_\perp^2}, \frac{V_y'-V_{oy}}{C_\perp^2}, \frac{V_z'-V_{oz}}{C_\parallel^2}\right] f_{bo}(\vec{V}') = -\vec{V}_{eq}\, f_{bo}(\vec{V}'),$$

where we have defined

$$\vec{V}_{eq} = \left[\frac{V'_x}{C_\perp^2} , \frac{V'_y - V_{oy}}{C_\perp^2} , \frac{V'_z - V_{oz}}{C_\parallel^2} \right] .$$

Assuming the perturbed quantities to be harmonic in space and time, we may write

$$\left. \begin{aligned} f_{b1}(\vec{r},\vec{V},t) &= f_{b1}(\vec{V}) \ \exp\{ i \ [\vec{k}.\vec{r} - \omega t] \} \\ \phi_1(\vec{r} \ ,t) \quad &= \phi_{1k\omega} \ \exp\{ i \ [\vec{k}.\vec{r} - \omega t] \} \end{aligned} \right\} . \qquad 3.1.5$$

Then $\nabla\phi_1(r',t') = i \vec{k} \ \phi_1(r',t')$ and (3.1.4) becomes

$$f_{b1}(\vec{r},\vec{V},t) = -\frac{ie}{m_i} \int_{-\infty}^{t} \vec{k}\cdot\vec{V}_{eq} \ \phi_1(\vec{r}',t') \ f_{bo}(\vec{V}') \ dt' . \qquad 3.1.6$$

Since the ions are magnetized their gyration about the field lines is significant. Upon solving the equations of motion (3.1.2) we obtain

$$\left. \begin{aligned} V'_x &= V'_\perp \cos(-\Omega_i t' + \theta) \\ V'_y - V_{oy} &= V'_\perp \sin(-\Omega_i t' + \theta) \\ V'_z &= \text{constant} \end{aligned} \right\} , \qquad 3.1.7$$

where $V'_\perp = \{V'^2_x + (V'_y - V_{oy})^2\}^{1/2}$ is the speed along a circular orbit perpendicular to the magnetic field lines. The situation at $t' = 0$ is illustrated in fig 3.1.2 .

FIG 3.1.2

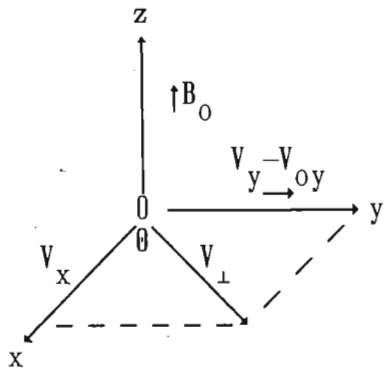

$$\vec{V}'(0) = \vec{V} = [V_\perp \cos\theta \ , V_\perp \sin\theta \ , \ V_z]$$

The negative sign (coefficient of Ω_i in 3.1.7) arises because the angle between $V'_\perp$ and the x–axis decreases as t' increases. This accounts for the different spin directions of the electrons and ions. The ions have spin vector antiparallel to $\vec{B}_0$. Since motion along the field is unaffected by the field, V'_z = constant.

We resolve $\mathbb{k}$ into components parallel and perpendicular to $\vec{B}_0$ as shown in fig 3.1.3 . Thus

$$\mathbb{k} = [k_x \ , k_y \ , k_z] = [k_\perp \cos\psi \ , k_\perp \sin\psi \ , k_z] \ . \qquad 3.1.8$$

FIG 3.1.3

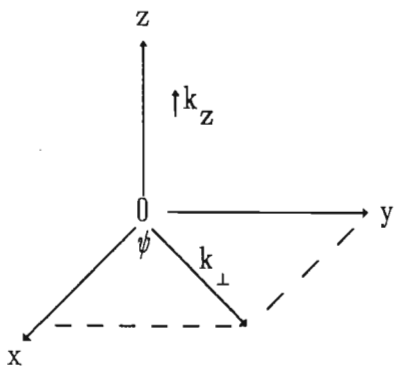

It can then be shown that

$$\vec{k}\cdot\vec{V}_{eq} = \frac{k_\perp V'_\perp}{C_\perp^2}\cos(\Omega_i t' + \psi - \theta) + \frac{k_z}{C_\parallel^2}(V'_z - V_{oz}) .$$

Using the above expression and (3.1.5) in (3.1.6), we get

$$f_{b1}(\vec{V})\exp\{ i\,[\vec{k}\cdot\vec{r} - \omega t]\} = f_{b1}(\vec{r},\vec{V},t) = -\frac{ie}{m_i} f_{bo}(\vec{V})\left[\frac{k_\perp V_\perp}{C_\perp^2}\times\right.$$
$$\left.\int_{-\infty}^{t}\phi_1\cos(\Omega_i t' + \psi - \theta)\,dt' + \frac{k_z}{C_\parallel^2}(V_z - V_{oz})\int_{-\infty}^{t}\phi_1\,dt'\right] . \qquad 3.1.9$$

Evaluating the right hand side of the above equation at $t = 0$:

$$f_{b1}(\vec{V}) = -\frac{ie}{m_i} f_{bo}(\vec{V})\,\phi_{1k\omega}\left[\frac{k_\perp V_\perp}{C_\perp^2}\int_{-\infty}^{0}\cos(\Omega_i t' + \psi - \theta)\exp\{ i\,[\vec{k}\cdot(\vec{r}' - \vec{r}) - \omega t']\}\,dt'\right.$$
$$\left. + \frac{k_z}{C_\parallel^2}(V_z - V_{oz})\int_{-\infty}^{0}\exp\{ i\,[\vec{k}\cdot(\vec{r}' - \vec{r}) - \omega t']\}\,dt'\right] \qquad 3.1.10$$

Solving the equations (3.1.7) with $\vec{r}'(0) = \vec{r} = [x_o\ ,\ y_o\ ,\ z_o]$, we obtain the approximate orbit equations

$$\vec{r}' - \vec{r} = \frac{V'_\perp}{\Omega_i}[\ \sin\theta - \sin(-\Omega_i t' + \theta)\ ]\hat{x}$$
$$+\left[\frac{V_\perp'}{\Omega_i}\{-\cos\theta + \cos(-\Omega_i t' + \theta)\} + V_{oy}t'\right]\hat{y} + V'_z t'\,\hat{z} . \qquad 3.1.11$$

Using (3.1.8) and (3.1.11), the second integral in (3.1.10) reduces to

$$\int_{-\infty}^{0} \exp[\, i\mu \sin(\theta - \psi)\,] \exp[\, -i\mu \sin(\theta - \psi - \Omega_i t')\,] \times$$
$$\exp[\, i\,\{\vec{k}.\vec{V}_0 + k_z(V_z' - V_{oz}) - \omega\}t'\,]\, dt' , \qquad 3.1.12$$

where $\mu = k_\perp V_\perp / \Omega_i$. The integration (3.1.12) is manipulated with the aid of the identity [15]

$$\exp(\, i\,\mu \sin\beta) = \Sigma_{l=-\infty}^{\infty} \exp(\, i\, l\, \beta)\, J_l(\mu) , \qquad 3.1.13$$

where J_l is the ordinary Bessel function of the first kind of order l, to yield

$$\sum_{p=-\infty}^{\infty} \sum_{q=-\infty}^{\infty} \frac{\exp[i(p-q)(\theta-\psi)]J_p(\mu)J_q(\mu)}{i[q\Omega_i + \vec{k}\cdot\vec{V}_0 + k_z(V_z - V_{oz}) - \omega]} . \qquad 3.1.14$$

The first integral in (3.1.10) is manipulated using the identity

$$\cos\beta = \frac{e^{i\beta} + e^{-i\beta}}{2}$$

and separates into two parts, of which the first part, namely

$$\frac{1}{2}\int_{-\infty}^{0} \exp\,[\, i\,(\psi - \theta + \Omega_i t')]\, \exp\,[\, i\,\{\vec{k}\cdot(\vec{r}' - \vec{r}) - \omega t'\}\,]\, dt'$$

is evaluated as before by using the orbit equations (3.1.11) and the identity (3.1.13). It reduces to

$$\frac{1}{2}\sum_{p=-\infty}^{\infty} \sum_{q=-\infty}^{\infty} \frac{\exp[i(p-q-1)(\theta-\psi)]J_p(\mu)J_q(\mu)}{i[(q+1)\Omega_i + \vec{k}\cdot\vec{V}_0 + k_z(V_z - V_{oz}) - \omega]} . \qquad 3.1.15$$

Similarly the second part yields

$$\frac{1}{2}\sum_{p=-\infty}^{\infty}\sum_{q=-\infty}^{\infty}\frac{\exp[i(p-q+1)(\theta-\psi)]J_p(\mu)J_q(\mu)}{i[(q-1)\Omega_i+\vec{k}\cdot\vec{V}_0+k_z(V_z-V_{oz})-\omega]}. \qquad 3.1.16$$

Using (3.1.14) – (3.1.16) in (3.1.10) we finally obtain

$$f_{b1}(\vec{V}) = -\frac{e}{m_i}f_{bo}(\vec{V})\,\phi_{1k\omega}\left[\frac{k_\perp V_\perp}{2C_\perp^2}\sum_{p=-\infty}^{\infty}\sum_{q=-\infty}^{\infty}J_p(\mu)\,J_q(\mu)\times\right.$$

$$\left\{\frac{\exp[i(p-q-1)(\theta-\psi)]}{[(q+1)\Omega_i+\vec{k}\cdot\vec{V}_0+k_z(V_z-V_{oz})-\omega]}+\frac{\exp[i(p-q+1)(\theta-\psi)]}{[(q-1)\Omega_i+\vec{k}\cdot\vec{V}_0+k_z(V_z-V_{oz})-\omega]}\right\}$$

$$\left.+\frac{k_z}{C_\parallel^2}(V_z-V_{oz})\sum_{p=-\infty}^{\infty}\sum_{q=-\infty}^{\infty}\frac{\exp[i(p-q)(\theta-\psi)]J_p(\mu)J_q(\mu)}{[q\Omega_i+\vec{k}\cdot\vec{V}_0+k_z(V_z-V_{oz})-\omega]}\right]. \qquad 3.1.17$$

The perturbed ion beam density is given by

$$n_{b1} = n_{b1k\omega}\exp\{\,i\,[\vec{k}\cdot\vec{r}-\omega t]\,\} = \int f_{b1}(\vec{V})\,d^3\vec{V}\,. \qquad 3.1.18$$

In performing the integration in (3.1.18) we transform to cylindrical coordinates in velocity space with

$$d^3\vec{V} = V_\perp\,dV_\perp\,dV_z\,d\theta\,.$$

We note that the triple integral in (3.1.18) can be separated into three parts corresponding to the terms of $f_{b1}(\vec{V})$ in (3.1.17). Using the expression (3.1.1) for the equilibrium velocity distribution $f_{bo}(\vec{V})$, the first part yields

$$-\frac{\pi e\phi_{1k\omega}k_{\perp}n_{bo}}{T_{\perp}(2\pi C_{\perp}^2)(2\pi C_{\|}^2)^{1/2}}\sum_{p=-\infty}^{\infty}\int_0^{\infty}\left[\int_{-\infty}^{\infty}\frac{\exp\{-[(V_z-V_{oz})^2/2C_{\|}^2]\}}{[p\Omega_i+\vec{k}\cdot\vec{V}_o+k_z(V_z-V_{oz})-\omega]}dV_z\right]\times$$

$$\exp\left[-\frac{V_{\perp}^2}{2C_{\perp}^2}\right]J_p(\mu)\,J_{p-1}(\mu)\,V_{\perp}^2\,dV_{\perp}\,, \qquad 3.1.19$$

where we have used the result

$$\int_0^{2\pi}\exp[\,i(p-q-1)\theta\,]\,d\theta=\begin{cases}0 & \text{if } p\neq q+1\\ 2\pi & \text{if } p=q+1\end{cases}.$$

At this stage we introduce the plasma dispersion function, known as the Z–function, defined by [16]

$$Z(\lambda)=\frac{1}{\sqrt{\pi}}\int_{-\infty}^{\infty}\frac{e^{-x^2}}{x-\lambda}\,dx \qquad \text{for } Im(\lambda)>0$$

or alternatively as

$$Z(\lambda)=2\,i\,e^{-\lambda^2}\int_{-\infty}^{i\lambda}e^{-t^2}\,dt\,.$$

Then the integral over dV_z in (3.1.19) can be written in terms of the $Z-$function and (3.1.19) becomes

$$-\frac{\pi e\phi_{1k\omega}k_{\perp}n_{bo}}{T_{\perp}(2\pi C_{\perp}^2)(2\pi C_{\|}^2)^{1/2}}\frac{\sqrt{\pi}}{k_z}\sum_{p=-\infty}^{\infty}\int_0^{\infty}J_p(\mu)\,J_{p-1}(\mu)\,Z\left[\frac{\omega-k\cdot V_o-p\Omega_i}{\sqrt{2}k_zC_{\|}}\right]\times$$

$$\exp\left[-\frac{V_{\perp}^2}{2C_{\perp}^2}\right]V_{\perp}^2\,dV_{\perp}\,. \qquad 3.1.20$$

Similarly the second part of the integral in (3.1.18) yields

$$-\frac{\pi e\phi_{1k\omega}k_\perp n_{bo}}{T_\perp(2\pi C_\perp^2)(2\pi C_\parallel^2)^{1/2}}\frac{\sqrt{\pi}}{k_z}\sum_{p=-\infty}^{\infty}\int_0^\infty J_p(\mu)\,J_{p+1}(\mu)\,Z\left[\frac{\omega-\vec{k}\cdot\vec{V}_o-p\Omega_i}{\sqrt{2}k_z C_\parallel}\right]\times$$
$$\exp\left[-\frac{V_\perp^2}{2C_\perp^2}\right]V_\perp^2\,dV_\perp\,. \qquad 3.1.21$$

The last part of the integral in (3.1.18) is shown (appendix A) to reduce to

$$-\frac{e\phi_{1k\omega}n_{bo}}{T_\parallel C_\perp^2}\sum_{p=-\infty}^{\infty}\int_0^\infty J_p^2(\mu)\,[1+z_b\,Z(z_b)]\,\exp\left[-\frac{V_\perp^2}{2C_\perp^2}\right]V_\perp\,dV_\perp\,, \qquad 3.1.22$$

where $z_b = (\omega-\vec{k}\cdot\vec{V}_o-p\Omega_i)/\sqrt{2}k_z C_\parallel$. Combining the results (3.1.20) – (3.1.22) we obtain

$$n_{b1k\omega} = -\frac{e\phi_{1k\omega}n_{bo}}{C_\perp^2}\left[\frac{1}{\sqrt{2}k_z C_\parallel}\sum_{p=-\infty}^{\infty}\int_0^\infty p\Omega_i\,J_p^2(\mu)\,Z(z_b)\,\exp\left[-\frac{V_\perp^2}{2C_\perp^2}\right]V_\perp\,dV_\perp\right.$$
$$\left.+\frac{1}{T_\parallel}\sum_{p=-\infty}^{\infty}\int_0^\infty J_p^2(\mu)\,[1+z_b\,Z(z_b)]\,\exp\left[-\frac{V_\perp^2}{2C_\perp^2}\right]V_\perp\,dV_\perp\right], \qquad 3.1.23$$

where we have used the identity [15]

$$J_{p-1}(\mu)+J_{p+1}(\mu)=\frac{2pJ_p(\mu)}{\mu}$$

with $\mu = k_\perp V_\perp/\Omega_i$ in our analysis. The relation [15]

$$\int_0^\infty J_p^2(\beta x)\,\exp(-ux^2)\,x\,dx=\frac{1}{2u}\exp\left[-\frac{\beta^2}{2u}\right]I_p\left[\frac{\beta^2}{2u}\right],$$

where I_p is the Modified Bessel function of the first kind of order p, is used to perform the integration over $dV_\perp$ and yields

$$n_{b1k\omega} = -\frac{e\phi_{1k\omega} n_{bo}}{T_\perp}\left[\frac{1}{\sqrt{2}k_z C_\parallel}\sum_{p=-\infty}^{\infty} p\Omega_i\, Z(z_b)\exp\left[-\frac{k_\perp^2 C_\perp^2}{\Omega_i^2}\right] I_p\left[\frac{k_\perp^2 C_\perp^2}{\Omega_i^2}\right]\right.$$
$$\left. + \frac{T_\perp}{T_\parallel}\sum_{p=-\infty}^{\infty}\left[1 + z_b Z(z_b)\right]\exp\left[-\frac{k_\perp^2 C_\perp^2}{\Omega_i^2}\right] I_p\left[\frac{k_\perp^2 C_\perp^2}{\Omega_i^2}\right]\right] . \qquad 3.1.24$$

Letting $a_b = k_\perp^2 C_\perp^2/\Omega_i^2$, $\Gamma_{pb} = e^{-a_b} I_p(a_b)$ and using the identity [15] $\Sigma_{p=-\infty}^{\infty} \Gamma_{pb} = 1$, we can write (3.1.24) as

$$n_{b1k\omega} = -\frac{e\phi_{1k\omega} n_{bo}}{T_\perp}\left[\frac{T_\perp}{T_\parallel}\left\{1 + \frac{\omega - \vec{k}.\vec{V}_o}{\sqrt{2}k_z C_\parallel}\sum_{p=-\infty}^{\infty} Z(z_b)\,\Gamma_{pb}\right\}\right.$$
$$\left. + \left\{1 - \frac{T_\perp}{T_\parallel}\right\}\sum_{p=-\infty}^{\infty}\frac{p\Omega_i}{\sqrt{2}k_z C_\parallel} Z(z_b)\,\Gamma_{pb}\right] . \qquad 3.1.25$$

3.2 CONTRIBUTION OF THE BACKGROUND SPECIES TO THE DISPERSION RELATION

The background ion and electron distributions are assumed to be stationary isotropic Maxwellians given by

$$f_{io} = \frac{n_{io}}{(2\pi V_i^2)^{3/2}}\exp\left[-\frac{V^2}{2V_i^2}\right] ,$$
$$f_{eo} = \frac{n_{eo}}{(2\pi V_e^2)^{3/2}}\exp\left[-\frac{V^2}{2V_e^2}\right] ,$$

respectively. Charge neutrality requires $n_{eo} = n_{io} + n_{bo}$. Using an analysis similar to

that for the drifting ions we have obtained the perturbation in the background ion and electron densities $n_{i1k\omega}$ and $n_{e1k\omega}$. However these can easily be obtained from (3.1.25) by setting $T_\perp = T_\parallel = T_j$ $(j = i,e)$ and $\vec{V}_0 = 0$, since the background distributions are isotropic and stationary, and using the appropriate equilibrium densities (n_{io} or n_{eo}). For the stationary ions we obtain

$$n_{i1k\omega} = -\frac{e\phi_{1k\omega} n_{io}}{T_i}\left[1 + \frac{\omega}{\sqrt{2}k_z V_i}\sum_{p=-\infty}^{\infty} Z\left[\frac{\omega - p\Omega_i}{\sqrt{2}k_z V_i}\right]\Gamma_{pi}\right]. \qquad 3.2.1$$

For the electrons we replace (in eqn 3.2.1) e by $-e$, m_i by m_e, Ω_i by $-\Omega_e$, T_i by T_e and V_i by V_e, where $V_e = (T_e/m_e)^{1/2}$ is the electron thermal speed, to obtain

$$n_{e1k\omega} = \frac{e\phi_{1k\omega} n_{eo}}{T_e}\left[1 + \frac{\omega}{\sqrt{2}k_z V_e}\sum_{p=-\infty}^{\infty} Z\left[\frac{\omega - p\Omega_e}{\sqrt{2}k_z V_e}\right]\Gamma_{pe}\right], \qquad 3.2.2$$

where $\Gamma_{pj} = \Gamma_{pj}(a_j) = e^{-a_j} I_p(a_j)$ and $a_j = k_\perp^2 V_j^2/\Omega_j^2$ $(j = i,e)$. In the electrostatic approximation Poisson's equation

$$\nabla^2\phi = 4\pi e\left[n_e - n_i - n_b\right]$$

reduces to

$$\phi_{1k\omega} = \frac{4\pi e}{k^2}\left(n_{i1k\omega} + n_{b1k\omega} - n_{e1k\omega}\right).$$

Using (3.1.25), (3.2.1) and (3.2.2) we obtain the dispersion relation

$$1 + k^2\lambda_{de}^2 + \frac{\omega}{\sqrt{2}k_z V_e}\sum_{p=-\infty}^{\infty} Z(z_e)\,\Gamma_{pe}$$

$$+\frac{\lambda_{de}^2}{\lambda_{di}^2}\left[1 + \frac{\omega}{\sqrt{2}k_z V_i}\sum_{p=-\infty}^{\infty} Z(z_i)\,\Gamma_{pi}\right] + \frac{\lambda_{de}^2}{\lambda_{db}^2}\left[\delta\left\{1 + \frac{\omega - \vec{k}.\vec{V}_o}{\sqrt{2}k_z C_{||}}\sum_{p=-\infty}^{\infty} Z(z_b)\,\Gamma_{pb}\right\}\right.$$

$$\left. + \frac{\beta}{\sqrt{2}k_z C_{||}}\sum_{p=-\infty}^{\infty} p\Omega_i\, Z(z_b)\,\Gamma_{pb}\right] = F(\omega) = 0 \qquad 3.2.3$$

for electrostatic waves in a uniform plasma with magnetized ions and electrons in which the electrons and a fraction of the ions form a stationary background, while the rest of the ions constitute an anisotropic beam drifting at an arbitrary direction to the magnetic field. Here $1/\lambda_{dj}^2 = 4\pi e^2 n_{jo}/T_j$ (j=i,e) is the characteristic Debye length of the background ions and electrons, $1/\lambda_{db}^2 = 4\pi e^2 n_{bo}/T_\perp$ is associated with the beam ions, $z_i = (\omega - p\Omega_i)/\sqrt{2}k_z V_i$, $z_e = (\omega - p\Omega_e)/\sqrt{2}k_z V_e$, $z_b = (\omega - \vec{k}.\vec{V}_o - p\Omega_i)/\sqrt{2}k_z C_{||}$, $\delta = T_\perp/T_{||}$ and $\beta = 1 - \delta$.

Setting $T_\perp = T_{||}$ in (3.2.3) we obtain the dispersion relation of Kindel and Kennel[17].

3.3 APPROXIMATE SOLUTIONS OF THE DISPERSION RELATION

We consider low frequency waves (of which the ion acoustic is an example) in a plasma with hot electrons and relatively cold ions. Thus we assume

$$(1)\ T_e \gg T_i,\ T_\perp,\ T_{||}\ (\sim 0)\ ,$$
$$(2)\ |\omega| \ll \Omega_e\ .$$

Then the power series and asymptotic expansions for the Z–function [16], namely

$$Z(z) = i\sqrt{\pi}\, e^{-z^2} - 2z\left[1 - \frac{2z^2}{3} + \frac{4z^4}{15} - \ldots\right] \qquad 3.3.1$$

for $|z| \ll 1$, and

$$Z(z) = i\sqrt{\pi}\delta\, e^{-z^2} - \frac{1}{z}\left[1 + \frac{1}{2z^2} + \frac{3}{4z^4} + \ldots\right] \qquad 3.3.2$$

for $|z| \gg 1$, where

$$\delta = \begin{cases} 0 & \text{if } \mathrm{Im}(z) > 0 \\ 1 & \text{if } \mathrm{Im}(z) = 0 \\ 2 & \text{if } \mathrm{Im}(z) < 0\,, \end{cases}$$

are used to reduce the dispersion relation (3.2.3) to an approximate form. With our assumptions

$$z_e = \frac{\omega - p\Omega_e}{\sqrt{2}k_z V_e} \approx \frac{-p\Omega_e}{\sqrt{2}k_z V_e} \quad \text{for } p \neq 0\,.$$

Then

$$\sum_{-\infty}^{\infty} Z(z_e)\,\Gamma_{pe} \approx Z\left[\frac{\omega}{\sqrt{2}k_z V_e}\right]\Gamma_{oe} + \sum_{1}^{\infty}\left[\, Z\left[\frac{-p\Omega_e}{\sqrt{2}k_z V_e}\right] + Z\left[\frac{p\Omega_e}{\sqrt{2}k_z V_e}\right]\right]\Gamma_{pe} = Z(z_{oe})\,\Gamma_{oe}\,,$$

where $z_{oe} = \omega/\sqrt{2}k_z V_e$ and we have used $Z(\lambda) + Z(-\lambda) = 0$, which can easily be proved from the definition of the Z–function (section 3.1). Further for large T_e, we may assume that $|z_{oe}| \ll 1$. Then using expansion (3.3.1) we may write

$$\sum_{-\infty}^{\infty} Z(z_e)\,\Gamma_{pe} \approx (i\sqrt{\pi} - 2z_{oe})\,\Gamma_{oe}\,. \qquad 3.3.3$$

Since for the cold background ions $|a_i| = |k_\perp^2 V_\perp^2/\Omega_i^2| \ll 1$ and $\Gamma_p(x) \ll 1$ for $p \neq 0$,

$$\Gamma_p(x) = e^{-x} I_p(x) \approx \left(\frac{x}{2}\right)^p \frac{1}{p!}(1 - x) \text{ for } |x| \ll 1 \text{ [15]}\,, \qquad 3.3.4$$

we retain only the zero order term in the ion summation. Thus

$$\sum_{-\infty}^{\infty} Z(z_i)\,\Gamma_{pi} \approx Z(z_{oi})\,\Gamma_{oi} \approx \left[-\frac{1}{z_{oi}} - \frac{1}{2z_{oi}^3}\right]\Gamma_{oi}\,, \qquad 3.3.5$$

where $z_{oi} = \omega/\sqrt{2}k_z V_i$ and we have used the expansion (3.3.2) since $|z_{oi}| \gg 1$. Similarly, for the cold beam ions

$$\sum_{-\infty}^{\infty} Z(z_b)\,\Gamma_{pb} \approx Z(z_{ob})\,\Gamma_{ob} \approx \left[-\frac{1}{z_{ob}} - \frac{1}{2z_{ob}^3}\right]\Gamma_{ob}\,, \qquad 3.3.6$$

where $z_{ob} = (\omega - \vec{k}\cdot\vec{V}_0)/\sqrt{2}k_z C_{\|}$. For the $\sum_{-\infty}^{\infty} p\,Z(z_b)\,\Gamma_{pb}$ term we retain the first order terms $(p = \pm 1)$ to obtain

$$\sum_{-\infty}^{\infty} p\,Z(z_b)\,\Gamma_{pb} \approx \frac{-2\Omega_i}{\bar{\omega}^2 - \Omega_i^2}\left(\sqrt{2}k_z C_{\|}\Gamma_{1b}\right)\,, \qquad 3.3.7$$

where $\bar{\omega} = \omega - \vec{k}.\vec{V}_0$ is a Doppler – shifted frequency. Using (3.3.3),(3.3.5)–(3.3.7) in the dispersion relation (3.2.3) we obtain

$$1 + k^2\lambda_{de}^2 = a\left[\frac{\Gamma_{oi}}{2z_{oi}^2} - (1 - \Gamma_{oi})\right] + b\left[\frac{2\Omega_i^2\beta\Gamma_{1b}}{\bar{\omega}^2 - \Omega_i^2} + \delta\left[\frac{\Gamma_{ob}}{2z_{ob}^2} - (1 - \Gamma_{ob})\right]\right] - i\sqrt{\pi}\,z_{oe}\Gamma_{oe}\,, \qquad 3.3.8$$

where $a = \lambda_{de}^2/\lambda_{di}^2 = (T_e/T_i)(n_{io}/n_{eo})$ and $b = \lambda_{de}^2/\lambda_{db}^2 = (T_e/T_\perp)(n_{bo}/n_{eo})$, and we recall $\delta = T_\perp/T_{\|}$, $\beta = 1 - \delta$. From (3.3.4) we can show that

$$1 - \Gamma_{oi} = a_i = \frac{k_\perp^2 V_i^2}{\Omega_i^2}$$

$$1 - \Gamma_{ob} = a_b = \frac{k_\perp^2 C_\perp^2}{\Omega_i^2} .$$

Using the above results eqn (3.3.8) becomes

$$1 + k^2\lambda_{de}^2 = a\left[\frac{k_z^2 V_i^2}{\omega^2}\Gamma_{oi} - \frac{k_\perp^2 V_i^2}{\Omega_i^2}\right] + b\left[\frac{2\Omega_i^2\beta\Gamma_{1b}}{\bar{\omega}^2-\Omega_i^2}\right.$$

$$\left. + \delta\left[\frac{k_z^2 C_\parallel^2}{\bar{\omega}^2}\Gamma_{ob} - \frac{k_\perp^2 C_\perp^2}{\Omega_i^2}\right]\right] - i\sqrt{\pi}\,\frac{\omega}{\sqrt{2}k_z V_e}\Gamma_{oe} . \qquad 3.3.9$$

We solve eqn (3.3.9) by setting $\omega = \omega_r + i\gamma$ and assuming that

$$(1)\ \left|\frac{\gamma}{\omega_r}\right| \ll 1$$

$$(2)\ \left|\frac{\gamma}{\bar{\omega}_r}\right| \ll 1$$

$$(3)\ |\bar{\omega}|^2 \ll \Omega_i^2 .$$

With these assumptions the following approximations are made

$$\frac{1}{\omega^2} = \frac{1}{\omega_r^2(1+i\gamma/\omega_r)^2} \approx \frac{1}{\omega_r^2}\left[1 - \frac{2i\gamma}{\omega_r}\right]$$

$$\bar{\omega}^2 = (\bar{\omega}_r + i\gamma)^2 \approx \bar{\omega}_r^2\left[1 + \frac{2i\gamma}{\bar{\omega}_r}\right]$$

$$\frac{1}{\bar{\omega}^2-\Omega_i^2} = \frac{1}{-\Omega_i^2(1-\bar{\omega}^2/\Omega_i^2)} \approx -\frac{1}{\Omega_i^2}\left(1 + \bar{\omega}^2/\Omega_i^2\right) \approx -\frac{1}{\Omega_i^2}\left[1 + \frac{2i\gamma\bar{\omega}_r}{\Omega_i^2}\right] .$$

Using the above approximations equation (3.3.9) becomes

$$1 + k^2\lambda_{de}^2 = a\left[\frac{k_z^2 V_i^2}{\omega_r^2}\Gamma_{oi}\left[1 - \frac{2i\gamma}{\omega_r}\right] - \frac{k_\perp^2 V_i^2}{\Omega_i^2}\right] + b\left[-2\beta\Gamma_{1b}\left[1 + \frac{2i\gamma\bar{\omega}_r}{\Omega_i^2}\right]\right.$$
$$\left. + \delta\left\{\frac{k_z^2 C_\parallel^2}{\bar{\omega}_r^2}\Gamma_{ob}\left[1 - \frac{2i\gamma}{\omega_r}\right] - \frac{k_\perp^2 C_\perp^2}{\Omega_i^2}\right\}\right] - \frac{i\sqrt{\pi}}{\sqrt{2}k_z V_e}\Gamma_{oe}(\omega_r + i\gamma)\,. \qquad 3.3.10$$

Taking the real part of (3.3.10), assuming that $|\gamma/V_e k_z| \ll 1$ and noting that $0 \leq \Gamma_{oe} \leq 1$ for all a_e, we obtain

$$1 + k^2\lambda_{de}^2 = a\left[\frac{k_z^2 V_i^2}{\omega_r^2}\Gamma_{oi} - \frac{k_\perp^2 V_i^2}{\Omega_i^2}\right]$$
$$+ b\left[-2\beta\Gamma_{1b} + \delta\left[\frac{k_z^2 C_\parallel^2}{\bar{\omega}_r^2}\Gamma_{ob} - \frac{k_\perp^2 C_\perp^2}{\Omega_i^2}\right]\right]. \qquad 3.3.11$$

We note that since we have assumed $|\gamma| \ll |\omega_r|$, the assumption $|\gamma/V_e k_z| \ll 1$ is satisfied if the wave phase speed (ω_r/k_z) along $\vec{B}_0$ is less than the electron thermal speed. We consider special cases of the dispersion relation (3.3.11).

(a) STATIONARY SINGLE ION SPECIES

For $n_{bo} = 0$ $(b = 0)$, that is a two component plasma with stationary ions, eqn (3.3.11) reduces to

$$\omega_r = \pm \frac{k_z c_s}{\sqrt{1 + k^2\lambda_{de}^2 + k_\perp^2\rho_s^2}} \qquad 3.3.12$$

which is the dispersion relation for ion acoustic waves as found by Zakharov and Kuznetsov[18]. In the absence of perpendicular dispersion $(k_\perp = 0)$ eqn (3.3.12) reduces to

the result of Kindel and Kennel [17].

(b) ISOTROPIC ION BEAM, STATIONARY ELECTRONS

For $T_\perp = T_\parallel$ and $n_{io} = 0$ $(a = 0)$, that is for isotropic ions streaming through background electrons, eqn (3.3.11) yields the fast and slow beam modes.

$$\omega_r = \vec{k}\cdot\vec{V}_0 \pm \frac{k_z c_s}{\sqrt{1+k^2\lambda_{de}^2+k_\perp^2\rho_s^2}} .$$

The imaginary part of eqn (3.3.10) yields

$$a\left[\frac{k_z^2 v_i^2}{\omega_r^2}\Gamma_{oi}\left[-\frac{2\gamma}{\omega_r}\right]\right] + b\left[-2\beta\Gamma_{1b}\frac{2\gamma}{\bar{\omega}_r}\frac{\bar{\omega}_r^2}{\Omega_i^2} + \delta\left\{\frac{k_z^2 c_\parallel^2}{\bar{\omega}_r^2}\Gamma_{ob}\left[-\frac{2\gamma}{\bar{\omega}_r}\right]\right\}\right] - \frac{\sqrt{\pi}\Gamma_{oe}}{\sqrt{2}k_z v_e}\omega_r = 0 ,$$

from which we obtain an expression for the normalized growth rate γ/ω_r, namely

$$\frac{\gamma}{\omega_r} = -\frac{\sqrt{\pi}\ \Gamma_{oe}\omega_r}{2\sqrt{2}k_z v_e}\left[a\frac{k_z^2 v_i^2}{\omega_r^2}\Gamma_{oi} + b\omega_r\left[\frac{2\beta\bar{\omega}_r}{\Omega_i^2}\Gamma_{1b} + \delta\frac{k_z^2 c_\parallel^2}{\bar{\omega}_r^3}\Gamma_{ob}\right]\right]^{-1} . \qquad 3.3.13$$

(c) UNMAGNETIZED PLASMA

For an unmagnetized plasma with isotropic ions we set $\Omega_j = 0$ $(j=i,e)$ and $\beta = 0$ in the dispersion relation (3.2.3). We obtain

$$0 = k^2\lambda_{de}^2 + 1 + z_{oe}Z(z_{oe}) + a[1 + z_{oi}Z(z_{oi})] + b[1 + z_{ob}Z(z_{ob})] , \qquad 3.3.14$$

where we have used the identities [15]

$$\Sigma_{p=-\infty}^{\infty} \Gamma_p = 1$$

and

$$\Sigma_{p=-\infty}^{\infty} p\, \Gamma_p = 0 \ .$$

The latter identity follows since Γ_p is an even function. Using the identity [16]

$$Z'(\lambda) = -2[1 + \lambda Z(\lambda)]$$

we can reduce eqn (3.3.14) to

$$2k^2\lambda_{de}^2 = Z'(z_{oe}) + aZ'(z_{oi}) + bZ'(z_{ob}) \ ,$$

which can be rewritten as

$$1 - \frac{1}{2k^2\lambda_{de}^2} Z'\left[\frac{\omega}{\sqrt{2}k_z V_e}\right] - \frac{1}{2k^2\lambda_{di}^2} Z'\left[\frac{\omega}{\sqrt{2}k_z V_i}\right] - \frac{1}{2k^2\lambda_{db}^2} Z'\left[\frac{\omega - \vec{k}\cdot\vec{V}_o}{\sqrt{2}k_z C_{||}}\right] = 0 \qquad 3.3.15$$

The result (3.3.15) has been derived by Akimoto and Omidi [6].

CHAPTER FOUR

ION BEAM – PLASMA INTERACTION

4.1 INTRODUCTION

In this chapter we present numerical solutions of the dispersion relation (3.2.3). "Unfortunately the (numerical) investigation of this relation is one of that large class of tasks that is trivial in principle but not in practice, owing to the multiplicity of parameters and variables involved and to the unpleasant nature of the functions." [19]. Details of the Cauchy Rootfinder are presented in appendix C. Beam drifts perpendicular and parallel to the external magnetic field $\vec{B}_0$ are separately considered. The results are presented in normalized form. The beam and background ions are assumed to have equal mass. Time is normalized by the inverse ion gyrofrequency (Ω_i^{-1}), speed by the ion sound speed $C_s = (T_e/m_i)^{1/2}$, distance by $\rho_s = C_s/\Omega_i$ (the ion gyroradius at the electron temperature), density by the electron density n_{eo} and temperatures by the electron temperature T_e.

Standard values of parameters used are: $n_{bo} = 0.1$, $\omega_{pe}/\Omega_e = 0.4$, $k = 1.0$ and 5.0 , $m_e/m_i = 1/1836$ (corresponding to a hydrogen plasma). For simplicity, we restrict our analysis to the two–dimensional y–z plane.

At the outset, it must be pointed out that very careful analysis is required to identify the low frequency modes observed. This is so because the ion acoustic wave and the two–stream like instabilities have overlapping phase speeds. In this regard, Winske et al. [20] have pointed out that the actual separation is somewhat artificial.

4.2 PERPENDICULAR DRIFT WITH k = 1

We note that for k = 1 we have $k\lambda_{de} = 0.06$ and $k\rho_i = 0.32$. Thus we consider extremely long wavelengths. Figure 4.2.1 is a plot of the normalized growth rate γ versus k_y/k for normalized velocities V_{oy} in the range $1.5 - 6$ for an isotropic ion beam ($T_\perp/T_\parallel = 1$). Here and in subsequent graphs k = 1 is held fixed and the angle of propagation θ between $\vec{k}$ and the beam direction ($\vec{V}_{oy}$) is varied from 0° to 90°. We note that $k_y/k = \cos\theta$.

For V_{oy} in the range $1.5 - 2.5$ γ_{max} (maximum growth) decreases with V_{oy} while for the range $2.5 - 6$ γ_{max} increases with V_{oy}. This seems to indicate the presence of two different plasma waves. This is clearly seen for $V_{oy} = 2.5$ where two unstable modes exist. An examination of the corresponding real frequency plots depicted in fig 4.2.2 indicate that the phase speeds of both the growing modes are entirely different.

TABLE 4.2.1

V_{oy}	k_y/k (at γ_{max})	ω_r	ω_{ria}	$k.V_o - \omega_r$
1.5	0.96	1.32	1.35	0.12
2.0	0.85	1.397	1.53	0.30
2.5	0.725	1.41	1.595	0.40
	0.475	0.86	0.91	0.327
2.75	0.45	0.895	0.955	0.343
3.0	0.425	0.918	0.989	0.357
4.0	0.35	0.989	1.104	0.411
6.0	0.25	1.05	1.19	0.45

Table 4.2.1 is obtained in the following manner. For each of the velocities of fig 4.2.1 k_y/k at maximum growth (γ_{max}) is determined. The corresponding real frequency (ω_r) is obtained from fig 4.2.2 . The ion acoustic slow beam mode frequency (ω_{ria}) is calculated using [21]

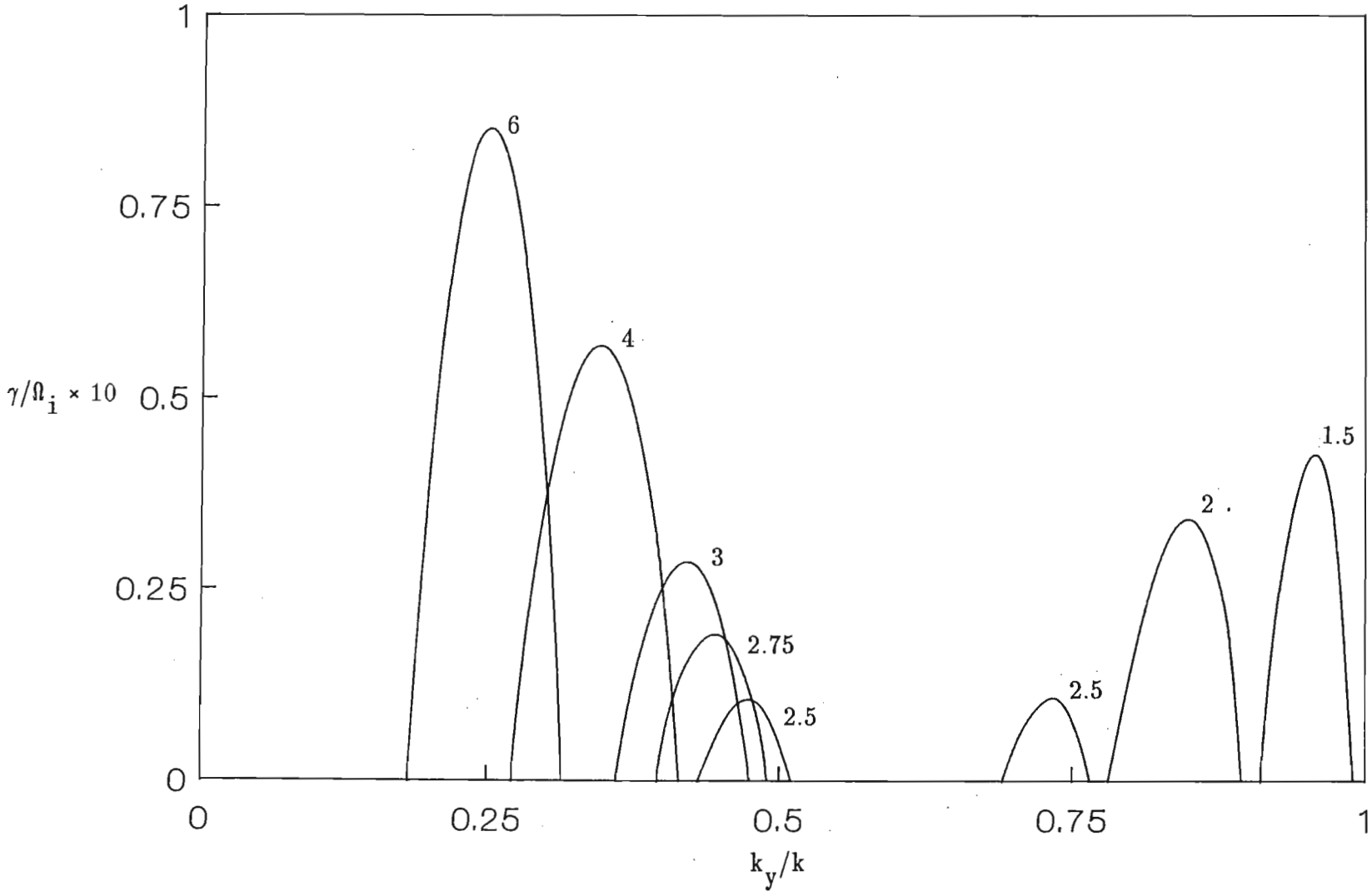

FIG 4.2.1 Normalized growth rate as a function of k_y/k for the isotropic case $T_\perp/T_\parallel = 1$. The parameter labelling the curves is the beam speed V_{oy}. Here $T_\perp = T_\parallel = T_i = 0.1\ T_e$, $k\rho_s = 1$, $\omega_{pe}/\Omega_e = 0.4$, $n_{b0} = 0.1\ n_{e0}$

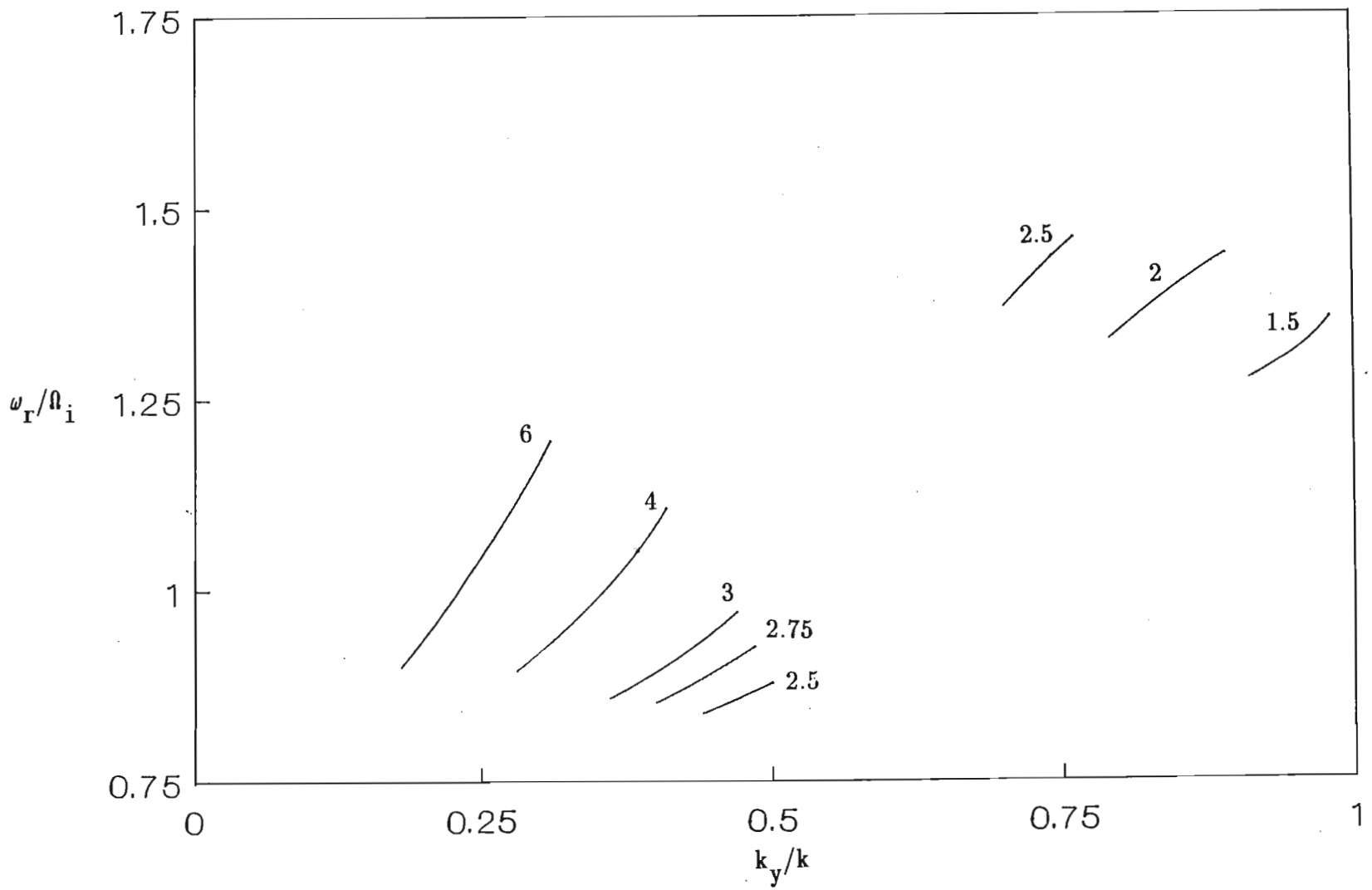

FIG 4.2.2 Normalized real frequency versus k_y/k for the isotropic case $T_\perp/T_\parallel = 1$. The parameter labelling the curves is the beam speed V_{oy}. Other fixed parameters have the same value as in fig 4.2.1 .

$$\omega_{ria} = \mathbb{k}.\vec{V}_0 - \left[\frac{n_{bo}}{n_{eo}}\right]^{1/2} \frac{k_z C_s}{(1+k^2\lambda_{de}^2+k_\perp^2\rho_s^2)^{1/2}} . \qquad 4.2.1$$

In the range $V_{oy} = 2.5 - 6$, ω_r is close to the slow beam ion acoustic frequency and the wave is thus associated with the ion acoustic mode. The maximum growth rate increases with V_{oy} as more free energy is available to drive the instability.

Before we proceed further we explain the meaning of beam resonance. If $\vec{V}_0$ is the velocity of the beam, then the projection of $\vec{V}_0$ in the direction of wave propagation is $V_0\cos\theta$, where θ is the angle between the beam direction and the direction of wave propagation (fig 4.2.3).

FIG 4.2.3

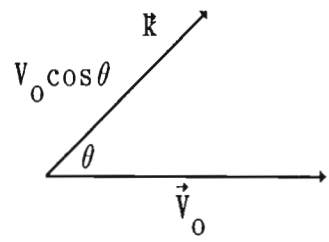

The wave can gain maximum energy from the beam when the phase speed V_ϕ of the wave satisfies

$$V_\phi = \frac{\omega_r}{k} = V_0\cos\theta . \qquad 4.2.2$$

This can be written as

$$\omega_r = \mathbb{k}.\vec{V}_0 , \qquad 4.2.3$$

and is an exact beam resonant condition mentioned by Gary and Omidi [7]. The condition (4.2.3) is an ideal condition for growth. However growth can still occur if $V_0\cos\theta \approx V_\phi$, when the beam ions with velocity near $V_0\cos\theta$ do not effectively see the rapidly varying

electric field of the wave and exchange energy with the wave. The deviation from exact resonance is calculated in table 4.2.1 .

In view of the above discussion and the data presented in table 4.2.1, in the range V_{oy} = 1.5 – 2.5 we identify the instability as the ion–ion streaming instability, which is a beam driven mode. This correlates with the the decrease in γ_{max} with V_{oy}, since as V_{oy} increases so too does the deviation from exact resonance. This increase in deviation from exact resonance with increase in V_{oy} accounts for the decrease in γ_{max} with V_{oy}. In addition, we also note that since both the ions and electrons are magnetized (ω_{pe}/Ω_e = 0.4) ,both ion and electron Landau damping is reduced at perpendicular propagation ($\perp \vec{B}_0$).

For a wave of fixed phase speed equation 4.2.2 implies that an increase in V_0 will decrease $\cos\theta$ and hence increase the angle of propagation. For a fixed phase speed in fig 4.2.2 (ω_r fixed, since k = constant) this shift in propagation angle (k_y/k decreasing for increasing V_{oy} in the range 1.5 – 2.5) is clearly noted. This increase in oblique propagation (to the beam) at higher beam speeds is characteristic of the ion–ion streaming instability and was found by Gary and Omidi [7], Akimoto and Omidi [6], Akimoto and Winske [5] and Gresillon et al. [1]. If we set $V_\phi = C_s$ (since $\omega_r \approx 1.0$ in fig 4.2.2) in equation 4.2.2 we get the condition $V_0\cos\theta = C_s$ for the propagation of the ion–ion streaming instability as found by Akimoto and Winske [5].

From equation 4.2.1 we see that for $V_0/C_s \gg k_z/k_y$ the ion acoustic instability becomes a beam driven mode. The transition from the ion–ion streaming mode to the ion acoustic mode at high beam velocities was found by the above mentioned authors. It is interesting to note that although the work of Gresillon et al. [1] was performed in an argon plasma while our calculations are for a hydrogen plasma, they also found the transition velocity from the ion–ion streaming to the ion acoustic instability to be 2.5 .

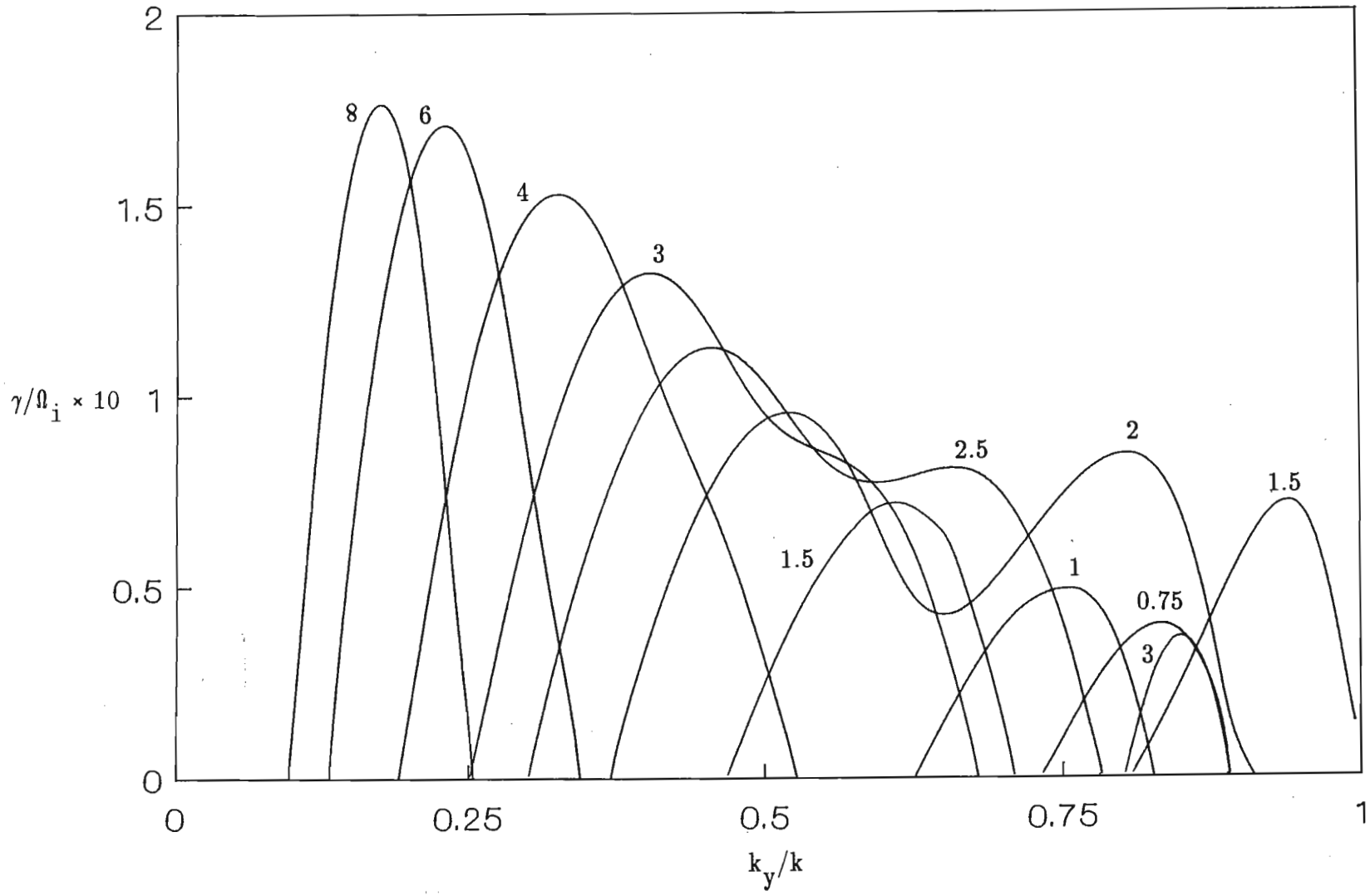

FIG 4.2.4 Normalized growth rate as a function of k_y/k for the anisotropic case $T_\perp/T_\parallel = 4$. The parameter labelling the curves is the beam speed V_{oy}. Here $T_\parallel = 0.025\ T_e$, $T_\perp = T_i = 0.1\ T_e$, while other fixed parameters have the same

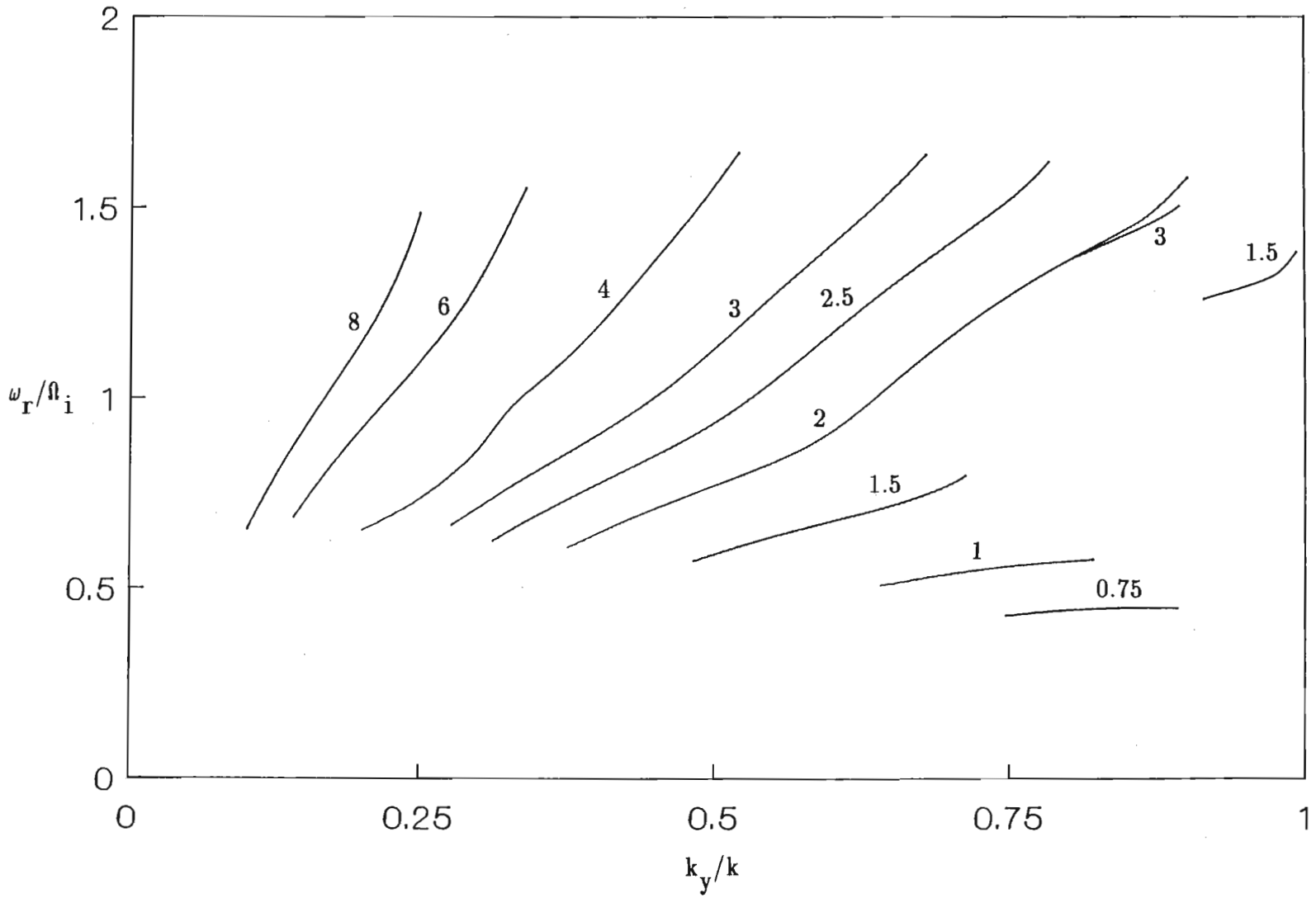

FIG 4.2.5 Normalized real frequency versus k_y/k for the parameters of fig 4.2.4 . The parameter labelling the curves is the beam speed V_{oy}.

In fig 4.2.4 we display the growth rates for an anisotropic ion beam with $T_\perp/T_\parallel = 4$. The corresponding real frequencies are plotted in fig 4.2.5 . It must be noted that here the perpendicular temperature ($T_\perp$) is held fixed ($T_\perp = 0.1\ T_e$), the same as for the isotropic case, while the parallel temperature is decreased ($T_\parallel = 0.025\ T_e$) to yield an anisotropy $T_\perp/T_\parallel = 4$.

In the range $V_{oy} = 0.75 - 8$ we have the ion acoustic instability where as before the maximum growth increases with velocity. In the range $V_{oy} = 1.5 - 3$ we have the ion–ion streaming instability where the maximum growth rate decreases with velocity. The distinction between these two modes is evident from fig 4.2.5 where for $V_{oy} = 1.5$ we have two separate modes, the ion–ion streaming mode propagating essentially parallel to the beam and the ion acoustic mode propagating oblique to the beam.

The left hand peak for $V_{oy} = 2$ occurs at $k_y/k \approx 0.52$ and corresponds to a real frequency of $\omega_r \approx 0.8$, which agrees with the computed value $\omega_{ria} = 0.77$ using the slow beam ion acoustic dispersion relation (4.2.1). For $V_{oy} = 2$, $k_y/k \approx 0.65$ at the dip in the growth rate curve (fig 4.2.4). The ω_r curve (fig 4.2.5) has an inflection point at $k_y/k \approx 0.65$ indicating a change in the nature of the instability. The growth rate curve ($V_{oy} = 2$) thus represents an overlap of the two instabilities.

For $V_{oy} = 4,6,8$ the maximum growth rates occur at $\omega_r \approx \Omega_i$ and could be associated with a resonance between the slow beam ion acoustic mode and the background ion cyclotron motion.

It is observed that the ion acoustic mode starts at a much lower threshold velocity (0.75) when the ion beam is anisotropic, surprisingly at a value less than C_s. For the isotropic case $V_{oy} > C_s$ is always necessary to excite the instability. This lower threshold allows for

the overlap with the ion–ion streaming mode for $V_{oy} > 1.5$.

It is seen from figs 4.2.4 and 4.2.5 that the ion–ion streaming instability propagates essentially parallel to the beam and shifts to oblique propagation as V_{oy} is increased from 1.5 to 2.5 . It reverts to parallel propagation as V_{oy} is increased to 3. This is unlike the isotropic case where larger beam velocities propagate obliquely.

The anisotropy also serves to increase the angular range of propagation. This is responsible for the merging in fig 4.2.4 of the two modes for $V_{oy} = 2.5$ that appear separately in fig 4.2.1 .

A comparison of figs 4.2.1 and 4.2.4 indicates an increase in the maximum growth rates with anisotropy. For $V_{oy} = 6$ the ratio of the maximum growth rates (anisotropic/isotropic) ≈ 2 while for $V_{oy} = 1.5$ this ratio is approximately 1.67 . The effect of the anisotropy on the growth is fully investigated in figs 4.2.6 and 4.2.7 . Figure 4.2.6 is a plot of growth rate versus k_y/k for beam speed $V_{oy} = 4$ while fig 4.2.7 is a similar plot for $V_{oy} = 2$. We note from figs 4.2.4 and 4.2.5 that the former beam speed corresponds to a purely ion acoustic mode while the latter ($V_{oy} = 2$) an overlap between the ion acoustic and ion–ion streaming instabilities takes place. The parameter labelling the curves is the beam anisotropy $T_\perp/T_\parallel$. We note that the anisotropy has little or no effect on the dip in fig 4.2.7 (which occurs at $\omega_r \approx \Omega_i$ and could be due to ion cyclotron damping) but shifts the peaks in fig 4.2.6 (where ion cyclotron resonance with the background ions could enhance wave growth) and fig 4.2.7 slightly to the left.

The effect of the anisotropy is to essentially increase the growth rates. This is easily explained. The total beam temperature is $T_b = (2T_\perp + T_\parallel)/3$. Since $T_\perp$ is kept fixed ($T_\perp = 0.1T_e$), increasing $T_\perp/T_\parallel$ corresponds to decreasing $T_\parallel$ and hence the total beam

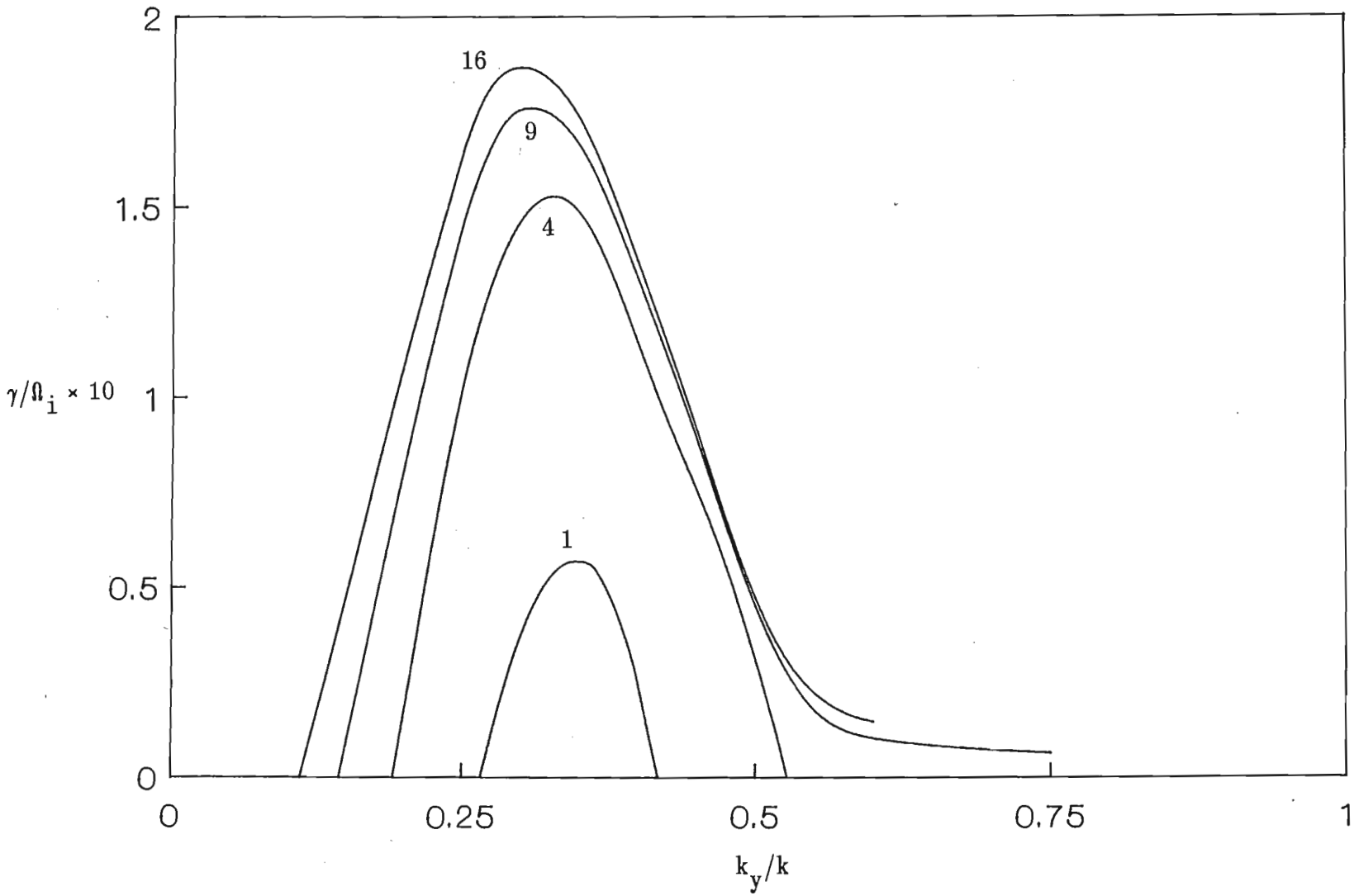

FIG 4.2.6 Normalized growth rate as a function of k_y/k for beam speed $V_{oy} = 4\ C_s$. The parameter labelling the curves is the beam anisotropy $T_\perp/T_\parallel$. Other fixed parameters have the same value as in fig 4.2.1 .

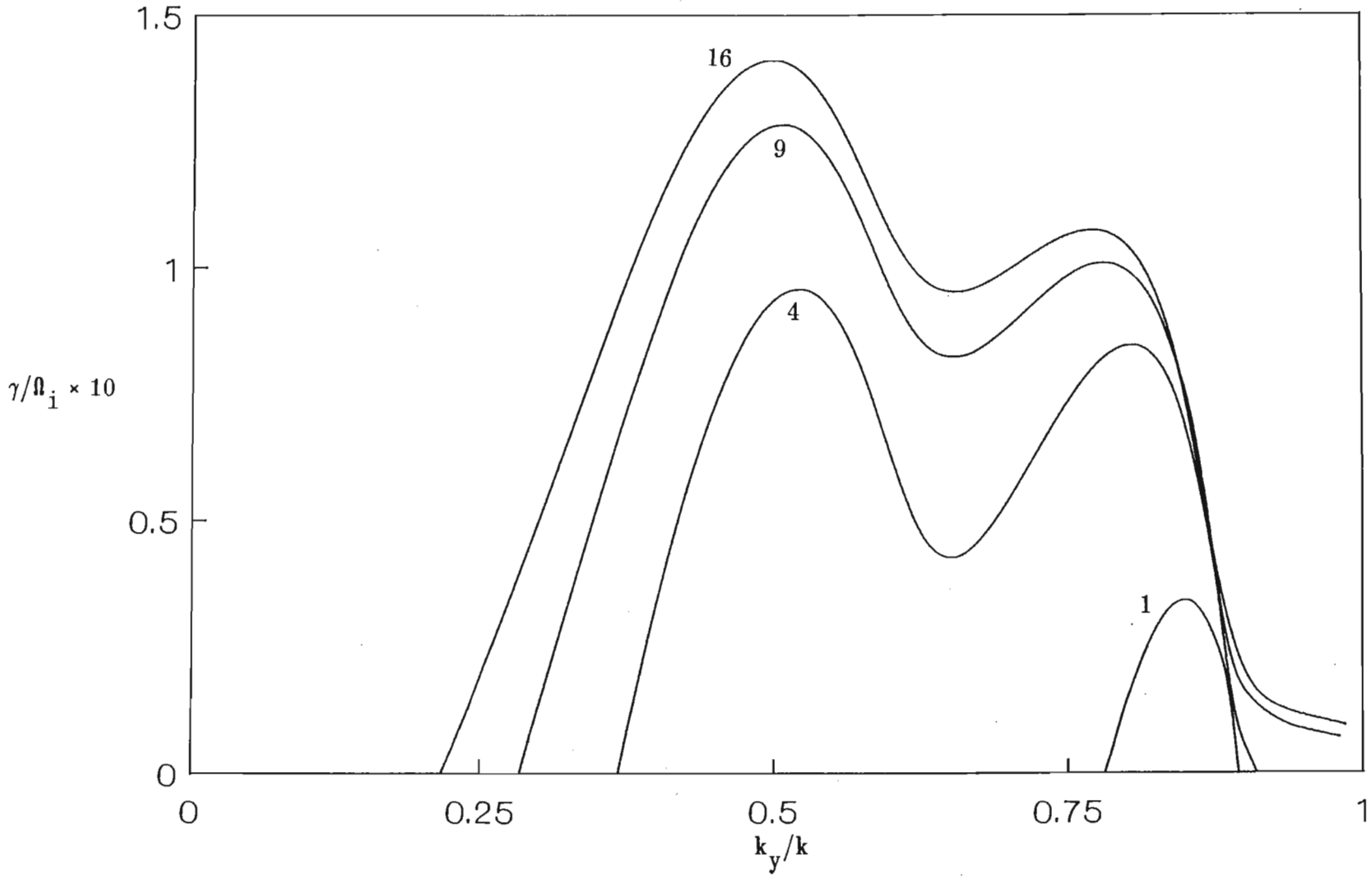

FIG 4.2.7 Normalized growth rate as a function of k_y/k for beam speed $V_{oy} = 2\ C_s$. The parameter labelling the curves is the beam anisotropy $T_\perp/T_\parallel$. Here $T_\perp = 0.1\ T_e$, while other fixed parameters have the same value as in fig 4.2.1 .

temperature T_b. This decrease in the total beam temperature increases the slope of the beam distribution and hence results in an increase in growth ($\gamma \propto \frac{\partial f}{\partial V}$). The enhancement of growth with decrease in T_b was also found by Akimoto and Omidi (fig3) [6] for an unmagnetized plasma. The enhancement of growth is essentially due to parallel (to $\vec{B}_0$) motion, since decreasing $T_{||}$ effectively reduces ion Landau damping along $\vec{B}_0$.

The effective temperature of the beam (T_{eff}) in the direction of wave propagation is obtained with the aid of fig 4.2.8 .

FIG 4.2.8

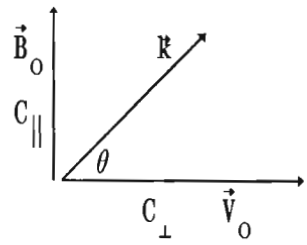

Here $C_{||} = (T_{||}/m_i)^{1/2}$ and $C_\perp = (T_\perp/m_i)^{1/2}$ are the thermal speeds in the parallel and perpendicular directions respectively. The projection of $\vec{C}_\perp$ in the direction of wave propagation is

$$V_1 = C_\perp \cos\theta$$

and the projection of $\vec{C}_{||}$ in the direction of wave propagation is

$$V_2 = C_{||} \sin\theta .$$

Taking the root mean square of these quantities, namely

$$\bar{V} = (V_1^2 + V_2^2)^{1/2}$$

we obtain

$$\bar{V} = V_{eff} = (T_{eff}/m_i)^{1/2} = (C_\perp^2 \cos^2\theta + C_{||} \sin^2\theta)^{1/2} ,$$

which can be simplified to yield

$$T_{eff} = T_\perp \cos^2\theta + T_{||} \sin^2\theta . \qquad 4.2.4$$

For the curves in fig 4.2.6 we calculate T_{eff} at maximum growth and present the results in table 4.2.2 .

TABLE 4.2.2

$T_\perp/T_{||}$	k_y/k (at γ_{max})	T_{eff}
1	0.348	0.1
4	0.326	0.0329
9	0.315	0.0199
16	0.309	0.0152

The shift of the peaks towards the left is now easily explained. With an increase in beam anisotropy, at maximum growth the wave propagates in a direction such that the effective temperature of the beam as seen by the wave is decreased. This decrease in effective temperature reduces ion beam Landau damping.

In fig 4.2.7 the overlap of the ion–ion streaming and ion acoustic instabilities is displayed. It is seen that as the anisotropy increases, γ_{max} of the ion acoustic mode dominates over that of the ion–ion streaming instability. One may argue that since the ion acoustic instability is kinetic in nature (due to a resonance in velocity space) while the two–stream instability is not, the former should be more sensitive to changes in velocity distribution. Thus the decrease in parallel (to $\vec{B}_0$) ion Landau damping with decreasing $T_{||}$ (increasing $T_\perp/T_{||}$) enhances the growth rate of the ion acoustic instability more than that of the ion–ion streaming instability.

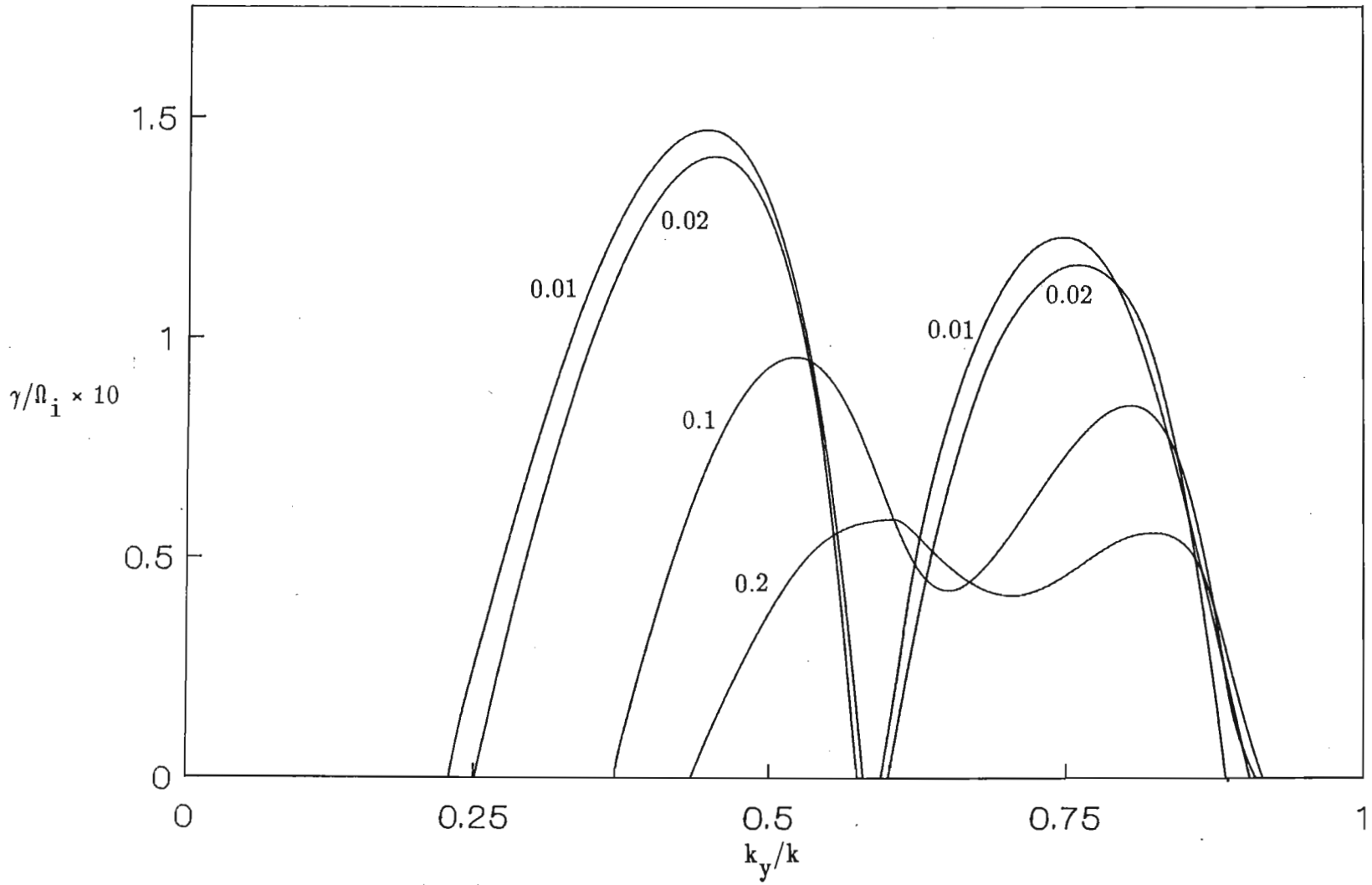

FIG 4.2.9 Normalized growth rate as a function of k_y/k for the anisotropic case $T_\perp/T_\parallel = 4$. The parameter labelling the curves is the background ion/electron temperature ratio T_i/T_e. Here $V_{oy} = 2\ C_s$ while other fixed parameters have the same value as in fig 4.2.4 .

The curves in fig 4.2.9 represent the normalized growth rates versus k_y/k for different values of the background ion to electron temperature ratio T_i/T_e. A decrease in T_i/T_e enhances both the ion–ion streaming and ion acoustic modes. As for the ion beam case, a decrease in T_i/T_e decreases ion Landau damping of the wave. It is well known that a necessary condition for the ion acoustic wave to propagate is that $T_i \ll T_e$. Although the source of free energy for the ion beam instability is the ion beam, high energy electrons also play an active role in driving the instability [22] as is evident in fig 4.2.9 . It is seen from fig 4.2.9 that for $T_i/T_e \leq 0.02$ the overlap between the two types of instability is destroyed. They propagate in clearly defined angular regions.

Figure 4.2.10 shows the normalized growth rates versus k_y/k for different values of the ion beam density. Initially an increase in ion beam density $(0.1 - 0.3)$ enhances both modes as the free energy available increases. It is seen that the ion–acoustic mode is enhanced more than the ion–ion mode as n_{bo} increases. In fact, the latter reaches a maximum for $n_{bo} \approx 0.3$.

4.3 PARALLEL (to $\vec{B}_0$) DRIFT WITH k = 1

In fig 4.3.1 we plot a graph of the normalized growth rate γ versus k_y/k for an isotropic ion beam, while fig 4.3.2 shows the corresponding real frequencies. The parameter labelling the curves is the normalized beam speed V_{oz} along $\vec{B}_0$. For the threshold drift speed for instability $V_{oz} = 1.25$, we identify the wave as the slow beam ion acoustic mode since this mode satisfies the ion acoustic dispersion relation 4.2.1 . This is evident from fig 4.3.3 where we have plotted the theoretical real frequencies (4.2.1) for the ion acoustic wave for $V_{oz} = 1.25 - 2$. We have further found that increasing the ion beam temperature completely damps this mode at a critical temperature of $T_b = T_{||} = T_{\perp} = 0.2$, and is due to ion Landau damping. Further it is well known that for the ion acoustic mode the growth is

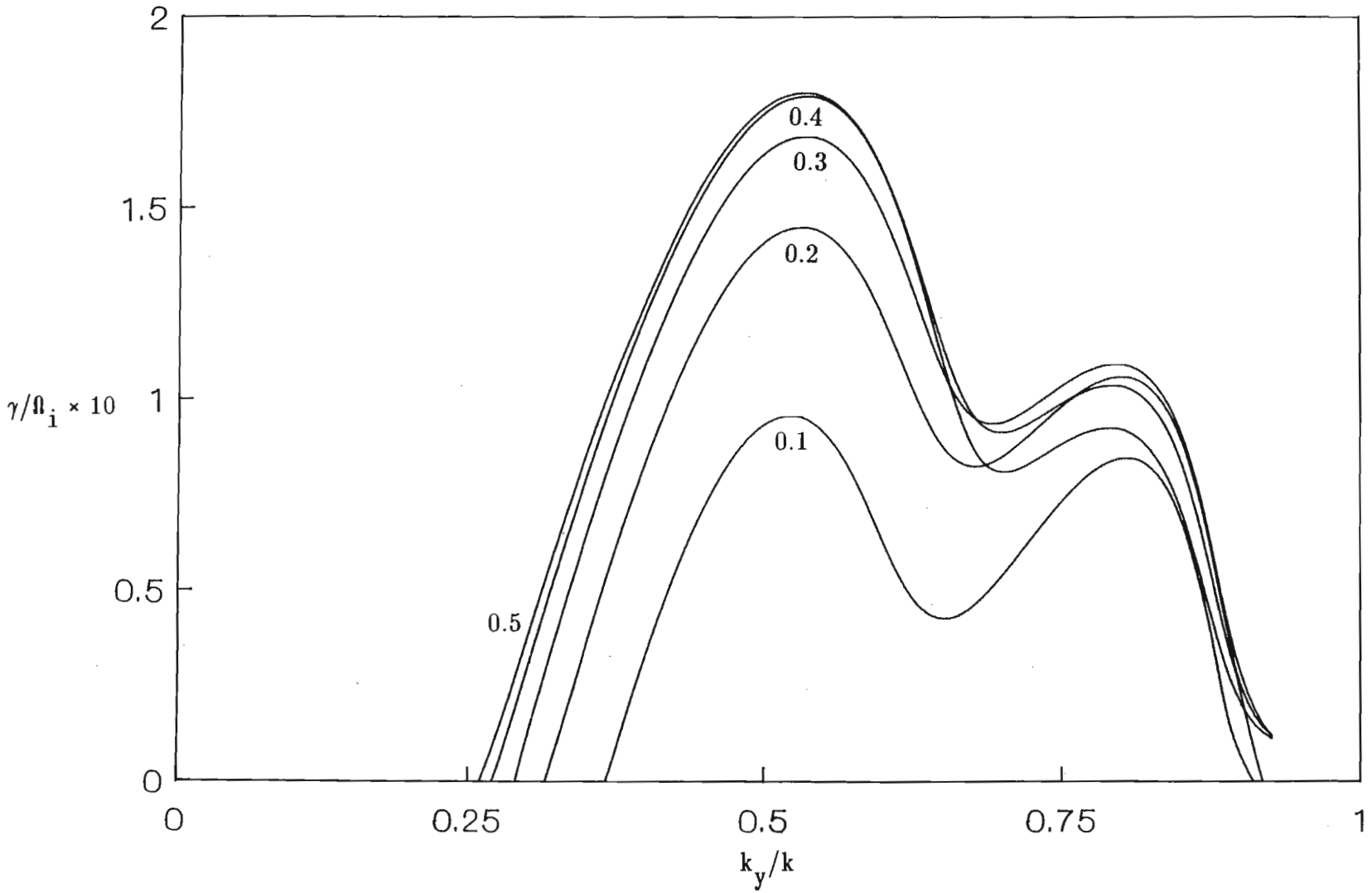

FIG 4.2.10 Normalized growth rate as a function of k_y/k for the anisotropic case $T_\perp/T_\parallel = 4$. The parameter labelling the curves is the normalized beam density n_{bo}/n_{eo}. Here $V_{oy} = 2\ C_s$ while other fixed parameters have the same value as in fig 4.2.4

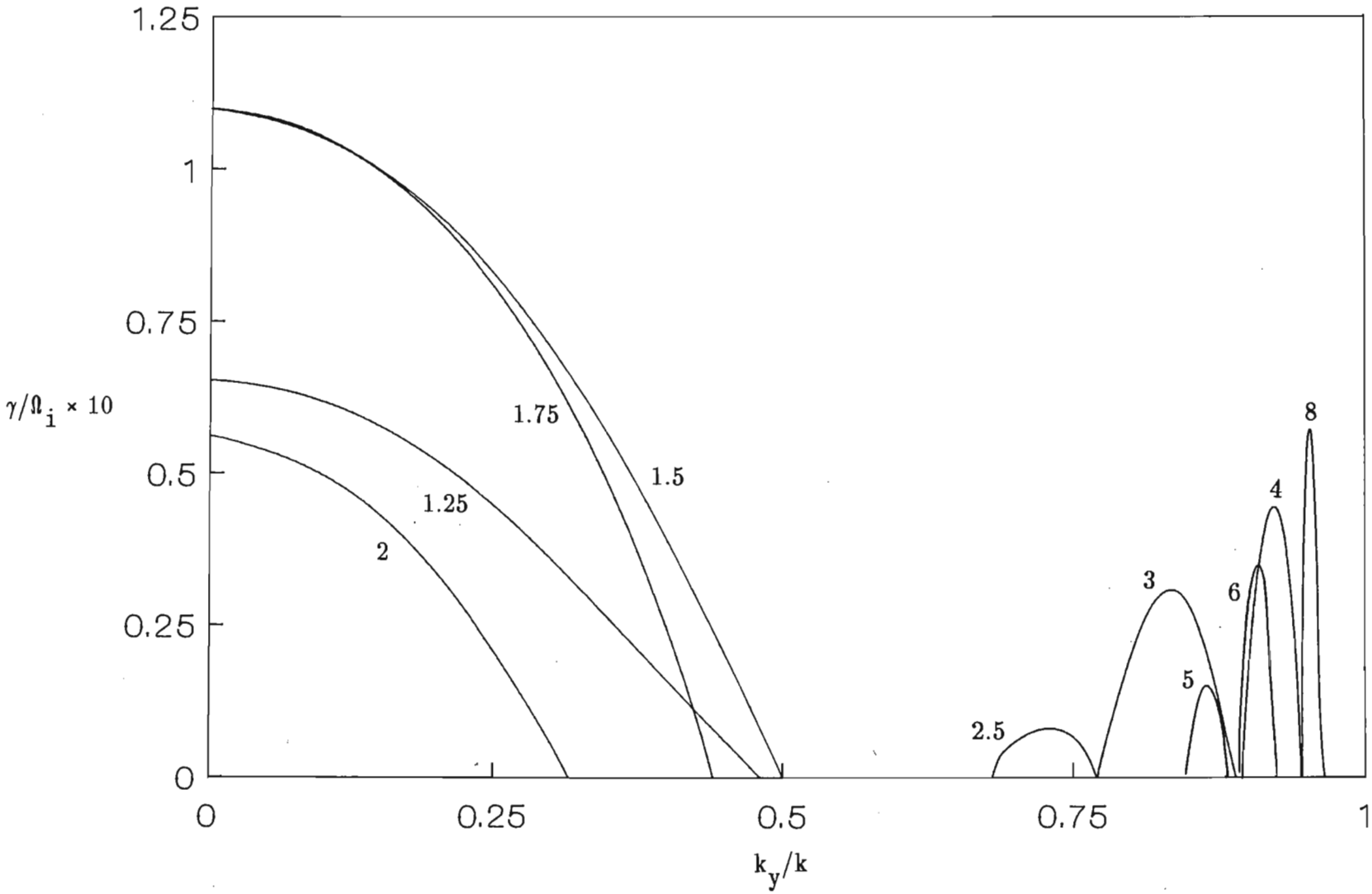

FIG 4.3.1 Normalized growth rate as a function of k_y/k for the isotropic case $T_\perp/T_\parallel = 1$. The parameter labelling the curves is the beam speed V_{oz}. Here $T_\perp = T_\parallel = T_i = 0.1\, T_e$, $k\rho_s = 1$, $\omega_{pe}/\Omega_e = 0.4$, $n_{bo} = 0.1\, n_{eo}$.

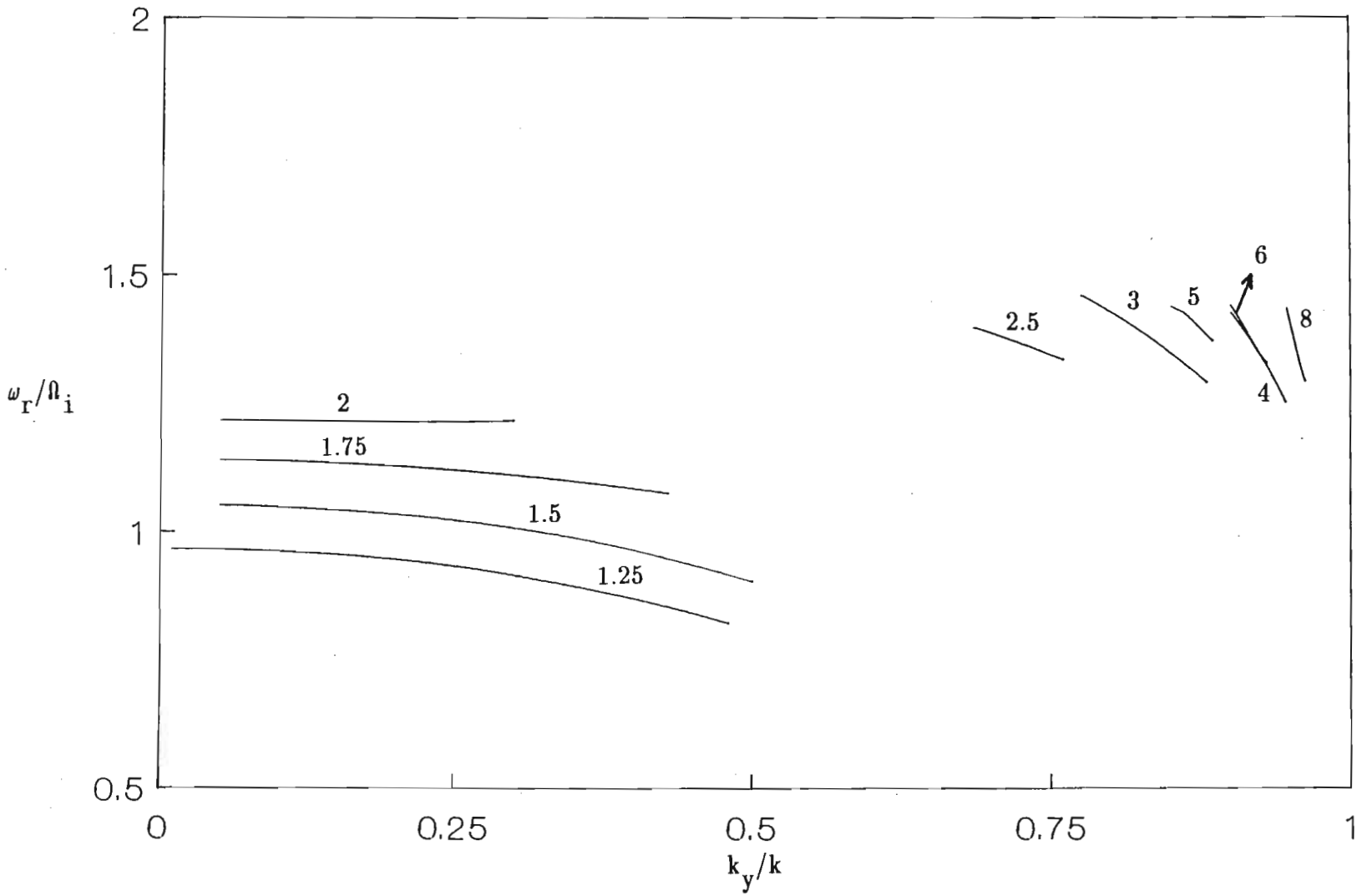

FIG 4.3.2 Normalized real frequency versus k_y/k for the parameters of fig 4.3.1 . The parameter labelling the curves is the beam speed V_{oz}.

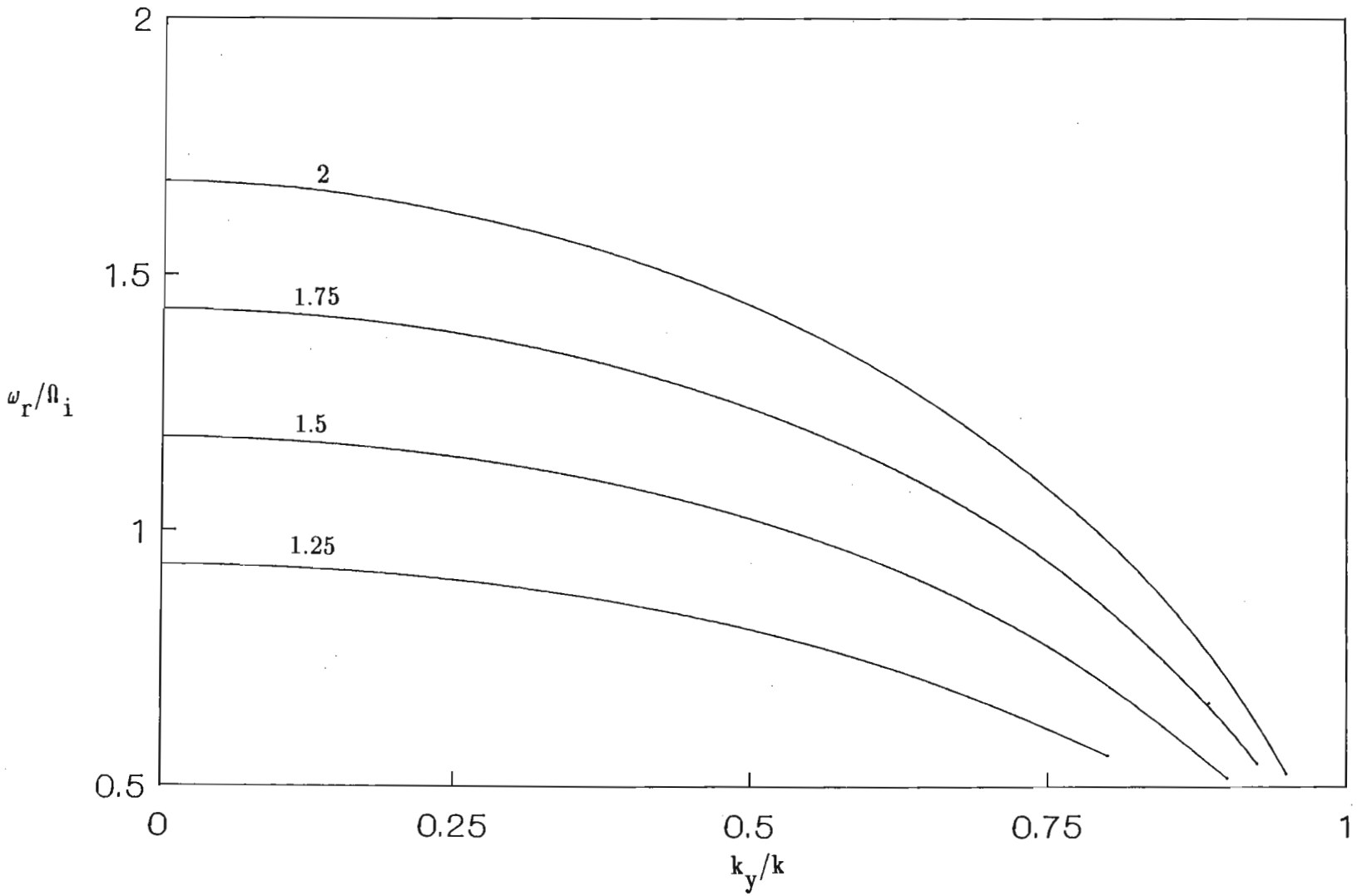

FIG 4.3.3 Normalized ion acoustic real frequency (eqn 4.2.1) versus k_y/k for the parameters of fig 4.3.1 . The parameter labelling the curves is the beam speed V_{oz}.

maximum at parallel propagation.

In table 4.3.1 we present the critical beam temperatures (isotropic case) for growth as a function of the beam velocities V_{oz} used in fig 4.3.1 . For values larger than those shown the wave was completely damped.

TABLE 4.3.1

V_{oz}	critical T_b
1.25	0.2
1.5	0.45
1.75	0.62
2.0	0.7
2.5	0.12
3.0	0.18
4.0	0.3
5.0	0.17
6.0	0.37
8.0	0.53

The ion–ion streaming instability can also have maximum growth for propagation parallel to $\vec{V}_0$ as found by other authors [5,6,7]. The growth curves for $V_{oz} = 1.5 - 2$ display such a behaviour. In addition, for these drift speeds γ_{max} decreases with V_{oz}. Such a behaviour has been observed for the ion–ion streaming instability by Akimoto and Omidi [6], Akimoto and Winske [5] and Gary and Omidi [7]. Furthermore the real frequency curves in fig 4.3.2 for $V_{oz} = 1.5 - 2.0$ do not satisfy the ion acoustic dispersion relation (4.2.1), as can be seen by comparing with the corresponding curves in fig 4.3.3 . Hence, we identify the instability corresponding to $V_{oz} = 1.5 - 2$ as the ion–ion streaming instability. Added evidence is provided by the critical $T_\perp = T_{||} = T_b$ values in table 4.3.1 . For V_{oz} in the range $1.5 - 2$, the mode damps at a relatively large beam temperature value (compared to the ion acoustic mode for $V_{oz} = 1.25$), thereby indicating its relative insensitivity to changes in ion velocity distribution functions, which is typical of two–stream instabilities.

The complete damping of the ion acoustic mode and a reduction in growth of the ion–ion streaming mode with increase in beam temperature was found by Akimoto and Omidi [6]. They also found that the critical beam temperature for complete damping is smaller for the ion acoustic mode than for the ion–ion streaming mode. Increasing the beam temperature increases ion Landau damping of the waves. This effect is discussed later.

For V_{oz} in the range $2.5 - 4$ we obtain an ion acoustic–like mode with phase velocity less than the ion acoustic phase velocity. Such modes were shown to exist by Fried and Gould [23] and were also found by Gary and Omidi [7]. The wave is completely damped at a critical beam temperature $T_b = 0.3$ ($V_{oz} = 4$) confirming the acoustic–like nature. The maximum growth increases with V_{oz} since the free energy available to drive the instability increases.

For velocities in the range $5 - 8$, ω_r at maximum growth satisfies

$$\omega_r \approx \vec{k}.\vec{V}_o - \Omega_i \qquad 4.3.1$$

with a definite shift in the associated k_y/k region of propagation as compared to $V_{oz} = 2.5 - 4$. We call this instability the beam cyclotron instability since it is driven by the cyclotron motion of the beam ions. A similar mode was observed by Goldman and Newman in their study of electromagnetic instabilities driven by an anisotropic electron beam [24].

The maximum growth of the ion–ion streaming instability at parallel to $\vec{V}_{oz}$ propagation is expected since the wave is then in total resonance with the beam. Gary and Omidi [7] in their fig 2 show that for $\theta = 0^\circ$ (wave propagation parallel to beam) the maximum growth decreases with velocity for $V_{oz} \geq 1.58$. However, it must be remembered that their situation corresponds to an unmagnetized plasma. The phase speed for the ion–ion

streaming mode is $V_\phi \approx 1$. When V_0 is close to V_ϕ the wave has maximum growth since more of the beam ions are in resonance with the instability. For larger beam speeds, say $V_{oz} = 2$, a smaller fraction of the beam ions have speed close to V_ϕ, hence a smaller fraction of the beam is in resonance with the wave, accounting for the decrease in growth.

We see from fig 4.3.1 that not only does γ_{max} increase with V_{oz} for the beam cyclotron mode, but propagation gets closer to the perpendicular (to $\vec{B}_0$). The latter point may be understood by rewriting equation 4.3.1 as

$$\omega_r + \Omega_i \approx k_z V_{oz} \qquad 4.3.2$$

For a mode of fixed phase speed or for ω_r fixed (since k = 1 is fixed) equation 4.3.2 implies that $k_z V_{oz}$ can be treated as a constant. Increasing V_{oz} should decrease k_z causing the mode to propagate more towards the perpendicular.

Figure 4.3.4 shows the normalized growth rate versus k_y/k for the anisotropic situation $T_\perp/T_\parallel = 4$ while fig 4.3.5 shows the corresponding real frequencies. Compared to the isotropic case the growth rates have increased noticeably.

The maximum growth rate for the ion acoustic mode ($V_{oz} = 1.25$) has increased by a factor of 2.6 . The growth is still maximum at parallel propagation but the angle of propagation has increased up to the perpendicular (to $\vec{B}_0$). The ion acoustic dispersion relation (4.2.1) can be rewritten as

$$\frac{\omega_r}{k_z} = V_{\phi z} = V_{oz} - \left[\frac{n_{bo}}{n_{eo}}\right]^{1/2} \frac{C_s}{(1+k^2\lambda_{de}^2+k_\perp^2\rho_s^2)^{1/2}},$$

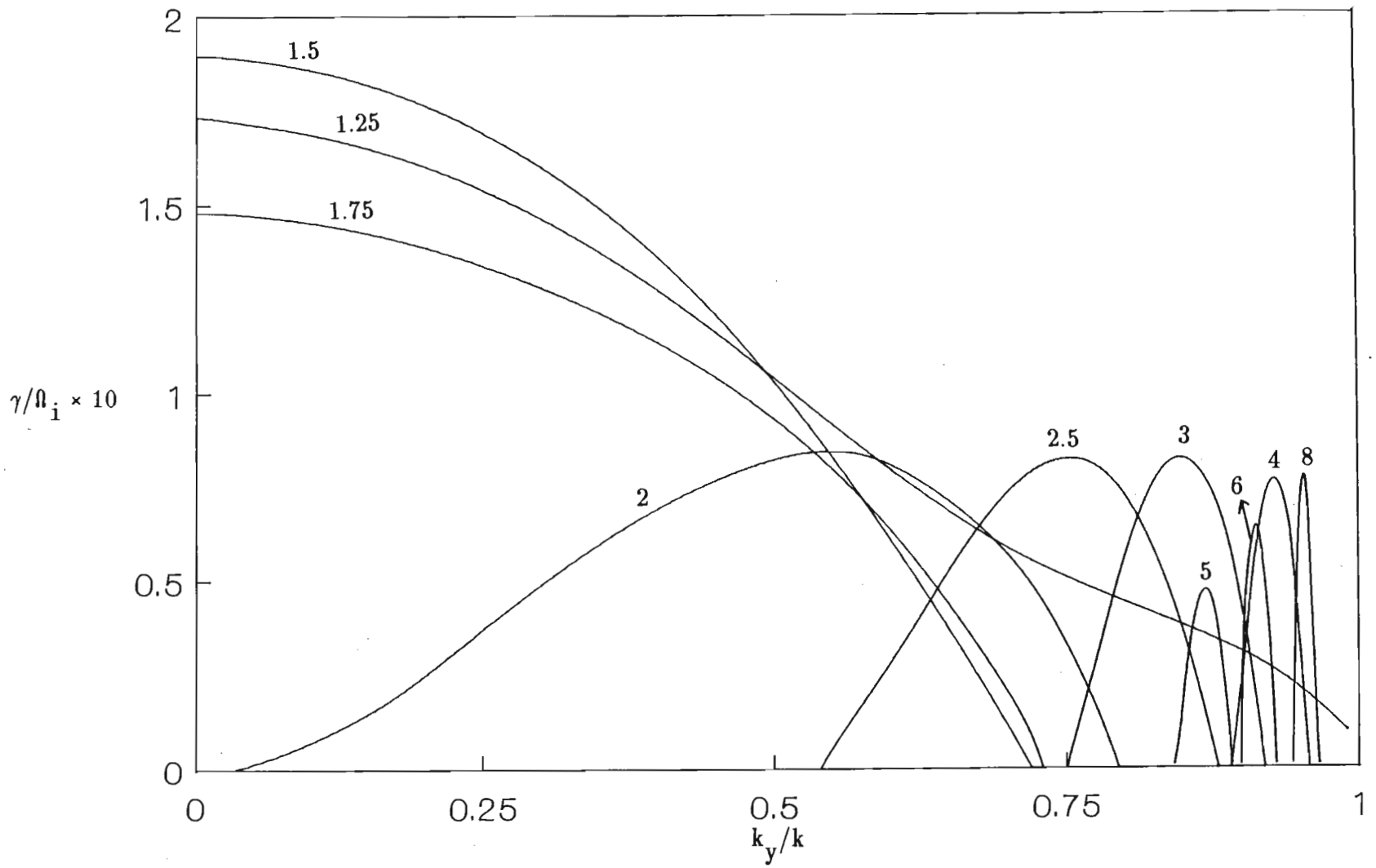

FIG 4.3.4 Normalized growth rate as a function of k_y/k for the anisotropic case $T_\perp/T_\parallel = 4$. The parameter labelling the curves is the beam speed V_{oz}. Here $T_\parallel = 0.025\ T_e$, $T_\perp = T_i = 0.1\ T_e$, while other fixed parameters have the same value as in fig 4.3.1 .

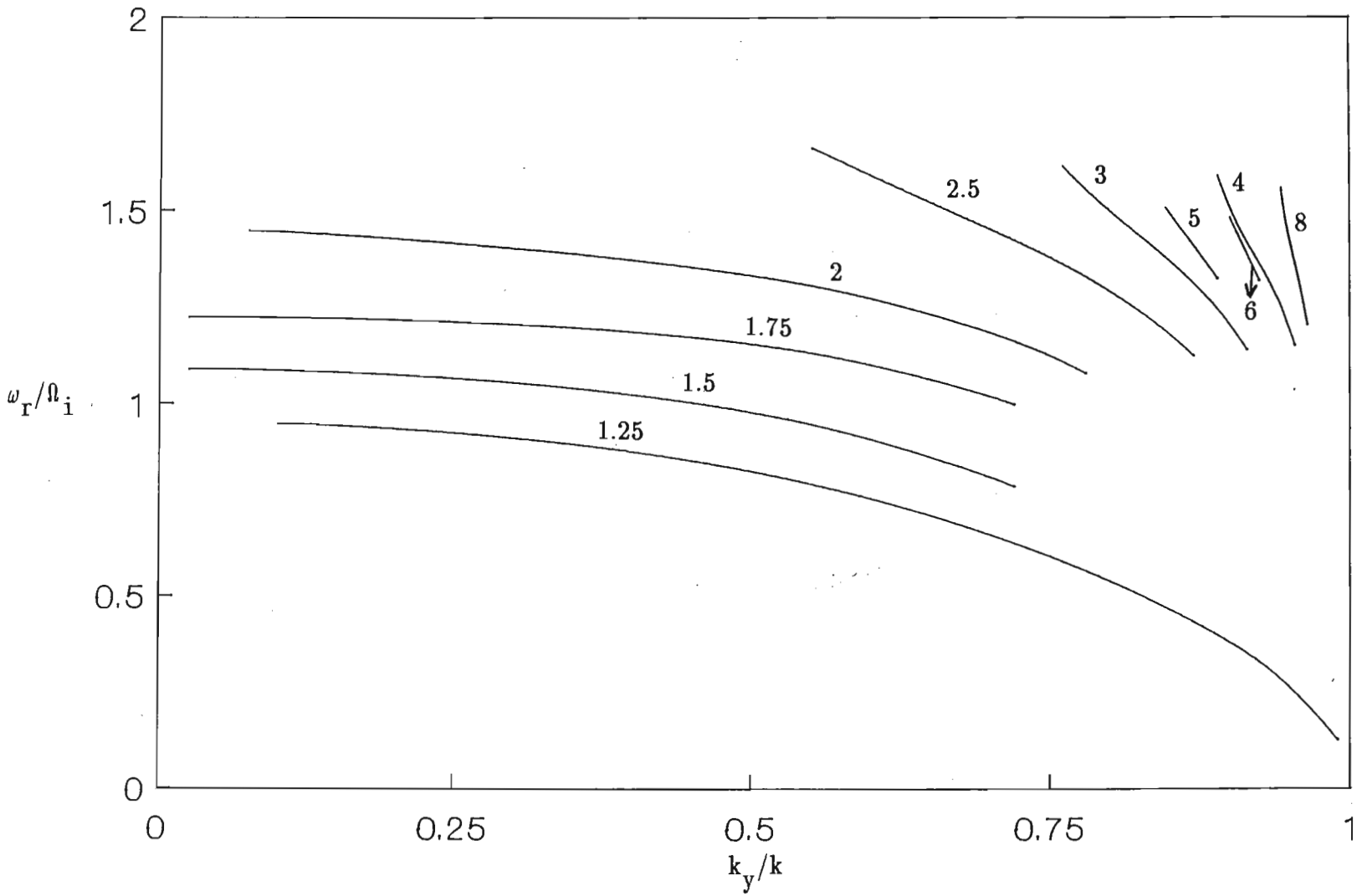

FIG 4.3.5 Normalized real frequency versus k_y/k for the parameters of fig 4.3.4 . The parameter labelling the curves is the beam speed V_{oz}.

so that $V_{\phi z} < V_{oz}$. This is a negative energy mode. We recall that the beam anisotropy $T_\perp/T_\parallel$ is increased by keeping $T_\perp$ fixed and decreasing $T_\parallel$. Reducing the parallel beam temperature ($T_\parallel$) narrows the beam distribution function $f_b(V_z)$ and increases the peak as depicted in fig 4.3.6 .

FIG 4.3.6

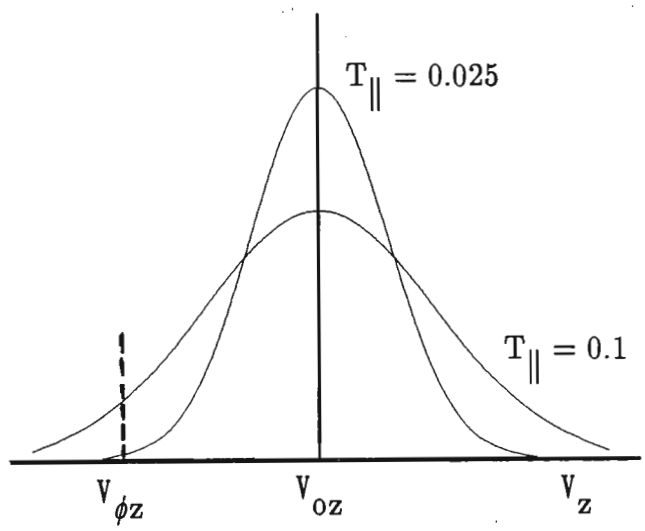

Thus the wave sees a larger positive slope $\frac{\partial f}{\partial V_z}$ at $V_{\phi z}$ for the curve $T_\parallel = 0.1$ than for $T_\parallel = 0.025$. Being a negative energy mode, this addition of more positive energy from resonant particles results in wave damping. This accounts for the increase in growth with anisotropy (decrease in $T_\parallel$). For the ion acoustic mode increasing $T_\perp$ while $T_\parallel$ is fixed is found to have little or no effect on the maximum growth. This is expected since this mode grows predominantly in the z – direction.

In the presence of the anisotropy, it is seen from fig 4.3.4 that the maximum growth for $V_{oz} = 2$ has shifted from $k_y/k = 0$ to $k_y/k \approx 0.55$. This shift appears to indicate a change in the nature of the instability. The total beam temperature $T_b = (2T_\perp + T_\parallel)/3$ was increased by increasing both $T_\perp$ and $T_\parallel$ while maintaining the anisotropy $T_\perp/T_\parallel = 4$. The

critical temperature for the $V_{oz} = 2$ mode was found to be $T_\perp = 0.31$, $T_{||} = 0.0775$, corresponding to $T_b = 0.23$. We note that this is much smaller than the isotropic case ($T_b = 0.7$) where the mode corresponded to an ion–ion streaming instability. For the sake of comparison we state the cut off temperatures for the $V_{oz} = 2.5$ mode. This is $T_{||} = 0.1$, $T_\perp = 0.4$, $T_b = 0.3$. This shift in propagation angle is also seen in fig 4.3.5 where the real frequency at maximum growth for $V_{oz} = 2$ shifts to the acoustic–like regime (close to $V_{oz} = 2.5, 3, 4$) as compared to fig 4.3.2 . Thus, the shift in γ_{max} from $k_y/k = 0$ to $k_y/k \approx 0.55$ coupled with a much lower cut off beam temperature (which is consistent with acoustic–like behaviour) allow us to conclude that for a drift speed $V_{oz} = 2$, the associated mode is ion–ion streaming in nature for an isotropic plasma ($T_\perp/T_{||} = 1$) and ion acoustic–like for an anisotropic plasma ($T_\perp/T_{||} = 4$). From fig 4.3.5, because of its extended tail for low k_y/k, we are led to believe that $V_{oz} = 2$ is a velocity representing the transition from the ion–ion streaming to the ion acoustic–like mode.

The peaks for $V_{oz} = 5,6,8$ still satisfy the beam cyclotron mode condition (4.3.1), however they are shifted towards the right. We shall account for the shift later.

In figure 4.3.7 we present a plot of the normalized growth rate versus k_y/k for $V_{oz} = 2$, for increasing anisotropy. The maximum growth rate is seen to saturate with anisotropy. This may be explained as follows. We recall that $T_\perp/T_{||}$ is increased by reducing $T_{||}$. Thus, beyond a $T_{||}$ value corresponding to $T_\perp/T_{||} \approx 16$, the associated effective ion Landau damping is negligibly small. Hence any further decrease in $T_{||}$ (with $T_\perp/T_{||}$ increasing) does not affect the instability growth rate.

The peaks are seen to shift towards the right with anisotropy. This is easy to understand since the effective temperature of the beam as seen by the wave is now

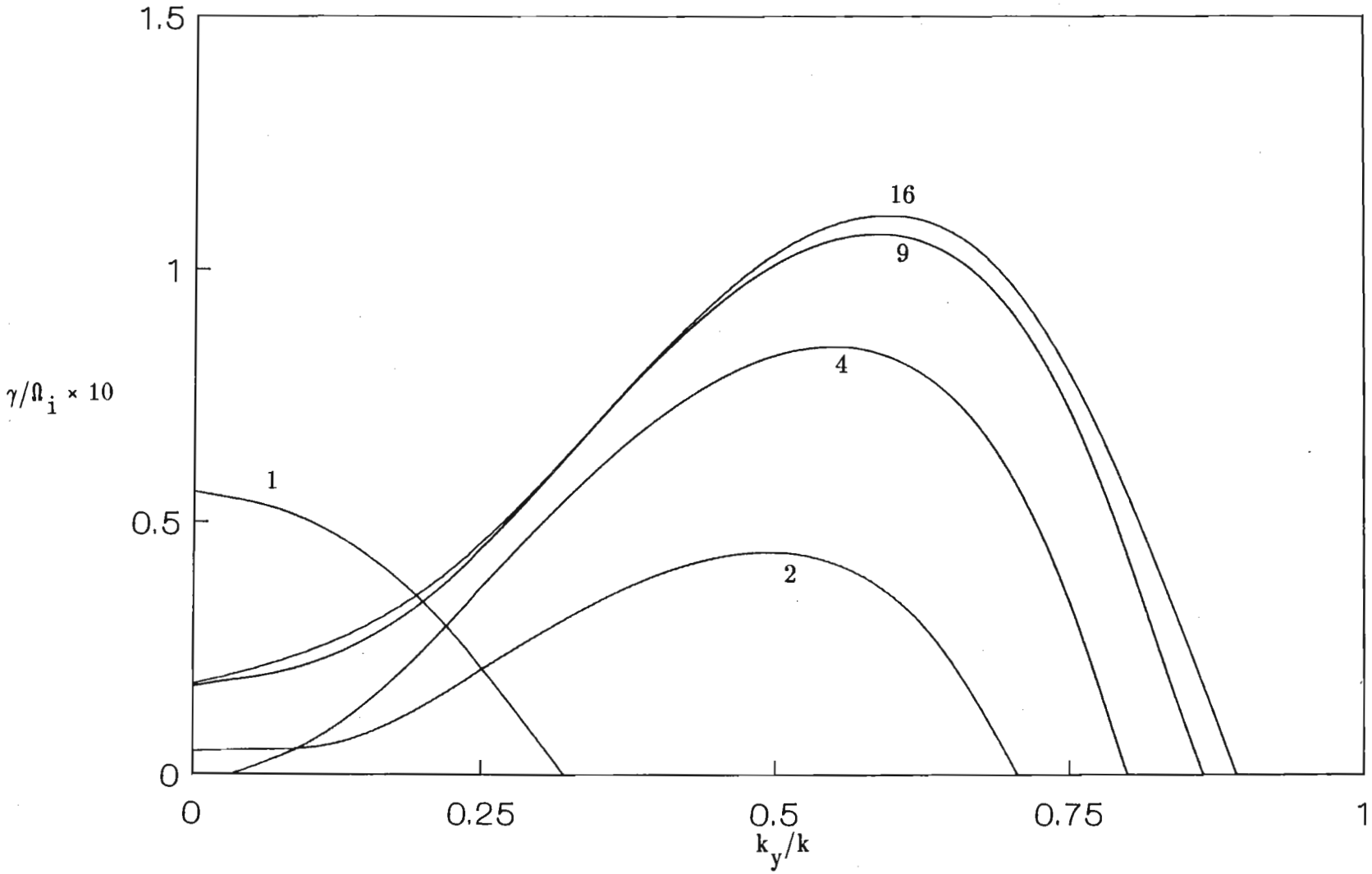

FIG 4.3.7 Normalized growth rate as a function of k_y/k for beam speed $V_{oz} = 2\ C_s$. The parameter labelling the curves is the beam anisotropy $T_\perp/T_\parallel$. Here $T_\perp = 0.1\ T_e$, while other fixed parameters have the same value as in fig 4.3.1 .

$$T_{eff} = T_{||} \cos^2\theta + T_{\perp} \sin^2\theta \,, \qquad 4.3.3$$

where as before θ is still the angle between the beam direction and the direction of wave propagation. The relation (4.3.3) has also been obtained by Akimoto and Winske [5]. For the plots in fig 4.3.7 we calculate T_{eff} at maximum growth and present the results in table 4.3.2 .

TABLE 4.3.2

$T_{\perp}/T_{||}$	k_y/k (at γ_{max})	T_{eff}
1	0	0.1
2	0.488	0.0619
4	0.545	0.0473
9	0.584	0.0414
16	0.589	0.0387

We recall that for $T_{\perp}/T_{||} > 1$, the mode corresponding to $V_{oz} = 2$ becomes acoustic–like in nature. Thus for the angles corresponding to maximum growth, the wave sees a lower effective beam temperature as $T_{\perp}/T_{||}$ increases. Consequently, as discussed after fig 4.3.6, the effective ion Landau damping decreases, leading to increased growth rate.

The effect of the beam density for the anisotropic case $T_{\perp}/T_{||} = 4$ with $V_{oz} = 2$ is illustrated in fig 4.3.8. For low beam densities ($0.05 < n_{bo} < 0.3$) the acoustic–like mode dominates the ion–ion streaming mode, while for larger beam densities the ion–ion streaming mode, with maximum growth for propagation parallel to $\vec{V}_{oz}$, is dominant. The fact that the acoustic–like mode dominates the ion–ion streaming mode at low beam densities ($n_{bo} = 0.05$) was also found by Akimoto and Omidi [6]. The increase in growth of the ion–ion streaming mode with density is due to the increase in beam energy. The transition from an acoustic–like mode ($n_{bo} = 0.05$) to an ion–ion streaming mode ($n_{bo} = 0.5$) is well illustrated.

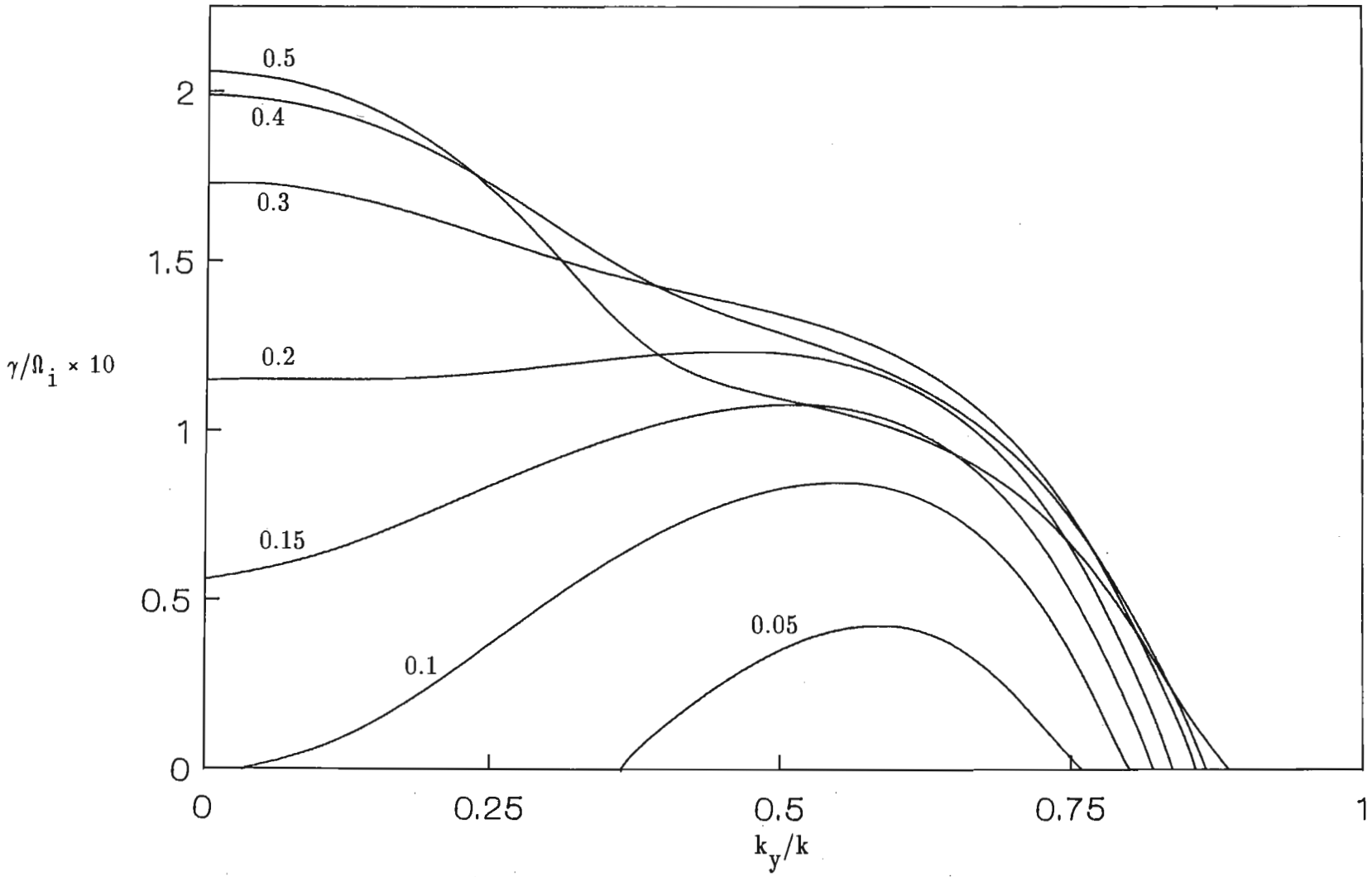

FIG 4.3.8 Normalized growth rate as a function of k_y/k for the anisotropic case $T_\perp/T_\parallel = 4$. The parameter labelling the curves is the normalized beam density n_{bo}/n_{eo}. Here $V_{oz} = 2\ C_s$ while other fixed parameters have the same value as in fig 4.3.4

In fig 4.3.9 we investigate the effect of the background ions by varying T_i/T_e for the anisotropic case $T_\perp/T_{||} = 4$ with beam speed $V_{oz} = 2$. At a value of $k_y/k \approx 0.64$ we have an increase of growth with decrease in background ion temperature. This is because Landau damping of the background ions is reduced. This is typical ion acoustic–like behaviour. For large T_i/T_e (0.25, 0.35) this acoustic–like mode is damped and shifts to parallel propagation indicating that conditions are ideal for the excitation of the ion–ion streaming instability which is less sensitive to ion Landau damping. Thus as T_i/T_e rises from 0.002 to 0.35, the nature of the instability changes from ion acoustic–like to ion–ion streaming type.

4.4 PERPENDICULAR DRIFT WITH k = 5

Here, for k = 5 we have $k\lambda_{de} = 0.292$ and $k\rho_i = 1.6$, which yields a typical wavelength for electrostatic ion cyclotron waves.

Figure 4.4.1 displays the normalized growth rate as a function of k_y/k for the isotropic case for different values of the beam velocity V_{oy}, while fig 4.4.2 is a plot of the corresponding real frequencies. Comparing fig 4.4.1 with fig 4.2.1 for the k = 1 case, we observe that the distinct separation between modes is no longer present. From fig 4.4.2 we note that ω_r increases with $\vec{k}.\vec{V}_0$. Hence the beam contributes to the dispersion of the mode. However, none of the modes satisfy the ion acoustic dispersion relation 4.2.1 .

For $V_{oy} = 1.25, 1.5$ we associate the instability with the ion–ion streaming mode which has maximum growth for propagation parallel to the beam, typically observed by Akimoto and Omidi [6], Akimoto and Winske [5] and Gary and Omidi [7]. Maximum growth increases with velocity until $V_{oy} = 1.6$. For speeds above this value, although the instability is two–stream like, it develops a few special characteristics. It is seen that at γ_{max}, $\vec{k}.\vec{V}_0$ is a

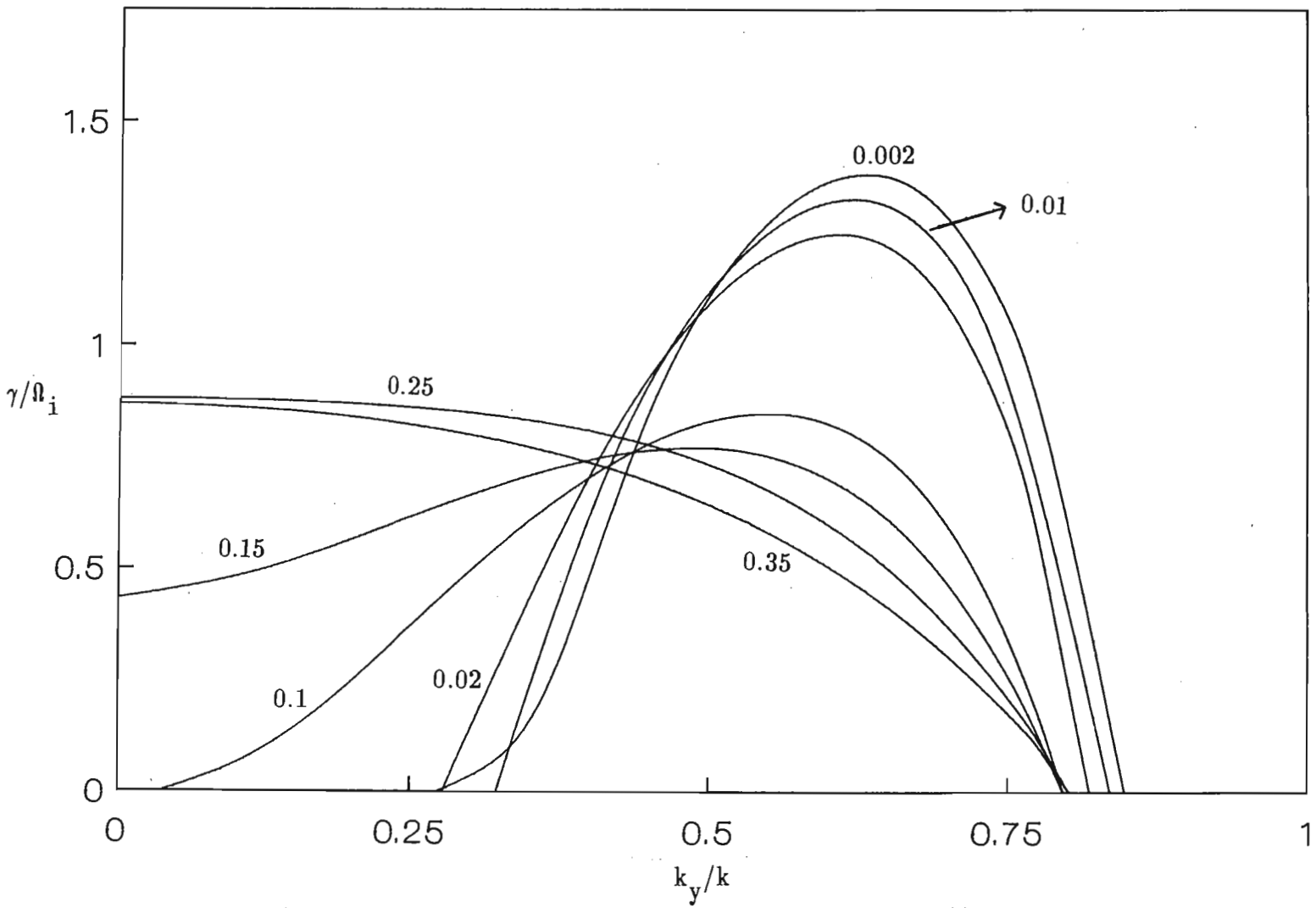

FIG 4.3.9 Normalized growth rate as a function of k_y/k for the anisotropic case $T_\perp/T_\parallel = 4$. The parameter labelling the curves is the background ion/electron temperature ratio T_i/T_e. Here $V_{oz} = 2\ C_s$ while other fixed parameters have the same value as in fig 4.3.4 .

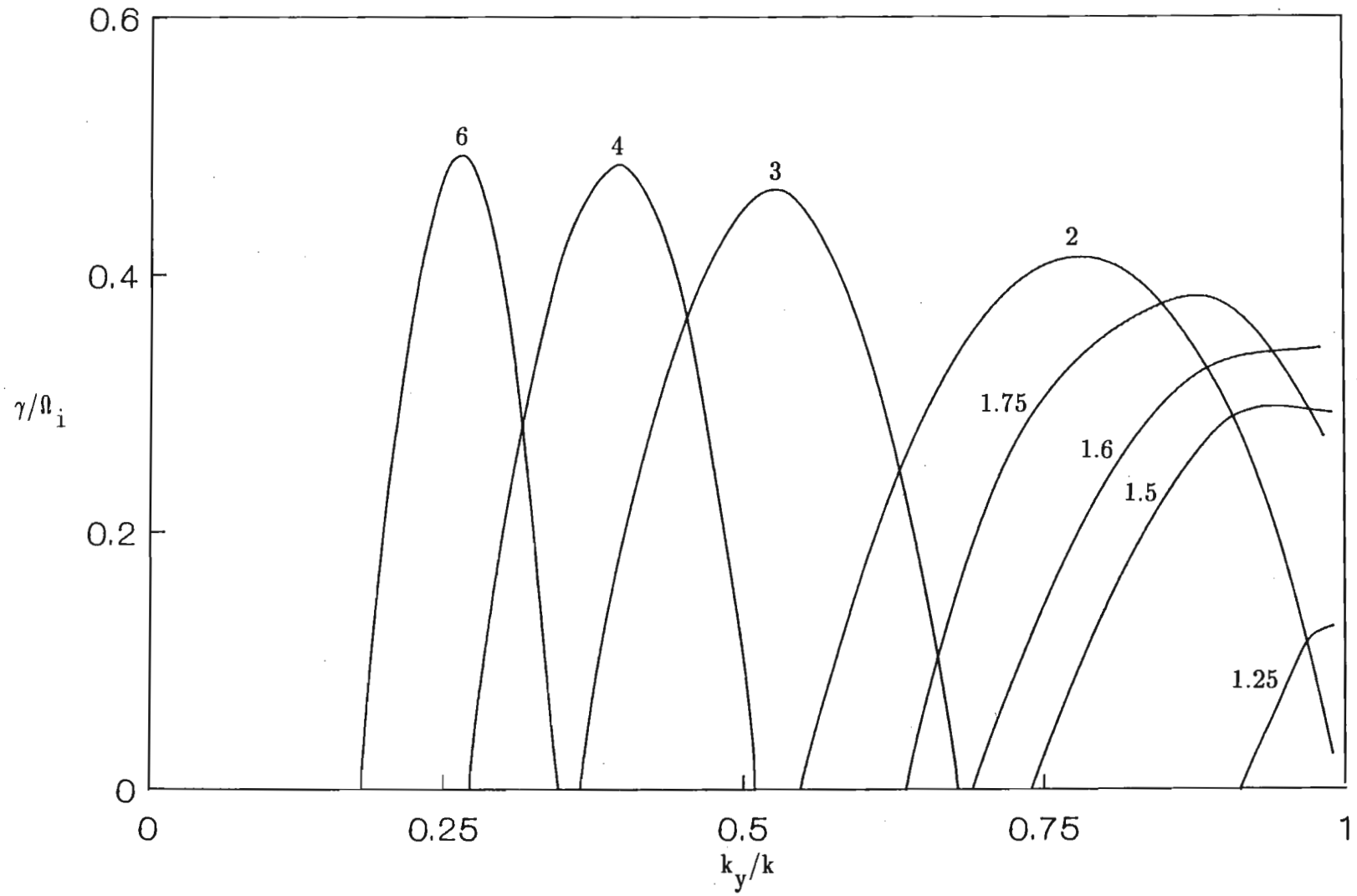

FIG 4.4.1 Normalized growth rate as a function of k_y/k for the isotropic case $T_\perp/T_\parallel = 1$. The parameter labelling the curves is the beam speed V_{oy}. Here $T_\perp = T_\parallel = T_i = 0.1\, T_e$, $k\rho_s = 5$, $\omega_{pe}/\Omega_e = 0.4$, $n_{bo} = 0.1\, n_{eo}$.

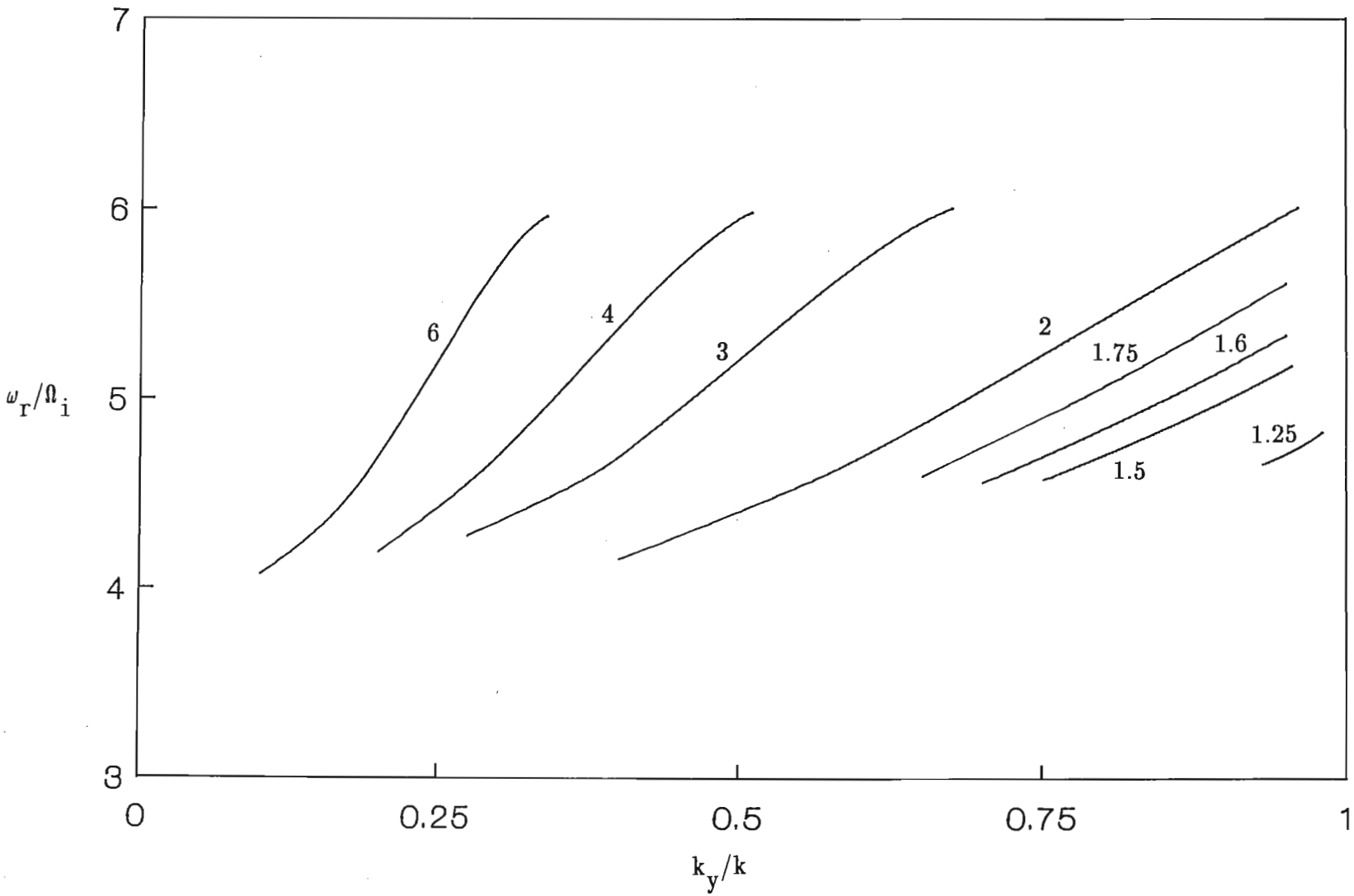

FIG 4.4.2 Normalized real frequency versus k_y/k for the parameters of fig 4.4.1 . The parameter labelling the curves is the beam speed V_{oy}.

constant for each drift speed, with $k_y V_{oy} \approx 7.9$. In addition, ω_r is constant at γ_{max}, with $\omega_r \approx 5.4$. Such a behaviour is typical of the modified two–stream instability (MTS instability)

In their theoretical study with counter–streaming ion beams ($\perp \vec{B}_0$) of equal density in a plasma with magnetized electrons and unmagnetized ions, Papadopoulos et al. [9] observed a zero–frequency MTS instability with $\mathbb{k}.\vec{V}_0 = \sqrt{3/8}\ \omega_{lh}$ and $\gamma = \omega_{lh}/2\sqrt{2}$ constant at maximum growth. Here ω_{lh} is the lower hybrid frequency defined as $\omega_{lh} = \omega_{pi}/[1+(\omega_{pe}/\Omega_e)^2]^{1/2}$, where ω_{pi} and ω_{pe} are the total ion and electron plasma frequencies respectively. The wave propagation vector $\mathbb{k}$ was perpendicular to $\vec{B}_0$. Allowing for oblique (to $\vec{B}_0$) propagation, McBride et al. [10] also obtained constant values $\omega_r = \sqrt{3/2}\ \omega_{lh}$ and $kV_0 = \sqrt{3}\ \omega_{lh}$ at maximum growth. They however considered the case of $k_z/k \approx (m_e/m_i)^{1/2}$ which allows for propagation very near to the perpendicular (to $\vec{B}_0$). Bharuthram and Johnstone [12] used the model of Papadopoulos et al. [9] but allowed for magnetization of the ions and anisotropy of the counter–streaming ion velocity distributions. At maximum growth they found that ω_r and $\mathbb{k}.\vec{V}_0$ were constant with $\omega_r = 0$ and $\mathbb{k}.\vec{V}_0 = 3\sqrt{2}/8\ \omega_{lh}$. Thus for beam speeds $V_{oy} \geq 1.6$ we label the instability as a MTS–type of instability, in contrast to that for $V_{oy} < 1.6$ which is typical of the ion–ion streaming instability in an unmagnetized plasma.

We note that for our case $\omega_{lh} \approx 15.1$. Since $3\sqrt{2}/8\ \omega_{lh} \approx 8.0$ we have good agreement with the result of Bharuthram and Johnstone [12]. This is expected since their model is the one that closely resembles ours. In addition, for our results ω_r at maximum growth satisfies

$$\omega_r \approx \mathbb{k}.\vec{V}_0 - \frac{\omega_{lhb}}{2}, \qquad 4.4.1$$

where $\omega_{lhb} = \omega_{pib}/[1+(\omega_{pe}/\Omega_e)^2]^{1/2}$. Here ω_{pib} is the plasma frequency of the beam ions.

Since $k_y V_{oy}$ is constant at maximum growth, increasing the velocity will result in k_{ymax} (k_y at γ_{max}) decreasing, causing propagation to shift closer to the direction of the magnetic field. This is clearly displayed in fig 4.4.1 . Since for low velocities propagation is much more oblique to the magnetic field $\vec{B}_0$, the effect of cyclotron damping is greater on these modes as compared to higher velocity modes, hence the lower γ_{max} for smaller beam speeds.

In figs 4.4.3 and 4.4.4 we consider the anisotropic case ($T_\perp/T_\parallel = 4$). The anisotropy once again increases the growth rate. The reason for this has been explained in sections 4.2 and 4.3 . We report that in their work Bharuthram and Johnstone [12] fixed $T_\parallel$ and increased $T_\perp$ inorder to obtain an anisotropy $T_\perp/T_\parallel > 1$. Hence their anisotropy corresponded to an increase of total beam temperature, resulting in a decrease in growth. We have done the opposite, namely kept $T_\perp$ fixed and decreased $T_\parallel$. Hence our anisotropy results in a decrease of total beam temperature, hence increase in growth. The shift of the peaks towards the left has been discussed in section 4.2 . For the MTS–type instability ($V_{oy} \geq 1.6$) $\vec{k}.\vec{V}_0$ is still constant at maximum growth but because of the shift of the peaks $\vec{k}.\vec{V}_0 \approx 7.1$ is lower than the isotropic case. The frequency $\omega_r \approx 5.15$ is also constant at maximum growth. For the ion–ion streaming mode corresponding to $V_{oy} = 1.5$, we note that the dip in the growth rate (fig 4.4.3) at $k_y/k \approx 0.92$ occurs at the fifth harmonic of the ion cyclotron frequency, $5\Omega_i$, indicating ion cyclotron damping.

In fig 4.4.5 we illustrate the effect of the anisotropy on a typical MTS–type of instability ($V_{oy} = 4$). The shift of the peaks towards the left and the increase in growth with anisotropy is consistent with our earlier findings, and has been discussed, for example, for

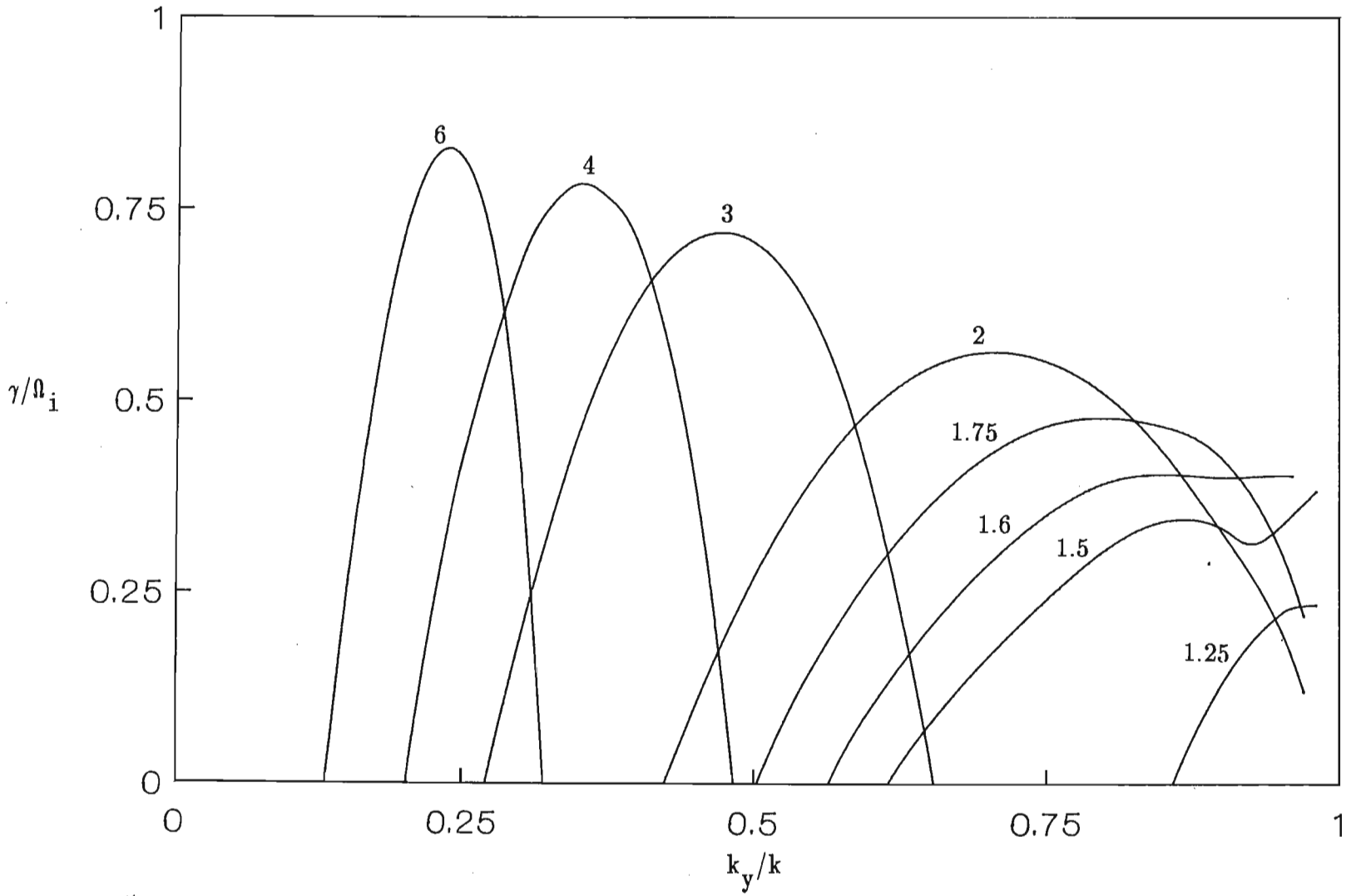

FIG 4.4.3 Normalized growth rate as a function of k_y/k for the anisotropic case $T_\perp/T_\parallel = 4$. The parameter labelling the curves is the beam speed V_{oy}. Here $T_\parallel = 0.025\ T_e$, $T_\perp = T_i = 0.1\ T_e$, while other fixed parameters have the same value as in fig 4.4.1 .

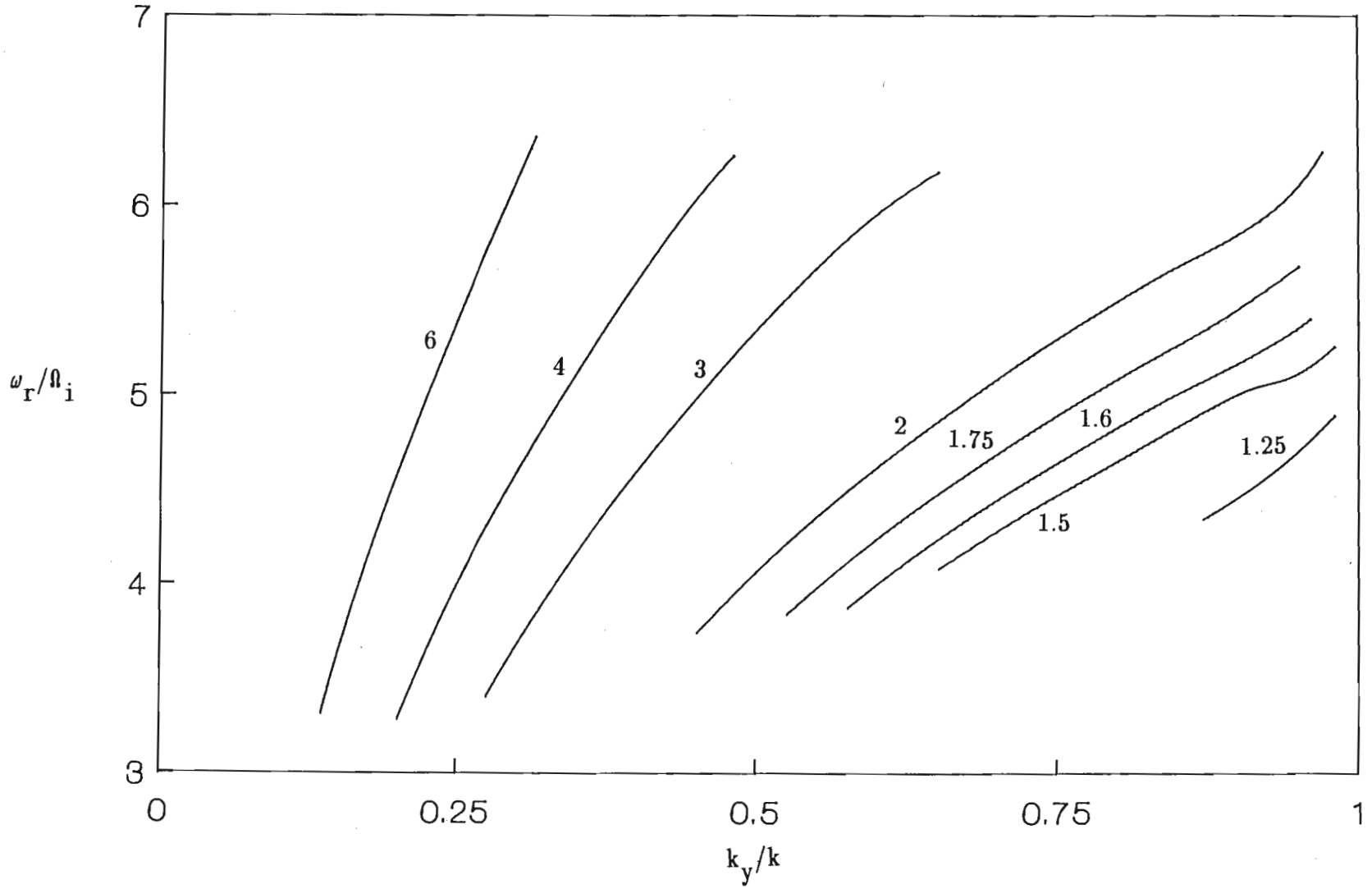

FIG 4.4.4 Normalized real frequency versus k_y/k for the parameters of fig 4.4.3 . The parameter labelling the curves is the beam speed V_{oy}.

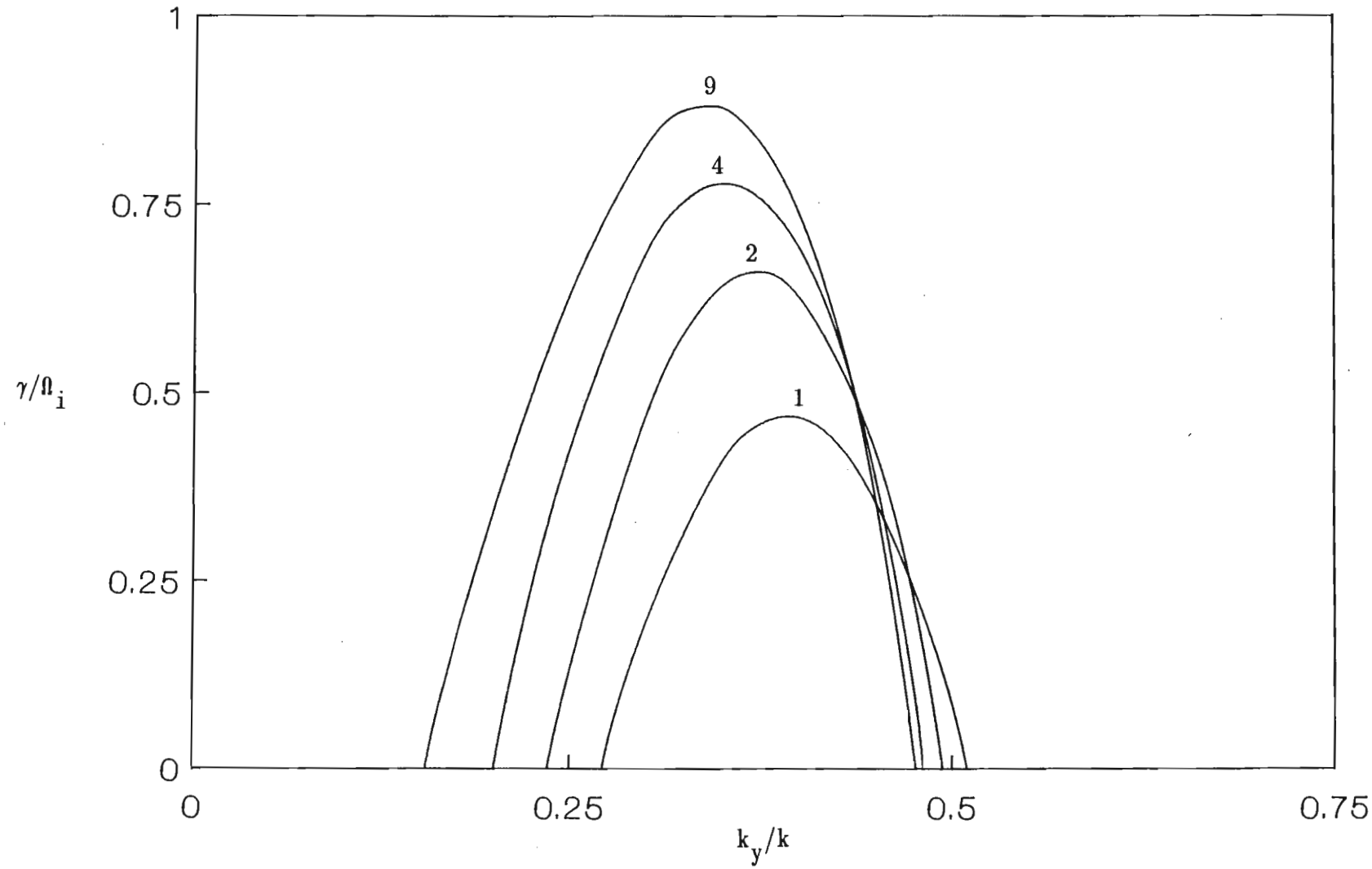

FIG 4.4.5 Normalized growth rate as a function of k_y/k for beam speed $V_{oy} = 4\ C_s$. The parameter labelling the curves is the beam anisotropy $T_\perp/T_\parallel$. Here $T_\perp = 0.1\ T_e$, while other fixed parameters have the same value as in fig 4.4.1 .

fig 4.2.6 . The effect of the beam density on the growth rates is investigated in figs 4.4.6 and 4.4.7, for both the isotropic and anisotropic cases. In both figures the growth rates increase with beam density. It is interesting to note that for $n_{bo} = 0.5$ we have 50% ion beam streaming through 50% background ions. The geometry is slightly different from that of Bharuthram and Johnstone [12] in that they had two counter–streaming ion beams of equal density (50%). Ignoring the relative electron drift, our case for $V_{oy} = 4$ correspond to theirs for $V_{oy} = 2$. Our maximum growth for the isotropic case (fig 4.4.6) for $n_{bo} = 0.5$ is approximately Ω_i. This agrees almost exactly with the maximum growth found by Bharuthram and Johnstone [12] for their $V_{oy} = 2$ case.

It is interesting to note from the results presented in this section that although we are in a Doppler shifted frame, both the ion–ion streaming and MTS–type of instabilities satisfy $\omega_r \approx kC_s$, as found by Gary and Omidi [7] and Fuselier et al. [8].

4.5 PARALLEL(to $\vec{B}_0$)DRIFT WITH k = 5

Figure 4.5.1 is a plot of the growth rate versus k_y/k for the isotropic case. The parameter labelling the curve is the beam speed V_{oz}. We firstly identify the modes.

For $V_{oz} = 1.25 - 1.5$ the maximum growth rate increases with velocity and occurs at parallel propagation. From fig 4.5.2 which shows the real frequencies we observe that the beam contributes to the dispersion of the mode. However, we find that these modes do not satisfy the ion acoustic dispersion relation (4.2.1). For $\theta = 0^\circ$ a plot of the growth rate versus velocity shows a peak at $V_{oz} = 1.6$. This is similar to the pattern obtained by Gary and Omidi [7] (fig 2), who found the peak to occur at $V_{oz} \approx 1.58$, for their unmagnetized plasma results. We note that ω_r and $\vec{k}.\vec{V}_0$ are not constant at maximum growth. Thus for $V_{oz} = 1.25 - 1.5$ we have the ion–ion streaming instability.

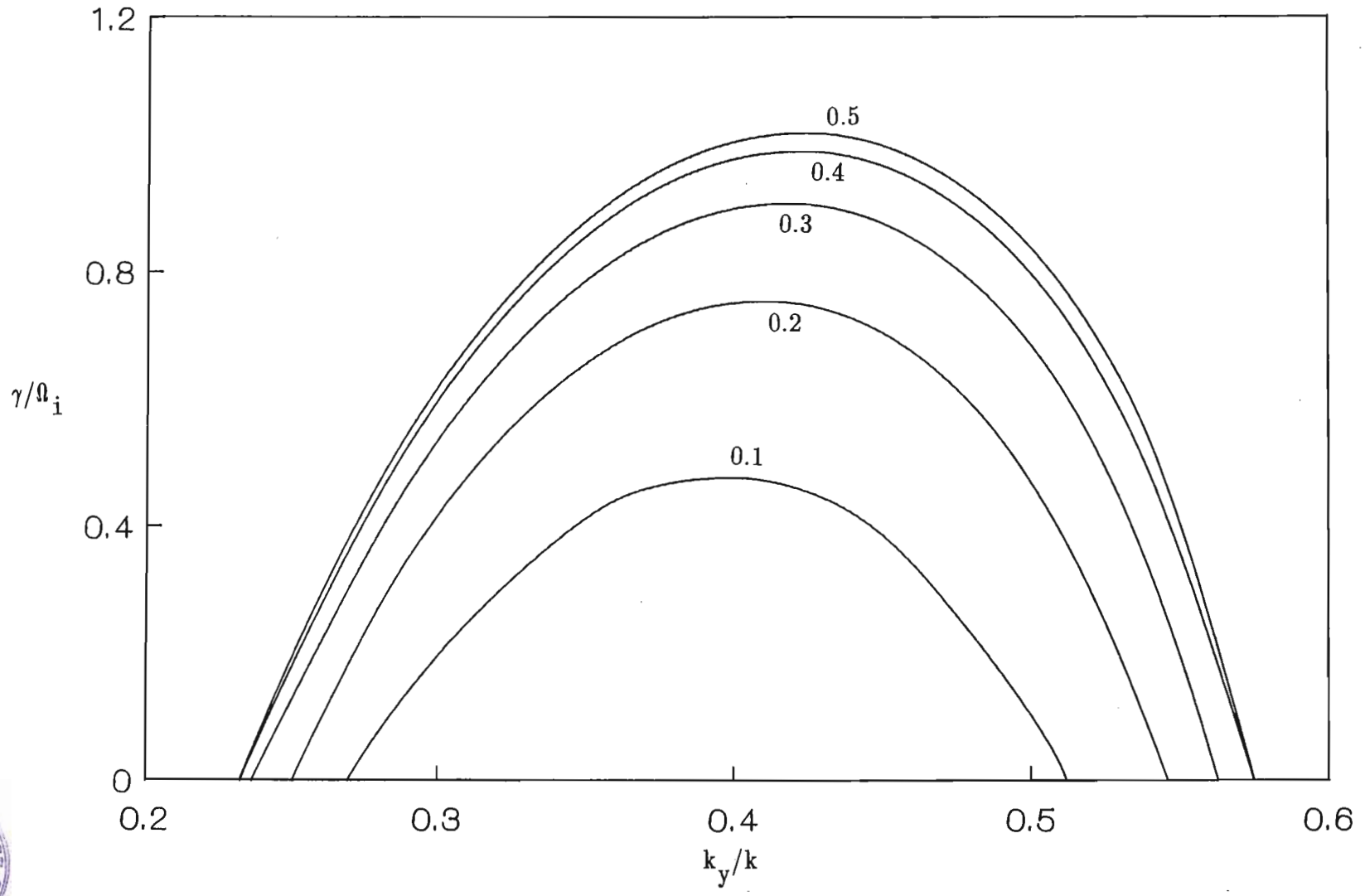

FIG 4.4.6 Normalized growth rate as a function of k_y/k for the isotropic case $T_\perp/T_\parallel = 1$. The parameter labelling the curves is the normalized beam density n_{bo}/n_{eo}. Here $V_{oy} = 4\ C_s$ while other fixed parameters have the same value as in fig 4.4.1 .

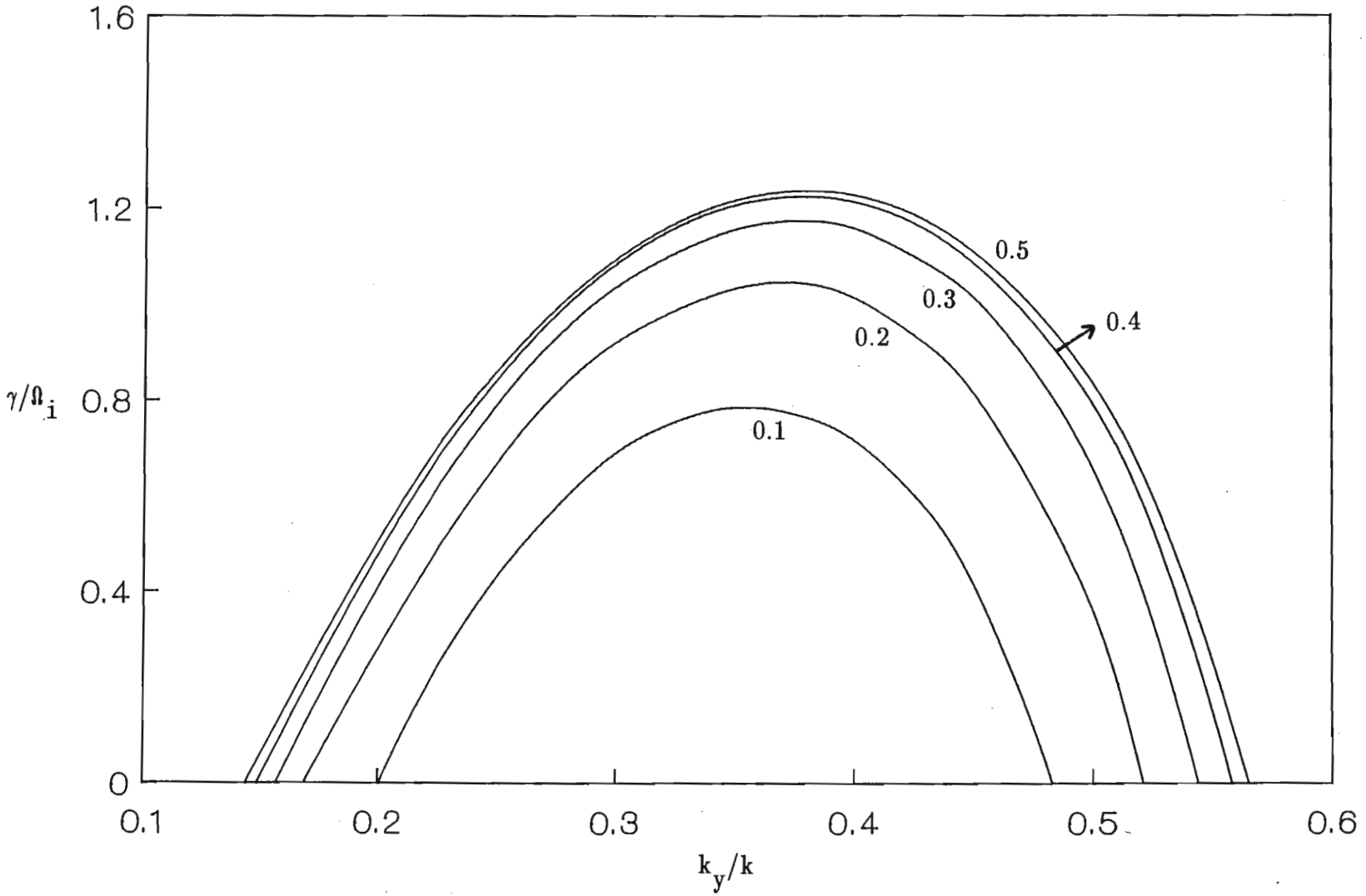

FIG 4.4.7 Normalized growth rate as a function of k_y/k for the anisotropic case $T_\perp/T_\parallel = 4$. The parameter labelling the curves is the normalized beam density n_{bo}/n_{eo}. Here $V_{oy} = 4\ C_s$ while other fixed parameters have the same value as in fig 4.4.3 .

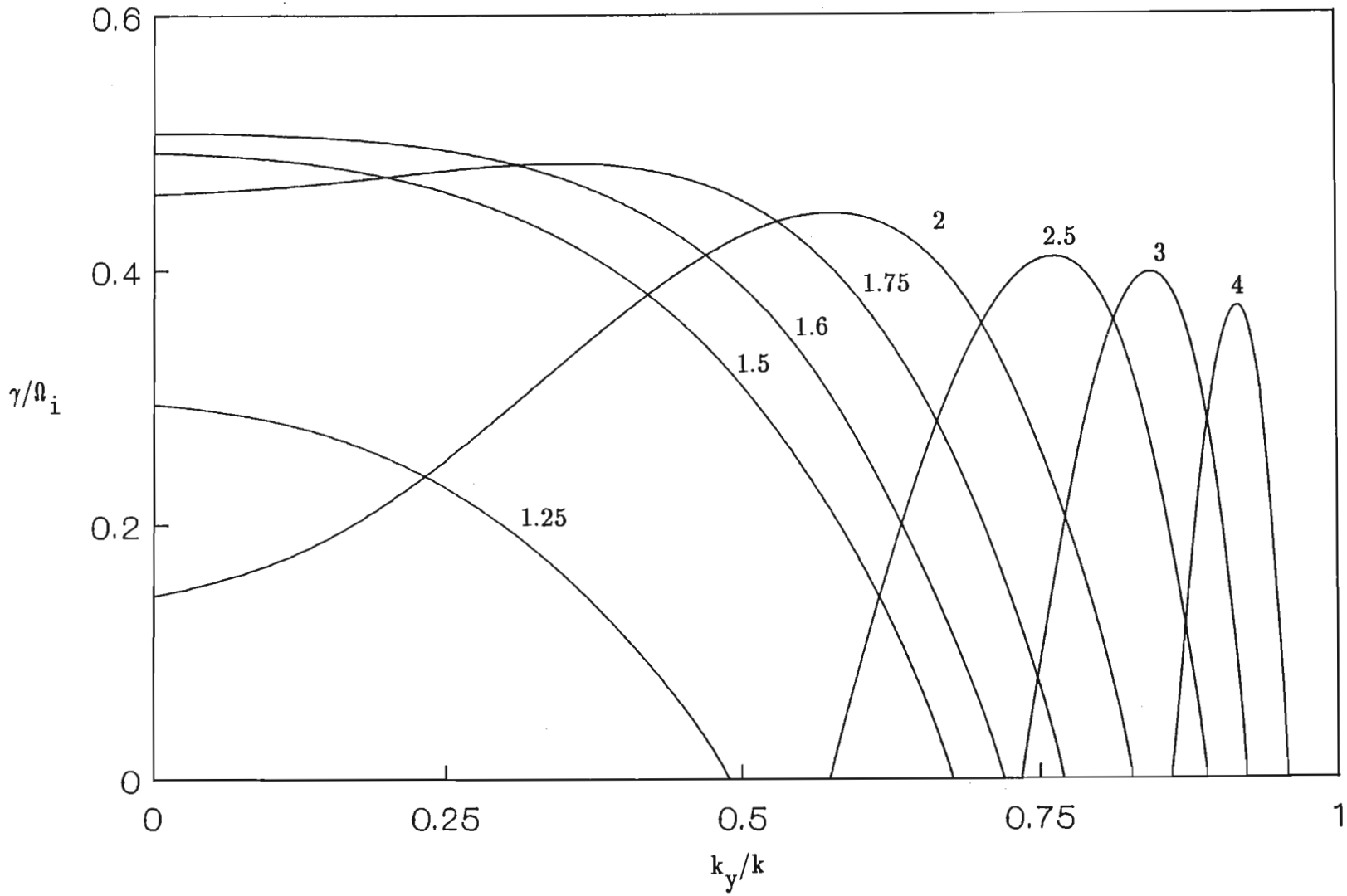

FIG 4.5.1 Normalized growth rate as a function of k_y/k for the isotropic case $T_\perp/T_\parallel = 1$. The parameter labelling the curves is the beam speed V_{oz}. Here $T_\perp = T_\parallel = T_i = 0.1\ T_e$, $k\rho_s = 5$, $\omega_{pe}/\Omega_e = 0.4$, $n_{bo} = 0.1\ n_{eo}$.

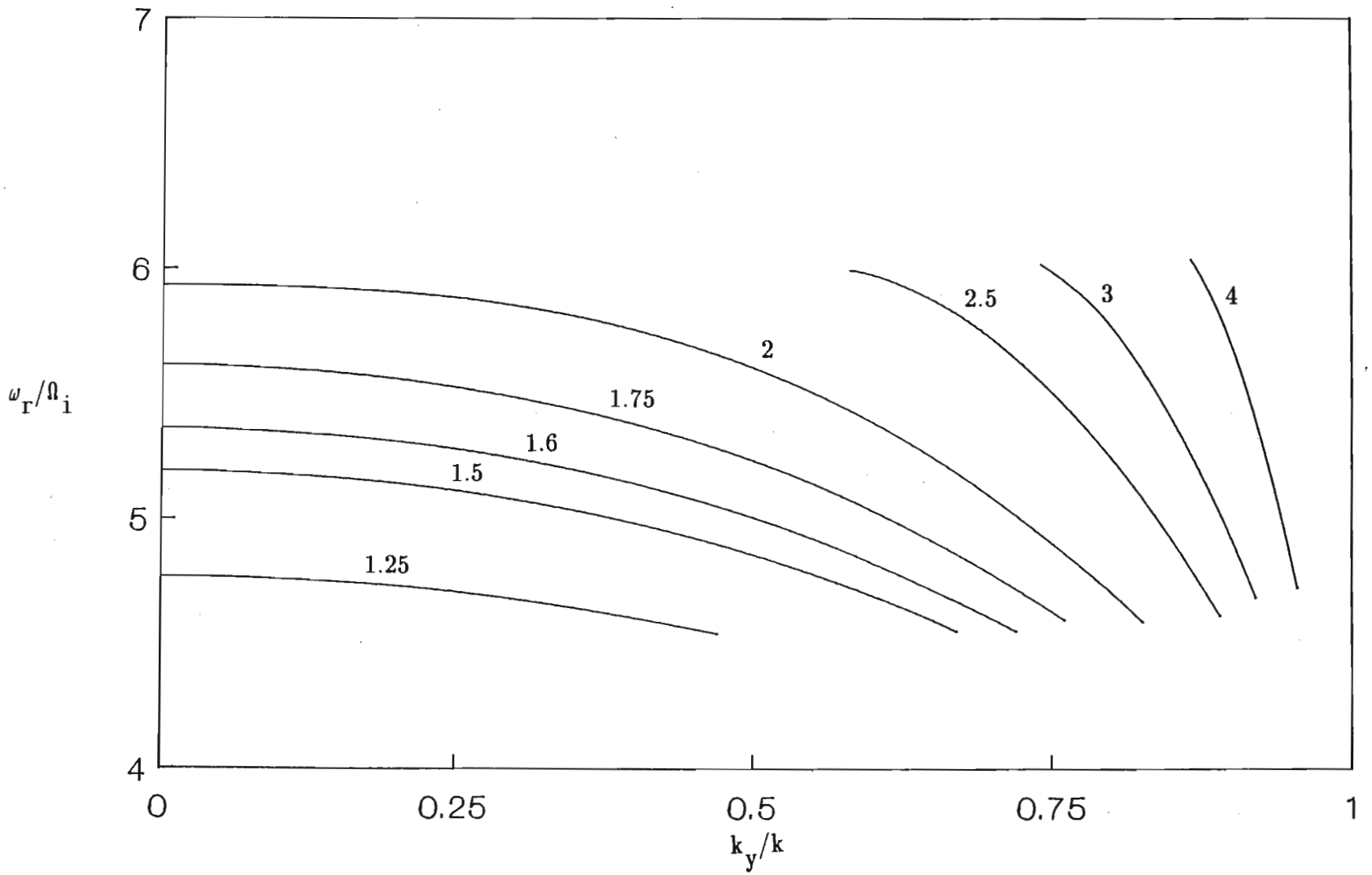

FIG 4.5.2 Normalized real frequency versus k_y/k for the parameters of fig 4.5.1 . The parameter labelling the curves is the beam speed V_{oz}.

For $V_{oz} = 1.6 - 4$, $\omega_r \approx 5.45$ is constant at maximum growth. In addition, at maximum growth, $k_z V_{oz} \approx 8$ is also constant, and ω_r also satisfies relation (4.4.1) as in the perpendicular drift case for k = 5. These velocities therefore excite the MTS–type of instability. Since $k_z V_{oz}$ is constant at maximum growth, larger velocities propagate more obliquely to $\vec{B}_0$. The difference with the perpendicular drift case is that now γ_{max} decreases with velocity. This is easily accounted for because of an increase in ion cyclotron damping with oblique propagation. In addition, the effect of electron magnetization increases with the obliqueness (to $\vec{B}_0$) of the propagation. In this regard, we point out that for an unmagnetized plasma, Gary and Omidi [7] found that γ_{max} was independent of the drift speed V_0. But, as ω_{pe}/Ω_e was lowered from 50 to 1, γ_{max} decreased with V_0. This drop – off was associated with the increase in the strength of electron magnetization (since the ions were unmagnetized). Thus our findings are consistent with the results of Gary and Omidi [7].

We note that for beam speeds in the range $1.6 < V_{oz} \leq 2$ we have an overlap of the two types of instabilities, as can be seen from fig 4.5.1, in particular for the "extended tail" of $V_{oz} = 2$. This then represents the transition regime from the ion–ion streaming instability (as found in an unmagnetized plasma) to the MTS–type of instability.

In fig 4.5.3 we investigate the anisotropic case ($T_\perp/T_{||} = 4$). Figure 4.5.4 shows the corresponding real frequencies. The effect of the anisotropy is to increase the growth rate, consistent with our earlier findings. For $V_{oz} = 1.6 - 4$ there is a slight shift of the peaks towards the right as compared to the isotropic case. This results in a slightly lower $k_z V_{oz}$ at maximum growth, namely $k_z V_{oz} \approx 7.95$ is constant and $\omega_r \approx 5.5$ is also constant at maximum growth.

By comparing with fig 4.5.1 we see that the anisotropy also lowers the threshold beam

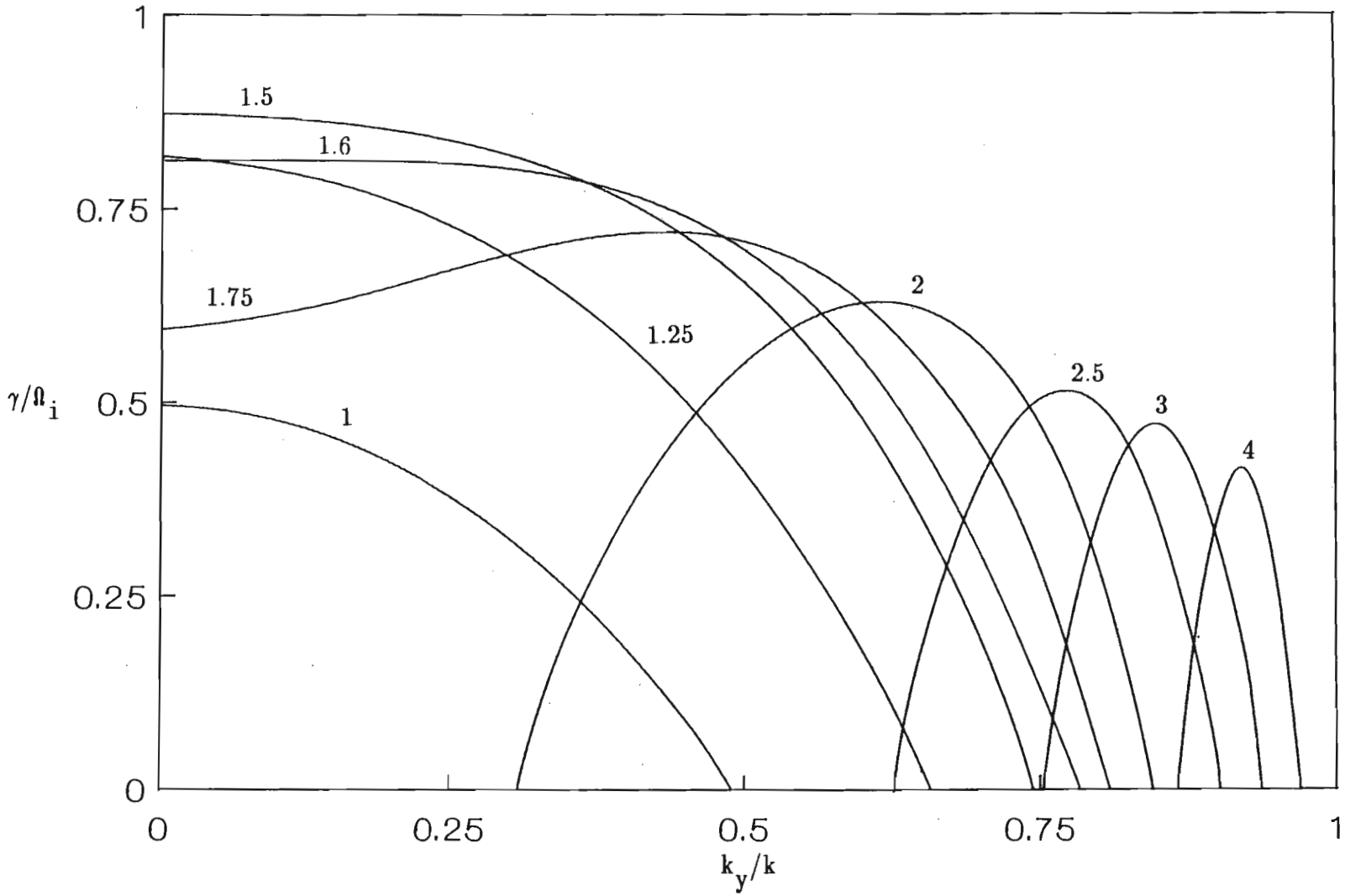

FIG 4.5.3 Normalized growth rate as a function of k_y/k for the anisotropic case $T_\perp/T_\parallel = 4$. The parameter labelling the curves is the beam speed V_{oz}. Here $T_\parallel = 0.025\ T_e$, $T_\perp = T_i = 0.1\ T_e$, while other fixed parameters have the same value as in fig 4.5.1 .

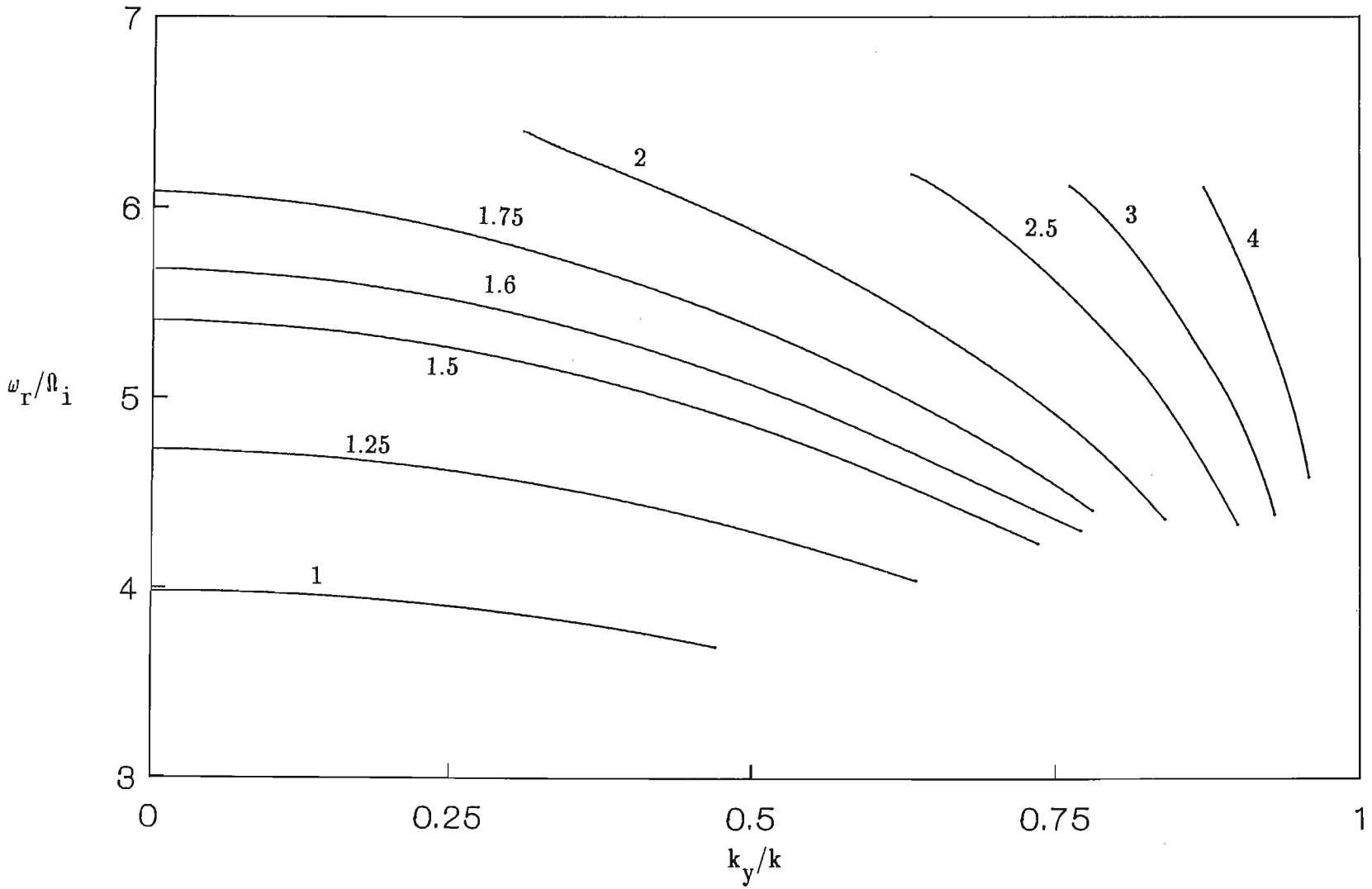

FIG 4.5.4 Normalized real frequency versus k_y/k for the parameters of fig 4.5.3 . The parameter labelling the curves is the beam speed V_{oz}.

velocity for the excitation for the ion–ion streaming instability. This is evident due to the appearance of the $V_{oz} = 1$ mode, which is not present for the isotropic case. The anisotropy also destroys the tail of the of the $V_{oz} = 2$ curve causing it to shift into the purely MTS–type instability regime. This shift is evident by comparing the real frequencies for the isotropic and anisotropic cases (figs 4.5.2 and 4.5.4).

The effect of further increasing the anisotropy is investigated in fig 4.5.5 for the $V_{oz} = 2$ mode. The effect of the anisotropy is to increase the maximum growth rate. For $k_y/k \leq 0.35$ increasing the anisotropy decreases the growth. This results in the anisotropy "killing" the parallel tail.

In figs 4.5.6 and 4.5.7 we show the effect of the beam density on the $V_{oz} = 2$ mode for the isotropic and anisotropic cases respectively. Increasing the beam density increases the growth rates. However, the growth is increased more in the z–direction since the relative streaming is in that direction. In fig 4.5.7 the increase in beam density and the associated energy available to excite an instability allows the ion–ion streaming instability to develop in the tail region of the MTS–type of instability for low k_y/k values.

4.6 EFFECT OF ION MAGNETIZATION

Figure 4.6.1 is a plot of the normalized growth rate versus ω_{pe}/Ω_e for a fixed angle $k_y/k = 0.4$ and velocity $V_{oy} = 4$ while fig 4.6.2 is a similar plot for $V_{oz} = 4$ and $k_y/k = 0.9$. Here we set $k = 5$. The parameter labelling the curves is the beam anisotropy $T_\perp/T_\parallel$.

For $\omega_{pe}/\Omega_e \geq 1$ the growth saturates with ω_{pe}/Ω_e. Increasing ω_{pe}/Ω_e while keeping all other plasma parameters fixed ($\vec{B}_0$ fixed) corresponds to increasing the total plasma density. We note that $\omega_{pe}/\Omega_e > 1$ corresponds to $\omega_{pi}/\Omega_i \gg 1$. Hence the ion cyclotron

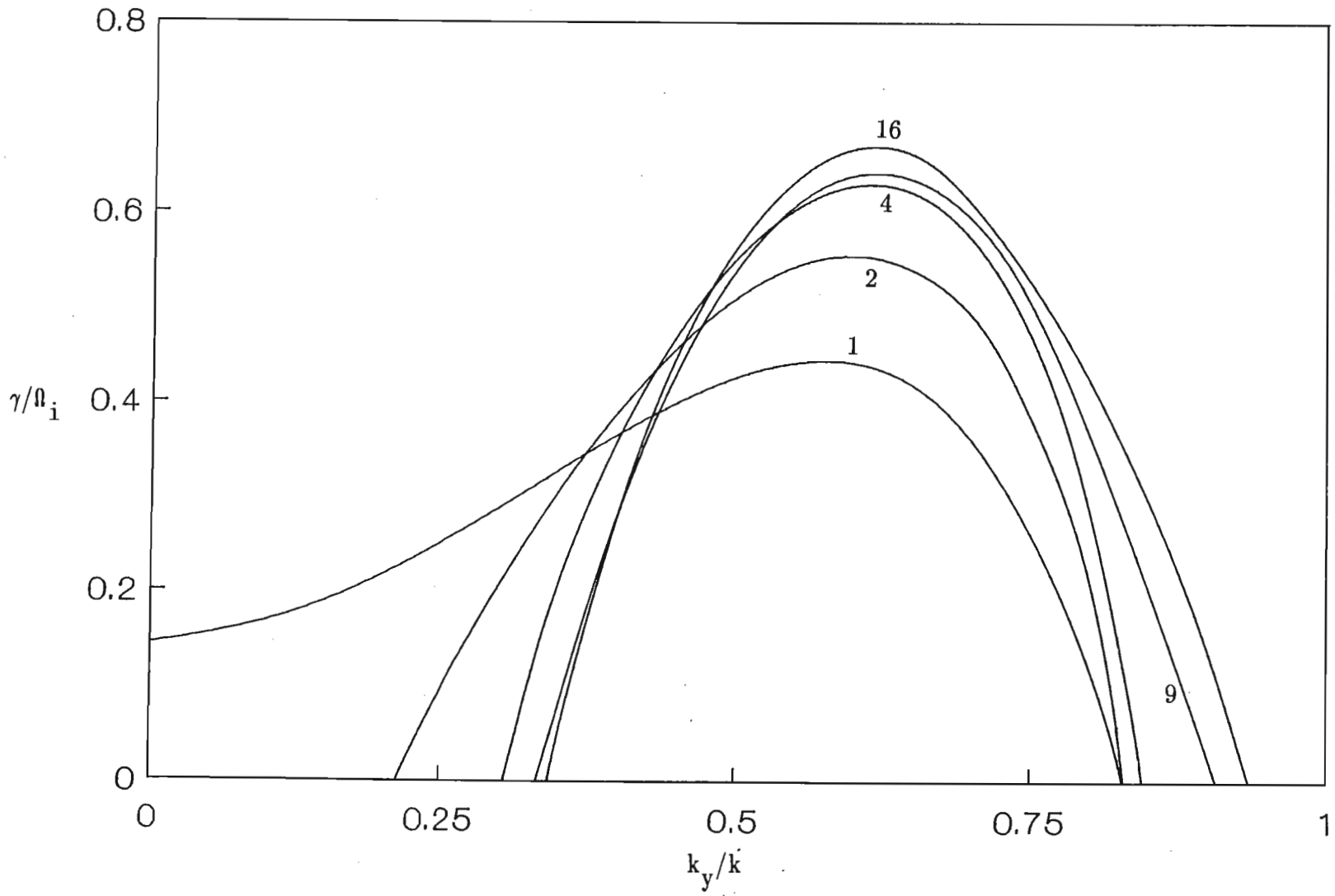

FIG 4.5.5 Normalized growth rate as a function of k_y/k for beam speed $V_{oz} = 2\ C_s$. The parameter labelling the curves is the beam anisotropy $T_\perp/T_\parallel$. Here $T_\perp = 0.1\ T_e$, while other fixed parameters have the same value as in fig 4.5.1 .

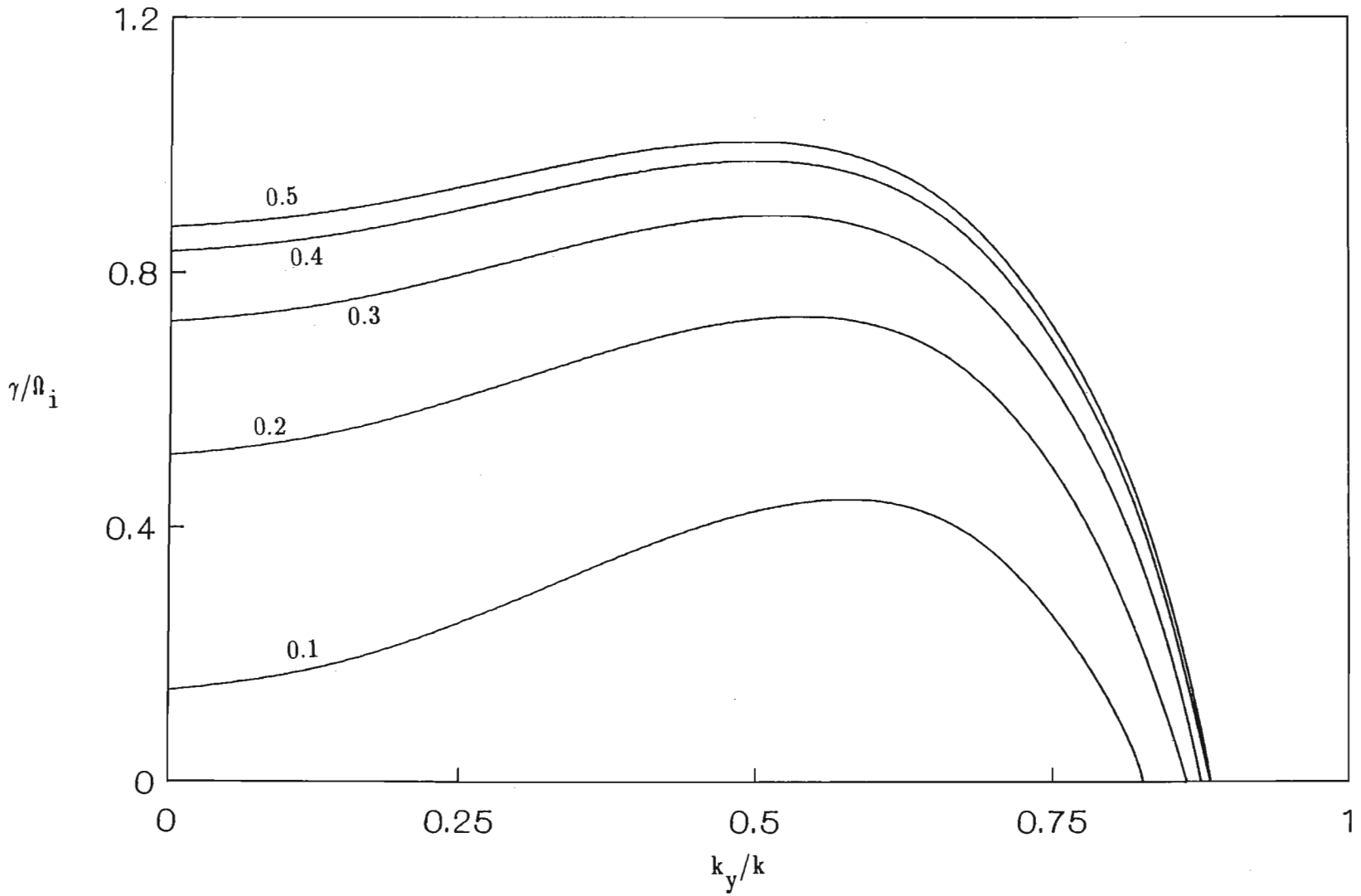

FIG 4.5.6 Normalized growth rate as a function of k_y/k for the isotropic case $T_\perp/T_\parallel = 1$. The parameter labelling the curves is the normalized beam density n_{bo}/n_{eo}. Here $V_{oz} = 2\ C_s$ while other fixed parameters have the same value as in fig 4.5.1 .

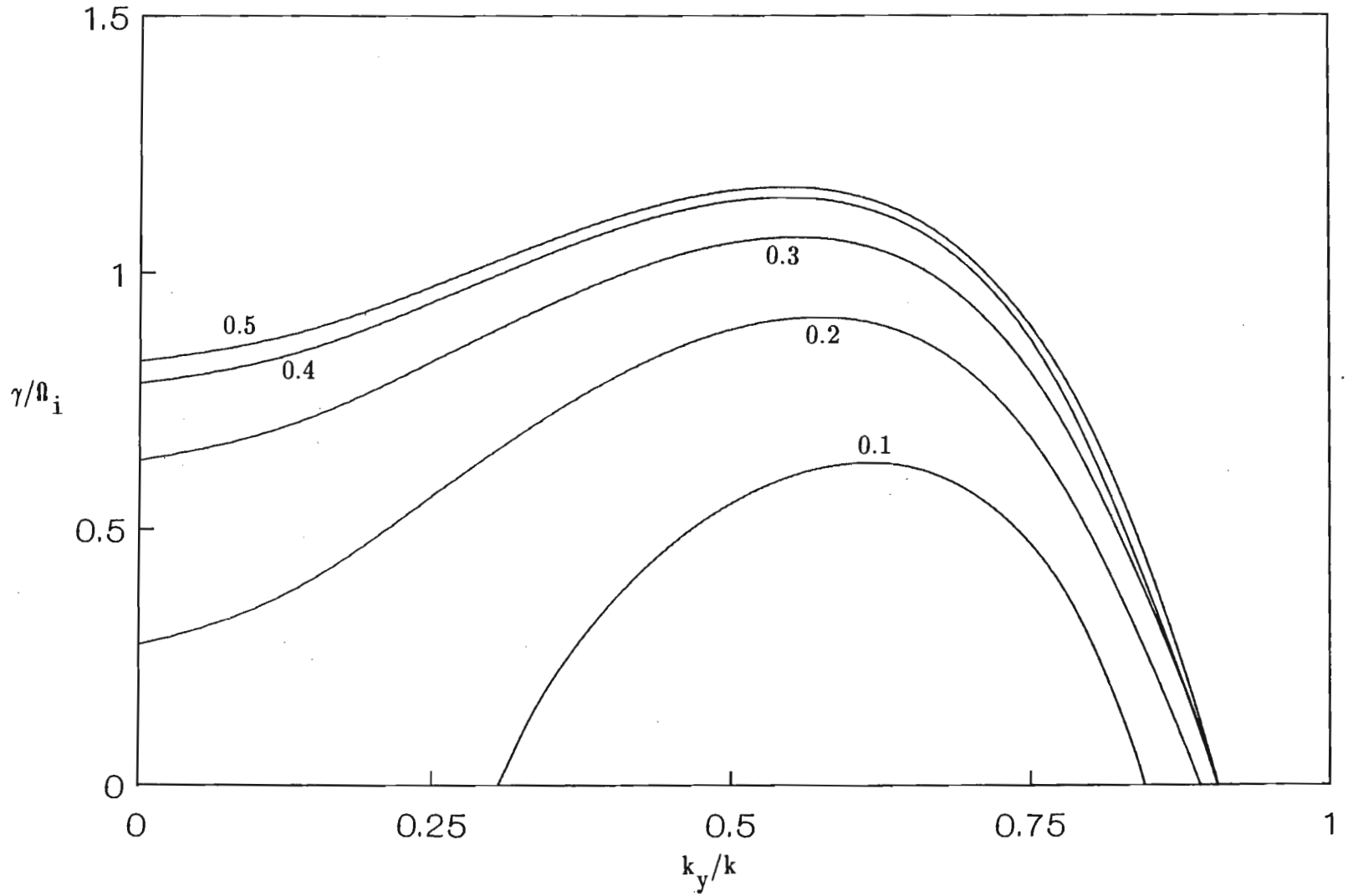

FIG 4.5.7 Normalized growth rate as a function of k_y/k for the anisotropic case $T_\perp/T_\parallel = 4$. The parameter labelling the curves is the normalized beam density n_{bo}/n_{eo}. Here $V_{oz} = 2\ C_s$ while other fixed parameters have the same value as in fig 4.5.3 .

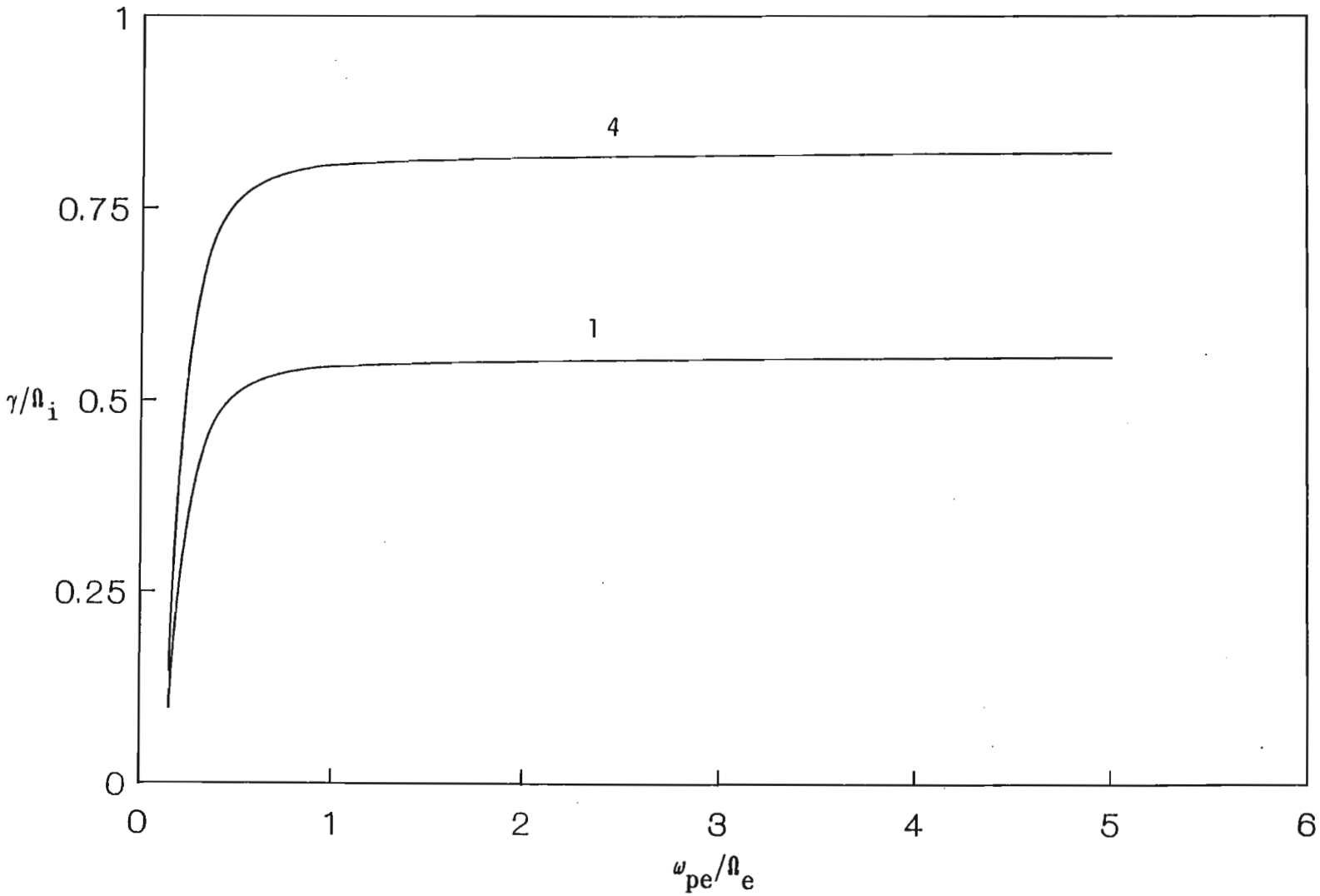

FIG 4.6.1 Normalized growth rate as a function of ω_{pe}/Ω_e. The parameter labelling the curves is the beam speed anisotropy $T_\perp/T_\parallel$. Here $T_\perp = T_i = 0.1\ T_e$, $k\rho_s = 5$, $k_y/k = 0.4$, $n_{bo} = 0.1\ n_{eo}$, $V_{oy} = 4\ C_s$.

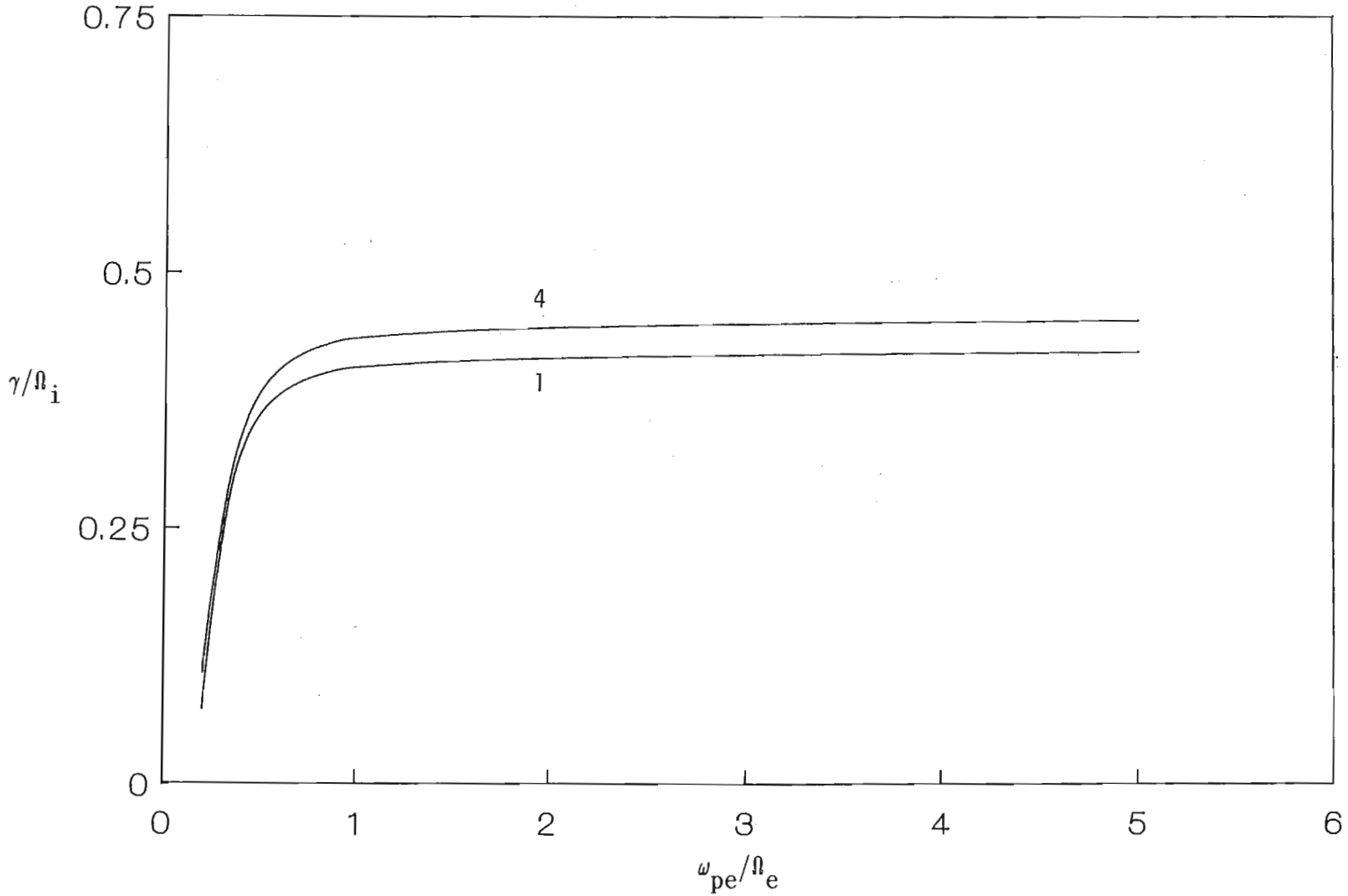

FIG 4.6.2 Normalized growth rate as a function of ω_{pe}/Ω_e. The parameter labelling the curves is the beam speed anisotropy $T_\perp/T_\parallel$. Here $k_y/k = 0.9$, $V_{oz} = 4\ C_s$, while other fixed parameters have the same value as in fig 4.6.1 .

period $2\pi/\Omega_i \gg 2\pi/\omega_{pi}$ (the ion plasma period). This case thus corresponds to the ions being effectively unmagnetized, hence ion cyclotron damping of the wave becomes weaker. In addition, the effect of electron magnetization decreases with increasing ω_{pe}/Ω_e. These factors could account for the saturation in growth rate.

For $\omega_{pe}/\Omega_e < 1$ decreasing ω_{pe}/Ω_e decreases growth. Decreasing ω_{pe}/Ω_e corresponds to increasing ion and electron magnetization, accompanied by cyclotron damping and hence a drop in growth rate. Our results are consistent with those of Gary and Omidi [7]. The growth for the anisotropic case usually dominates that of the isotropic case because of the decrease in total beam temperature due to the anisotropy. The latter effect, as explained earlier, enhances growth. However, for strongly magnetized electrons and ions ($\omega_{pe}/\Omega_e \ll 1$), the effect of cyclotron damping is so great that the growths for both the isotropic and anisotropic cases are the same.

The analysis carried out in the above four sections differs from most of the earlier work (Gary and Omidi [7], Akimoto and Omidi [6], Akimoto and Winske [5]) in that in our model both the ions and electrons are magnetized. In the above references, under the assumption $|\gamma| \gg \Omega_i$, the ions are assumed to be unmagnetized. Since in our results $|\gamma| \sim \Omega_i$, the effect of ion magnetization cannot be ignored.

We have thus extended a study of beam – driven low frequency electrostatic instabilities into the regime $|\gamma| \sim \Omega_i$ and find that two – stream type and ion acoustic – like modes display similar behaviour as compared to the case of unmagnetized ions.

CHAPTER FIVE

ELECTROMAGNETIC WAVE – PLASMA INTERACTION

5.1 INTRODUCTION

The dispersion relation for linear electromagnetic wave propagation in an unmagnetized plasma is $\omega^2 = \omega_{pe}^2 + k^2c^2$, where $\omega_{pe} = (4\pi n_o e^2/m_e)^{1/2}$ is the electron plasma frequency and c is the speed of light. From this it is clear that $\omega \geq \omega_{pe}$ and hence classical linear theory forbids the propagation of electromagnetic waves with $\omega < \omega_{pe}$ in the plasma. Since ω_{pe} depends on the density, for a plasma with non–uniform density there exists a critical cut off density beyond which propagation is prohibited. We consider nonlinear interactions which may reduce the local plasma frequency. When intense electromagnetic radiation is incident on a plasma, the electrons oscillate in the electric field of the radiation. The electron quiver velocity can be $\approx 0.6c$ [25] and hence relativistic effects have to be taken into account. As a result the mass of the electron is modulated in the presence of the field. This nonlinear increase in the electron mass leads to a downshift of the local plasma frequency ω_{pe}.

The ponderomotive force, caused by self interaction of large amplitude waves, is a low frequency, nonlinear force which acts on electrons (ions are massive and therefore not affected) expelling them from a region of high field intensity. The ambipolar field thus created pulls away the ions. Thus it reduces the local plasma density and hence ω_{pe}.

The downshift of the local electron plasma frequency by these two nonlinearities has an important consequence in that it permits the propagation of electromagnetic waves into the "overdense" region (beyond the cut off density) and hence allows the heating of regions of

the plasma which are forbidden by classical linear theory.

The study of nonlinear wave propagation is thus important to the work associated with laser pellet interaction, rf heating of magnetically confined fusion plasmas, wave driven particle accelerators and free electron lasers where intense electromagnetic waves are used.

However, the nonlinearities mentioned above have been shown to give rise to plasma instabilities, in particular the modulational and filamentation instabilities. In addition, they are the source of nonlinear potential structures such as solitons [25].

Yu, Shukla and Spatschek [26] studied the nonlinear propagation of intense circularly polarized electromagnetic waves in an unmagnetized plasma. They were the first to consider both the relativistic electron mass variation and relativistic ponderomotive force nonlinearities simultaneously. Their results showed the existence of finite amplitude wave localization in the form of soliton structures. For sufficiently strong relativistic effects, the existence of supersonic solitary waves was demonstrated.

The interaction of high power circularly polarized electromagnetic waves with an electron plasma was considered by Yu, Shukla and Tsintsadze [27]. In their model, the electron density was modulated by Langmuir (low frequency) oscillations while the ions formed a neutralizing background (Raman effect). They showed the existence of solitons of large amplitude.

Rao, Shukla and Yu [28] studied the problem of solitary wave propagation in a magnetized plasma. They did not assume the quasineutrality condition and included ion dynamics exactly. They considered three types of ion responses giving rise to the forced–Raman (FR), quasistatic (QS) and forced–quasistatic (FQ) interactions. It was found that intense

circularly polarized electromagnetic waves propagating along the external magnetic field could produce large amplitude solitary potential structures.

Shukla, Bharuthram and Tsintsadze [29] investigated the filamentation instability of an intense electromagnetic wave in an unmagnetized plasma. They allowed for fully relativistic effects as well as for a large amplitude electron quiver velocity and large amplitude electron density variations. They studied the three well known plasma responses mentioned above and obtained the spatial growth rates analytically. They showed the existence of a new relativistic filamentation instability at high laser intensities, which they attributed to the fully relativistic electron quiver velocity and finite amplitude density fluctuations associated with the FR interaction.

The modulational instability of an arbitrarily large amplitude electromagnetic wave in an unmagnetized plasma was examined by Shukla, Bharuthram and Tsintsadze [30]. They took into account the relativistic electron quiver velocity and the relativistic ponderomotive force. Three types of plasma slow responses, namely the FR, QS and FQ interactions were considered. The growth rates (temporal) associated with these interactions were analytically obtained. They showed that for $V_e/c \leq 0.12$, were V_e is the electron thermal speed, only the FR interaction participated in the modulational instability, while for larger plasma temperatures, all three interactions contributed to the instability.

A comprehensive review of nonlinear effects associated with relativistic electron mass variation and the ponderomotive force in unmagnetized, as well as magnetized plasmas was compiled by Shukla et al. [25]. They also studied the nonlinear propagation of intense electromagnetic waves in an electron–positron plasma.

Our investigation is an extension of the work in reference [30] to a magnetized plasma. The effect of cyclotron motion on the instability growth rate is clearly demonstrated.

5.2 BASIC EQUATIONS

In deriving our basic equations we closely follow the approach of Rao, Shukla and Yu [28]. We consider the propagation of an intense circularly polarized electromagnetic wave of frequency ω_0 and wavenumber k_0 along an external magnetic field $\vec{B}_0 = B_0\hat{z}$ in a two component electron–ion plasma. The plasma response is of two time scales: the high frequency motion of the electrons in the wave fields and the low frequency response of the ions and electrons due to the nonlinear ponderomotive force.

We use the fluid approach. Hence we use the two fluid relativistic equations namely: the equation of continuity

$$\frac{\partial n_j}{\partial t} + \nabla\cdot(n_j\vec{V}_j) = 0 \ , \tag{5.2.1}$$

and the equation of motion

$$\frac{\partial \vec{p}_j}{\partial t} + (\vec{V}_j\cdot\nabla)\vec{p}_j = e_j\left[\vec{E} + \frac{\vec{V}_j\times\vec{B}}{c} + \frac{\vec{V}_j\times\vec{B}_0}{c}\right] - \frac{T_j}{n_j}\nabla n_j \ , \tag{5.2.2}$$

together with Maxwell's equations

$$\nabla\times\vec{E} = -\frac{1}{c}\frac{\partial\vec{B}}{\partial t} \ , \tag{5.2.3}$$

$$\nabla\times\vec{B} = \frac{4\pi}{c}\sum_j n_j e_j\vec{V}_j + \frac{1}{c}\frac{\partial\vec{E}}{\partial t} \ , \tag{5.2.4}$$

$$\nabla\cdot\vec{E} = 4\pi e(n_i - n_e) \ , \tag{5.2.5}$$

$$\nabla\cdot\vec{B} = 0 \ , \tag{5.2.6}$$

where n_j, $\vec{V}_j$ and T_j are the number density, the fluid velocity and the temperature of the jth species (j=i,e), respectively,

$$\vec{p}_j = \frac{m_{jo}\vec{V}_j}{(1-V_j^2/c^2)^{1/2}} = m_{jo}\vec{V}_j\,(1+p_j^2/m_{jo}^2c^2)^{1/2} \qquad 5.2.7$$

is the relativistic momentum and m_{jo} is the rest mass of the jth species.

The wave fields $\vec{E}$ and $\vec{B}$ can be written in terms of the a scalar potential ϕ and a vector potential $\vec{A}$ as

$$\vec{B} = \nabla \times \vec{A}\ , \qquad 5.2.8$$

$$\vec{E} = -\frac{1}{c}\frac{\partial \vec{A}}{\partial t} - \nabla\phi\ , \qquad 5.2.9$$

and satisfy the gauge condition

$$\nabla\cdot\vec{A} + \frac{1}{c}\frac{\partial\phi}{\partial t} = 0\ . \qquad 5.2.10$$

Here ϕ is the low frequency potential perturbation induced by the strong electromagnetic wave. Substituting from equations (5.2.8) and (5.2.9) into the electron momentum equation (5.2.2) and using equation (5.2.7) we obtain

$$\frac{\partial\vec{p}_e}{\partial t} + \frac{1}{m_{eo}}(1+p_e^2/m_{eo}^2c^2)^{-1/2}\,(\vec{p}_e\cdot\nabla)\vec{p}_e = \frac{e}{c}\frac{\partial\vec{A}}{\partial t} + e\nabla\phi - \frac{e}{m_{eo}c}(1+p_e^2/m_{eo}^2c^2)^{-1/2}\,\vec{p}_e \times (\nabla\times\vec{A}) - \Omega_{eo}(1+p_e^2/m_{eo}^2c^2)^{-1/2}\,\vec{p}_e\times\hat{z} - T_e\nabla(\ln n_e)\ , \qquad 5.2.11$$

where $\Omega_{eo} = eB_0/m_{eo}c$ is the electron gyrofrequency. Since the plasma response is of two time scales, we separate the high and low frequency components of $\vec{A}$ and $\vec{p}_e$ and write for left–hand circularly polarized waves:

$$\left.\begin{aligned}\vec{A} &= A(z,t)(\hat{x} - i\hat{y})\exp[i(k_0 z - \omega_0 t)] + c.c \\ \vec{p}_e &= p(z,t)(\hat{x} - i\hat{y})\exp[i(k_0 z - \omega_0 t)] + c.c\end{aligned}\right\}, \qquad 5.2.12$$

where c.c denotes complex conjugate and A and p are normalized with respect to $m_{eo}c^2/e$ and $m_{eo}c$, respectively.

Here $A(z,t)$ and $p(z,t)$ are slowly varying complex functions of space and time. We have used the fact that the perpendicular momentum of the electrons is due to the high frequency response in the wave fields (transverse wave) whereas the parallel momentum due to the ponderomotive force, is a low frequency response. However, the effect of the parallel electron momentum on the low–frequency dynamics of the plasma is neglected.

Equation (5.2.11) with $\vec{A}$ and $\vec{p}_e$ in normalized form becomes

$$m_{eo}c\frac{\partial \vec{p}_e}{\partial t} + m_{eo}c^2(1+p^2)^{-1/2}(\vec{p}_e\cdot\nabla)\vec{p}_e = m_{eo}c\frac{\partial \vec{A}}{\partial t} + e\nabla\phi - m_{eo}c^2(1+p^2)^{-1/2}\vec{p}_e \times (\nabla\times\vec{A}) - m_{eo}c\Omega_{eo}(1+p^2)^{-1/2}\vec{p}_e\times\hat{z} - T_e\nabla(\ln n_e)\ . \qquad 5.2.13$$

We note that $\vec{p}_e$ represents the perpendicular (to $\vec{B}_0$) electron momentum. Since all terms that vary as $\exp[i(k_0 z - \omega_0 t)]$ behave independently of all terms that vary as $\exp[-i(k_0 z - \omega_0 t)]$, it is necessary only to substitute the first half of equation (5.2.12) into equation (5.2.13), that is, ignore the complex conjugate part [31]. With this substitution

$$\left.\begin{aligned} \frac{\partial \vec{p}_e}{\partial t} &= \left(\frac{\partial p}{\partial t} - i\omega_o p\right)\ (\hat{x} - i\hat{y})\ \exp[i(k_o z - \omega_o t)] \\ \frac{\partial \vec{A}}{\partial t} &= \left(\frac{\partial A}{\partial t} - i\omega_o A\right)\ (\hat{x} - i\hat{y})\ \exp[i(k_o z - \omega_o t)] \\ \vec{p}_e \times \hat{z} &= -ip\ (\hat{x} - i\hat{y})\ \exp[i(k_o z - \omega_o t)] \end{aligned}\right\} \qquad 5.2.14$$

and equation (5.2.13) is averaged over the fast time scale to yield (appendix B)

$$\frac{\partial p}{\partial t} - i\omega_o p = \frac{\partial A}{\partial t} - i\omega_o A + ip\Omega_{eo}(1+p^2)^{-1/2} \ . \qquad 5.2.15$$

Upon dividing by ω_o and noting that $|\frac{\partial p}{\partial t}/\omega_o| \ll |p|$ and $|\frac{\partial A}{\partial t}/\omega_o| \ll |A|$ since A and p are slowly varying quantities, equation (5.2.15) reduces to

$$-ip = -iA + ip\Omega_{eo}/\omega_o\ (1+p^2)^{-1/2} \ .$$

Letting $\alpha = \Omega_{eo}/\omega_o$, we solve for A in terms of p to obtain

$$A = p[1 + \alpha(1+p^2)^{-1/2}] \ , \qquad 5.2.16$$

in agreement with Rao, Shukla and Yu [28]. Thus by (5.2.12) we have

$$\vec{A} = \eta \vec{p}_e \ , \qquad 5.2.17$$

where $\eta = 1 + \alpha(1+p^2)^{-1/2}$. For the low frequency electron motion we can show (appendix B) from (5.2.11) that

$$m_{eo}c^2(1+p^2)^{-1/2}\,(\vec{p}_e\cdot\nabla)\vec{p}_e = e\nabla\phi - m_{eo}c^2(1+p^2)^{-1/2}\,\vec{p}_e \times (\nabla\times\vec{A}) - \nabla(\ln n_e)\ . \qquad 5.2.18$$

Using (5.2.17) and the identity

$$\vec{p}_e\times(\nabla\times\eta\vec{p}_e) = p^2\nabla\eta + 1/2\,\eta\nabla p^2 - \eta(\vec{p}_e\cdot\nabla)\vec{p}_e - (\vec{p}_e\cdot\nabla\eta)\vec{p}_e$$

equation (5.2.18) becomes

$$m_{eo}c^2\Gamma(\vec{p}_e\cdot\nabla)\vec{p}_e = e\nabla\phi - m_{eo}c^2\Gamma(p^2\nabla\eta + 1/2\,\eta\nabla p^2) + m_{eo}c^2\Gamma[\eta(\vec{p}_e\cdot\nabla)\vec{p}_e + (\vec{p}_e\cdot\nabla\eta)\vec{p}_e] - \nabla(\ln n_e)\ , \qquad 5.2.19$$

where $\Gamma = (1+p^2)^{-1/2}$. Taking the dot product of equation (5.2.19) with $\hat{z}$ and noting that $\vec{p}_e\cdot\hat{z} = 0$, we obtain

$$[\nabla\phi - \beta\Gamma(p^2\nabla\eta + 1/2\,\eta\nabla p^2) - \nabla(\ln n_e)]\cdot\hat{z} = 0\ , \qquad 5.2.20$$

where ϕ is normalized with respect to T_e/e and $\beta = m_{eo}c^2/T_e$. Since

$$\nabla\eta = \nabla[1 + a(1+p^2)^{-1/2}] = -a/2\,(1+p^2)^{-3/2}\,\nabla p^2\ ,$$

the second term in (5.2.20) can be written as

$$\Gamma(p^2\nabla\eta + 1/2\eta\,\nabla p^2) = a/2\,(1+p^2)^{-2}\,\nabla p^2 + 1/2\,(1+p^2)^{-1/2}\nabla p^2\ . \qquad 5.2.21$$

Since

$$\nabla(1+p^2)^{-1} = -(1+p^2)^{-2}\nabla p^2\ ,$$

and

$$\nabla(1+p^2)^{1/2} = 1/2\,(1+p^2)^{-1/2}\nabla p^2\ ,$$

the right hand side of (5.2.21) simplifies to

$$\nabla(1+p^2)^{1/2} - a/2\ \nabla(1+p^2)^{-1} .$$

Hence (5.2.20) becomes

$$[\nabla\phi - \beta\nabla\{(1+p^2)^{1/2} - a/2\ (1+p^2)^{-1}\} - \nabla(\ln n_e)] . \hat{z} = 0 , \qquad 5.2.22$$

which represents a low frequency electron momentum balance along $\vec{B}_0$.

In deriving the governing equation for the wave amplitude A we begin with the vector wave equation (5.2.25) which is derived as follows:

equation (5.2.4) can be written as

$$\nabla \times (\nabla \times \vec{A}) = \frac{4\pi}{c} \vec{J} + \frac{1}{c} \frac{\partial}{\partial t} \left(-\frac{1}{c} \frac{\partial \vec{A}}{\partial t} - \nabla\phi\right) , \qquad 5.2.23$$

where $\vec{J} = \sum_j n_j e_j \vec{V}_j$ is the current density and we have used (5.2.8) and (5.2.9) to substitute for $\vec{B}$ and $\vec{E}$. Using the identity

$$\nabla \times (\nabla \times \vec{A}) = \nabla(\nabla \cdot \vec{A}) - \nabla^2 \vec{A}$$

we can write (5.2.23) as

$$\nabla(\nabla \cdot \vec{A} + \frac{1}{c} \frac{\partial \phi}{\partial t}) = \nabla^2 \vec{A} + \frac{4\pi}{c} \vec{J} - \frac{1}{c^2} \frac{\partial^2 \vec{A}}{\partial t^2} . \qquad 5.2.24$$

Using the gauge condition (5.2.10), (5.2.24) simplifies to

$$\frac{\partial^2 \vec{A}}{\partial t^2} - c^2 \nabla^2 \vec{A} = 4\pi c \vec{J} . \qquad 5.2.25$$

Since the ions are massive we neglect their contribution to the high frequency current density and write

$$\vec{J} \approx -en_e\vec{V}_e \ . \qquad 5.2.26$$

Substituting (5.2.26) into (5.2.25) and using (5.2.7) for $\vec{V}_e$, with $\vec{A}$ and $\vec{p}_e$ normalized and n_e normalized with respect to the equilibrium density n_0, we obtain

$$\frac{\partial^2\vec{A}}{\partial t^2} - c^2\nabla^2\vec{A} = -\omega_{peo}^2 \frac{n_e\vec{p}_e}{(1+p^2)^{1/2}} \ , \qquad 5.2.27$$

where $\omega_{peo}^2 = (4\pi n_0 e^2/m_{eo})^{1/2}$ is the plasma frequency associated with the electron rest mass. Using (5.2.12) and (5.2.14) we can show that

$$\begin{aligned}\frac{\partial^2\vec{A}}{\partial t^2} &= \left[\frac{\partial^2 A}{\partial t^2} - 2i\omega_0\frac{\partial A}{\partial t} - \omega_0^2 A\right](\hat{x} - i\hat{y})\exp[i(k_0 z - \omega_0 t)] \\ &\approx \left[-2i\omega_0\frac{\partial A}{\partial t} - \omega_0^2 A\right](\hat{x} - i\hat{y})\exp[i(k_0 z - \omega_0 t)] \ , \qquad 5.2.28\end{aligned}$$

where we have used the approximation

$$\left|\frac{\partial^2 A}{\partial t^2}\Big/\left(\omega_0\frac{\partial A}{\partial t}\right)\right| \ll 1$$

since A is a slowly varying quantity, and

$$\frac{\partial^2\vec{A}}{\partial z^2} = \left[\frac{\partial^2 A}{\partial z^2} + 2ik_0\frac{\partial A}{\partial z} - k_0^2 A\right](\hat{x} - i\hat{y})\exp[i(k_0 z - \omega_0 t)] \ . \qquad 5.2.29$$

Substituting (5.2.28) and (5.2.29) into (5.2.27) and using (5.2.12) for $\vec{p}_e$ we obtain

$$\frac{2i\omega_o}{\omega_{peo}^2}\frac{\partial A}{\partial t} + \frac{(\omega_o^2 - k_o^2c^2)}{\omega_{peo}^2}A + \frac{c^2}{\omega_{peo}^2}\frac{\partial^2 A}{\partial z^2} + \frac{2ik_oc^2}{\omega_{peo}^2}\frac{\partial A}{\partial z} = \frac{n_e p}{(1+p^2)^{1/2}} . \qquad 5.2.30$$

Normalizing t and z with respect to the ion plasma period $\omega_{pi}^{-1} = (m_i/4\pi n_o e^2)^{1/2}$ and the electron Debye length $\lambda_{de} = (T_e/4\pi n_o e^2)^{1/2}$ respectively, and letting $\Delta = (\omega_o^2 - k_o^2c^2)/\omega_{peo}^2$, we can write (5.2.30) as

$$\frac{2i\omega_o\omega_{pi}}{\omega_{peo}^2}\frac{\partial A}{\partial t} + \Delta A + \frac{c^2}{\omega_{peo}^2\lambda_{de}^2}\frac{\partial^2 A}{\partial z^2} + \frac{2ik_oc^2}{\omega_{peo}^2\lambda_{de}}\frac{\partial A}{\partial z} = \frac{n_e p}{(1+p^2)^{1/2}} . \qquad 5.2.31$$

Letting $\epsilon = (m_{eo}/m_i)^{1/2}\,\omega_o/\omega_{peo} = (\omega_{pi}/\omega_{peo})\omega_o/\omega_{peo}$, $V_g = 2k_oc^2/(\omega_{peo}^2\lambda_{de})$ and noting that $c^2/(\omega_{peo}^2\lambda_{de}^2) = m_{eo}c^2/T_e = \beta$, (5.2.31) may be written as

$$2i\epsilon\frac{\partial A}{\partial t} + iV_g\frac{\partial A}{\partial z} + \beta\frac{\partial^2 A}{\partial z^2} + \Delta A = \frac{n_e p}{(1+p^2)^{1/2}} , \qquad 5.2.32$$

as found by Rao et al [28]. Integrating (5.2.22) with respect to z and using the boundary conditions $\phi = p = 0$, $n_e = 1$ when $|z| \to \infty$, we obtain for the ambipolar potential ϕ,

$$\phi = \beta\left[(1+p^2)^{1/2} - 1 + \frac{a}{2}\frac{p^2}{(1+p^2)}\right] + \ln n_e . \qquad 5.2.33$$

The equations (5.2.32) and (5.2.33) constitute the governing set for our study of the modulational instability of large amplitude cyclotron waves. We consider three types of slow plasma responses–the forced Raman(FR), forced–quasistatic(FQ) and the quasistatic(QS) interactions. Associated with each is a unique slow electron density response n_e.

FORCED – RAMAN INTERACTION (FR)

For intense laser beams the relativistic electron ponderomotive pressure (second term in 5.2.22) dominates the electron thermal pressure ($\propto \ln n_e$) and (5.2.33) simplifies to

$$\phi = \beta \left[(1+p^2)^{1/2} - 1 + \frac{\alpha}{2} \frac{p^2}{(1+p^2)} \right] , \qquad 5.2.34$$

which describes a balance of the ambipolar electric field by the ponderomotive force. For the FR interaction, on the electron time scale (ω_{pe}^{-1}), the ions do not respond and form a neutralizing background. Then $n_i = n_0$ and the normalized Poisson's equation yields

$$n_e = 1 + \nabla^2 \phi \ . \qquad 5.2.35$$

Upon substituting (5.2.34) and (5.2.35) into (5.2.32) and using the notation $\partial_t = \frac{\partial}{\partial t}$, $\partial_z = \frac{\partial}{\partial z}$, we obtain

$$(2i\epsilon\partial_t + iV_g\partial_z + \beta\partial_z^2 + \Delta)A$$
$$= \frac{p}{(1+p^2)^{1/2}} \left[1 + \beta\nabla^2 \left\{ (1+p^2)^{1/2} + \frac{\alpha}{2} \frac{p^2}{(1+p^2)} \right\} \right] , \qquad 5.2.36$$

where we recall $A = p[1 + \alpha(1+p^2)^{-1/2}]$ from (5.2.16).

The modulational instability analysis is carried out following the method of Karpman[32]. We let

$$p = (p_0 + \delta p)\, e^{-i\delta t} \ ,$$

where p_0 is a real constant and represents the pump wave amplitude, δp is the perturbation term with $|\delta p| \ll |p_0|$ and δ represents a nonlinear frequency shift. It is then easy to

approximate the following quantities:

$$p^2 = |p^2| \approx p_0^2 + p_0\tilde{\delta p} \ ,$$

where $\tilde{\delta p} = \delta p + \delta p^*$, (* denotes complex conjugate)

$$\frac{1}{(1+p^2)^{1/2}} \approx \frac{1}{(1+p_0^2)^{1/2}} - \frac{p_0\tilde{\delta p}}{2(1+p_0^2)^{3/2}}$$

$$A \approx \left[p_0+\delta p + \frac{(p_0+\delta p)a}{(1+p_0^2)^{1/2}} - \frac{a}{2}\frac{p_0^2\tilde{\delta p}}{(1+p_0^2)^{3/2}} \right] e^{-i\delta t} \qquad \text{by (5.2.16)}$$

$$\frac{p}{(1+p^2)^{1/2}} \approx \left[\frac{p_0+\delta p}{(1+p_0^2)^{1/2}} - \frac{p_0^2\tilde{\delta p}}{2(1+p_0^2)^{3/2}} \right] e^{-i\delta t}$$

$$(1+p^2)^{1/2} \approx (1+p_0^2)^{1/2}\left[1 + \frac{p_0\tilde{\delta p}}{2(1+p_0^2)}\right]$$

$$\frac{p^2}{(1+p^2)} \approx \left[\frac{p_0^2+p_0\tilde{\delta p}}{(1+p_0^2)} - \frac{p_0^3\tilde{\delta p}}{(1+p_0^2)^2} \right] .$$

Substituting the above approximations in (5.2.36), the pump terms (corresponding to zero order in perturbation) yield for the nonlinear frequency shift

$$\delta = \delta_R = \frac{1}{2\epsilon}\left[\frac{1}{(1+p_0^2)^{1/2}+a} - \Delta \right] , \qquad 5.2.37$$

while the first order perturbation terms yield

$$\{2\epsilon\delta_R+\Delta + i(2\epsilon\partial_t + V_g\partial_z) + \beta\partial_z^2\}\left[\left\{1 + \frac{a}{(1+p_0^2)^{1/2}}\right\}\delta p - \frac{a}{2}\frac{p_0^2\tilde{\delta p}}{(1+p_0^2)^{3/2}}\right]$$

$$= \left[\frac{\delta p}{(1+p_0^2)^{1/2}} - \frac{p_0^2\tilde{\delta p}}{2(1+p_0^2)^{3/2}}\right] + \frac{\beta}{2}\frac{p_0^2}{(1+p_0^2)}\left[1 + \frac{a}{(1+p_0^2)^{3/2}}\right]\nabla^2\tilde{\delta p}. \qquad 5.2.38$$

We write $\delta p = X + iY$ in (5.2.38) and separate into real and imaginary parts to obtain (from the real component)

$$(2\epsilon\delta_R + \Delta + \beta\partial_z^2)\left[1 + \frac{a}{(1+p_0^2)^{3/2}}\right]X - (2\epsilon\partial_t + V_g\partial_z)\left[1 + \frac{a}{(1+p_0^2)^{1/2}}\right]Y$$

$$= \frac{1}{(1+p_0^2)^{3/2}}X + \beta\frac{p_0^2}{(1+p_0^2)}\left[1 + \frac{a}{(1+p_0^2)^{3/2}}\right]\nabla^2 X\,, \qquad 5.2.39$$

and (from the imaginary component)

$$(2\epsilon\delta_R+\Delta + \beta\partial_z^2)\left[1 + \frac{a}{(1+p_0^2)^{1/2}}\right]Y + (2\epsilon\partial_t + V_g\partial_z)\left[1 + \frac{a}{(1+p_0^2)^{3/2}}\right]X$$

$$= \frac{1}{(1+p_0^2)^{1/2}}Y\,. \qquad 5.2.40$$

We perform a Fourier analysis by letting

$$\begin{bmatrix} X \\ Y \end{bmatrix} = \begin{bmatrix} \tilde{X} \\ \tilde{Y} \end{bmatrix} \exp[i(Kz - \Omega t)]\,,$$

where Ω and K are the frequency and wave number associated with the plasma slow motion. Equations (5.2.39) and (5.2.40) then yield, respectively

$$(2\epsilon\delta_R+\Delta-K^2\beta)\left[1+\frac{a}{(1+p_0^2)^{3/2}}\right]\tilde{X}-\{i(KV_g-2\epsilon\Omega)\}\left[1+\frac{a}{(1+p_0^2)^{1/2}}\right]\tilde{Y}$$

$$=\frac{1}{(1+p_0^2)^{3/2}}\tilde{X}-K^2\beta\frac{p_0^2}{(1+p_0^2)}\left[1+\frac{a}{(1+p_0^2)^{3/2}}\right]\tilde{X} \qquad 5.2.41$$

and

$$(2\epsilon\delta_R+\Delta-\beta K^2)\left[1+\frac{a}{(1+p_0^2)^{1/2}}\right]\tilde{Y}+i(KV_g-2\epsilon\Omega)\left[1+\frac{a}{(1+p_0^2)^{3/2}}\right]\tilde{X}$$

$$=\frac{1}{(1+p_0^2)^{1/2}}\tilde{Y}\,. \qquad 5.2.42$$

Solving for $\tilde{Y}$ from (5.2.42) and substituting into (5.2.41) we obtain

$$(2\epsilon\delta_R+\Delta-\beta K^2)[(1+p_0^2)^{3/2}+a]+\frac{1}{\beta K^2}(KV_g-2\epsilon\Omega)^2[(1+p_0^2)^{3/2}+a]$$

$$=1-\beta K^2\frac{p_0^2}{(1+p_0^2)}[(1+p_0^2)^{3/2}+a]\,. \qquad 5.2.43$$

We set $V_g' = V_g/2\epsilon$ and $\Omega = KV_g' + i\gamma_R$ in (5.2.43) to obtain the growth rate for the FR modulational instability

$$\gamma_R=\frac{K\sqrt{\beta}}{2\epsilon}\left[\frac{1}{(1+p_0^2)^{1/2}+a}-\frac{\beta K^2}{(1+p_0^2)}-\frac{1}{(1+p_0^2)^{3/2}+a}\right]^{1/2}. \qquad 5.2.44$$

The threshold condition corresponding to $\gamma_R = 0$ is given by

$$\beta K^2=\frac{p_0^2(1+p_0^2)^{3/2}}{[(1+p_0^2)^{1/2}+a][(1+p_0^2)^{3/2}+a]}\,. \qquad 5.2.45$$

We recall that $a = \Omega_{eo}/\omega_0$. Thus the limit $a = 0$ corresponds to an unmagnetized plasma

situation. In this case our results reduce to those of Shukla, Bharuthram and Tsintsadze [30]. It must be noted that our normalizations and definition of ϵ are different from theirs, and must be taken into cognizance when comparing results.

FORCED QUASISTATIC INTERACTION (FQ)

Here the ions actively participate. When the phase velocity of the ion fluctuations is much smaller than the ion thermal velocity, the ion thermal pressure balances the slow electric field [28]. We may assume an isothermal equation of state for the ions, leading to an expression for the ion number density given by

$$n_i = n_0 \exp(-e\phi/T_i) \ ,$$

which in normalized form reads as

$$n_i = \exp(-\sigma\phi) \ ,$$

where $\sigma = T_e/T_i$. The normalized Poisson's equation yields

$$n_e = \exp(-\sigma\phi) + \nabla^2\phi \ . \qquad 5.2.46$$

Here, as for the forced – Raman interaction, the electron thermal pressure is neglected in comparison to the ponderomotive pressure. Hence ϕ is given by (5.2.34) with

$$n_e = \exp\left[\beta_b - \beta_b \left\{ (1+p^2)^{1/2} + \frac{a}{2} \frac{p^2}{(1+p^2)} \right\} \right] + \beta\nabla^2 \left[(1+p^2)^{1/2} + \frac{a}{2} \frac{p^2}{(1+p^2)} \right] \ . \qquad 5.2.47$$

Following the procedure outlined for the forced–Raman case, we use (5.2.32) and (5.2.47) to obtain for the nonlinear frequency shift and modulational instability growth rate, respectively

$$\delta_{FQ} = \frac{1}{2\epsilon}\left[\frac{e^{Q}}{(1+p_0^2)^{1/2+a}} - \Delta\right], \tag{5.2.48}$$

$$\gamma_{FQ} = \frac{K\sqrt{\beta}}{2\epsilon}\left[\frac{p_0^2(1+p_0^2)^{1/2}\ e^{Q}}{[(1+p_0^2)^{1/2+a}][(1+p_0^2)^{3/2+a}]} + \frac{\beta_b p_0^2 e^{Q} - K^2\beta}{(1+p_0)^2}\right]^{1/2}, \tag{5.2.49}$$

with the threshold condition

$$\beta K^2 = p_0^2 e^{Q}\left[\frac{(1+p_0^2)^{3/2}}{[(1+p_0^2)^{1/2+a}][(1+p_0^2)^{3/2+a}]} + \beta_b\right], \tag{5.2.50}$$

where $\beta_b = \sigma\beta$ and $Q = \beta_b\left[1 - (1+p_0^2)^{1/2} - \frac{a}{2}\frac{p_0^2}{(1+p_0^2)}\right]$.

QUASISTATIC INTERACTION (QS)

For a plasma situation in which the ponderomotive force and thermal pressure exactly balance the ambipolar potential the electron density is represented by a modified Boltzmann distribution [25]. For Boltzmann ions we use the quasi–neutrality condition

$$n_e = n_i = e^{-\sigma\phi} \tag{5.2.51}$$

and substitute into (5.2.33) to obtain

$$\phi = \beta_Q \left[(1+p^2)^{1/2} - 1 + \frac{a}{2} \frac{p^2}{(1+p^2)} \right] , \qquad 5.2.52$$

where $\beta_Q = \beta\sigma/(1+\sigma)$. Substituting (5.2.52) into (5.2.51) we obtain the modified form for n_e

$$n_e = \exp\left[-\beta_Q \left\{ (1+p^2)^{1/2} - 1 + \frac{a}{2} \frac{p^2}{(1+p^2)} \right\} \right] . \qquad 5.2.53$$

Following a similar analysis to that for the forced Raman effect we obtain for the nonlinear frequency shift

$$\delta_Q = \frac{1}{2\epsilon} \left[\frac{e^S}{(1+p_0^2)^{1/2}+a} - \Delta \right] .$$

The growth rate for the associated modulational instability is given by

$$\gamma_Q = \frac{K\sqrt{\beta}}{2\epsilon} \left[\frac{p_0^2(1+p_0^2)^{1/2}\ e^S}{[(1+p_0^2)^{1/2}+a][(1+p_0^2)^{3/2}+a]} + \frac{\beta_Q p_0^2 e^S}{(1+p_0^2)} - K^2\beta \right]^{1/2}$$

with

$$\beta K^2 = p_0^2 e^S \left[\frac{(1+p_0^2)^{1/2}}{[(1+p_0^2)^{1/2}+a][(1+p_0^2)^{3/2}+a]} + \frac{\beta_Q}{(1+p_0^2)} \right]$$

at threshold. Here $S = \beta_Q \left[1 - (1+p_0^2)^{1/2} - \frac{a}{2} \frac{p_0^2}{(1+p_0^2)} \right]$

It is easy to show that for the unmagnetized plasma ($a = 0$) our results, for the FQ and QS interactions, just as for the FR interaction, reduce to those of Shukla, Bharuthram and Tsintsadze [30].

5.3 RESULTS

The growth rates (γ) associated with the three types of interactions have been numerically studied as a function of the perturbation wavenumber K, p_0 (related to the incident pump amplitude) and the ratio $\beta = c^2/V_{te}^2$. Figure 5.3.1 shows the variation of γ with K. It is seen that for the chosen values of β and p_0, the QS interaction has the strongest wave growth, also over a much wider range of K values than the FQ and FR interactions. In fig 5.3.2 we show γ against p_0. It is seen that for large pump amplitudes only the FR interaction contributes to wave growth. On the other hand, for low pump amplitude, FQ and QS interactions dominate. The dependence of wave growth on β is presented in fig 5.3.3 . It is observed that for $\beta > 50$ ($V_{te}/c < 0.14$) only the instability associated with FR grows, consistent with the findings in reference [30] for the unmagnetized case. As the plasma temperature is increased, β decreases, accompanied by a significant increase in growth due to QS and FQ interactions and a decrease in growth due to the FR interaction.

The variations of the growth rates associated with the FR, FQ and QS interactions with the parameters K, p_0 and β are qualitatively similar to those for the an unmagnetized plasma [30]. However, for the chosen parameters of reference [30], the maximum growth rates are found to be an order of magnitude smaller when the ambient magnetic field is included.

The above results have already been published in a summarized form [33].

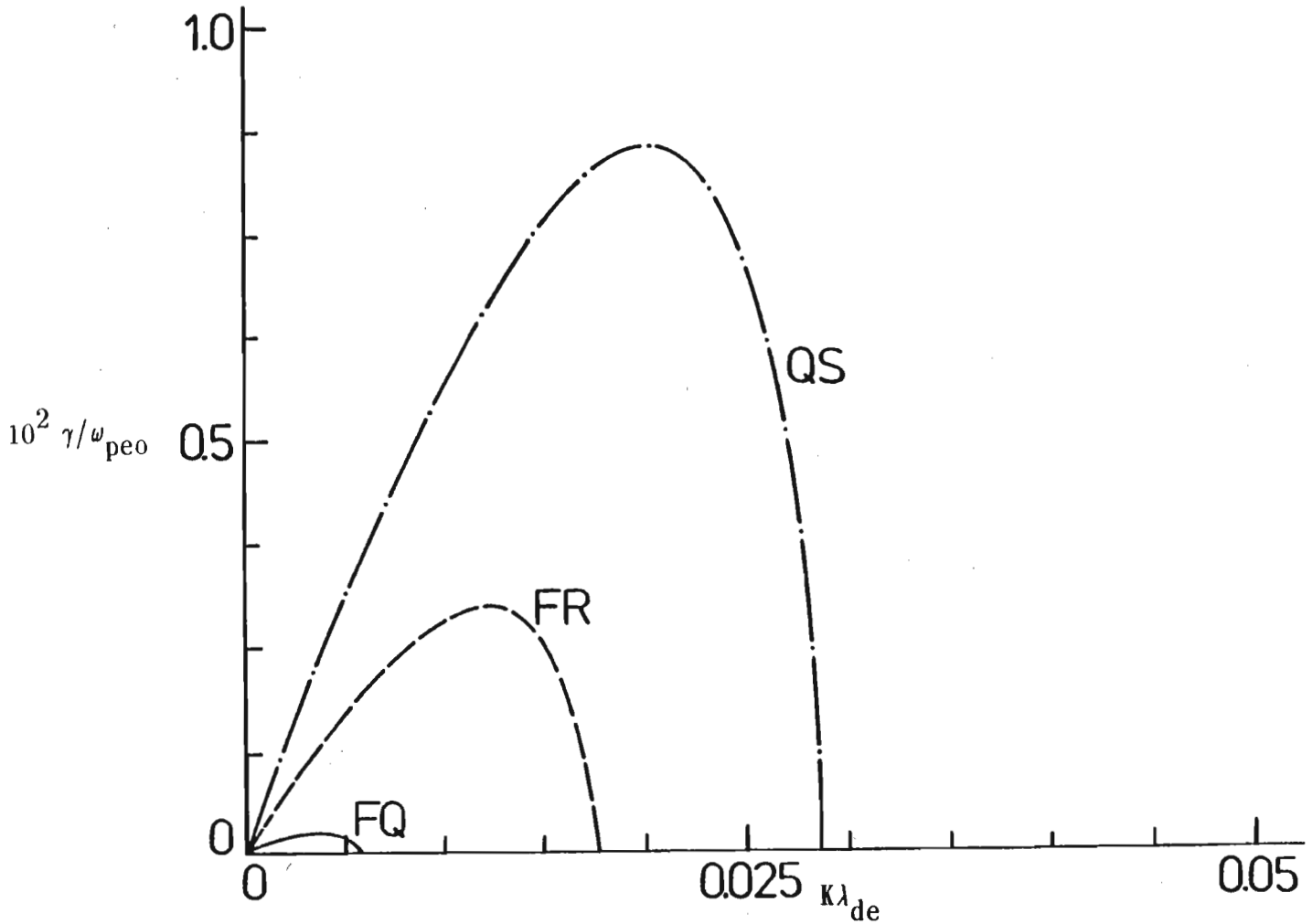

FIG 5.3.1 Normalized growth rate versus $K\lambda_{de}$. The parameter labelling the curves indicate the type of interaction: FR–forced Raman, FQ–forced quasistatic and QS–quasistatic. The graph has been produced for the CO_2 laser (wavelength λ = 10.06 μm) with intensity $I \approx 10^{16}$ W/cm^2, and the plasma parameters $n_o = 4 \times 10^{18}$ cm^{-3}, $T_e = T_i = 10$ keV and $B_o = 10$ MG.

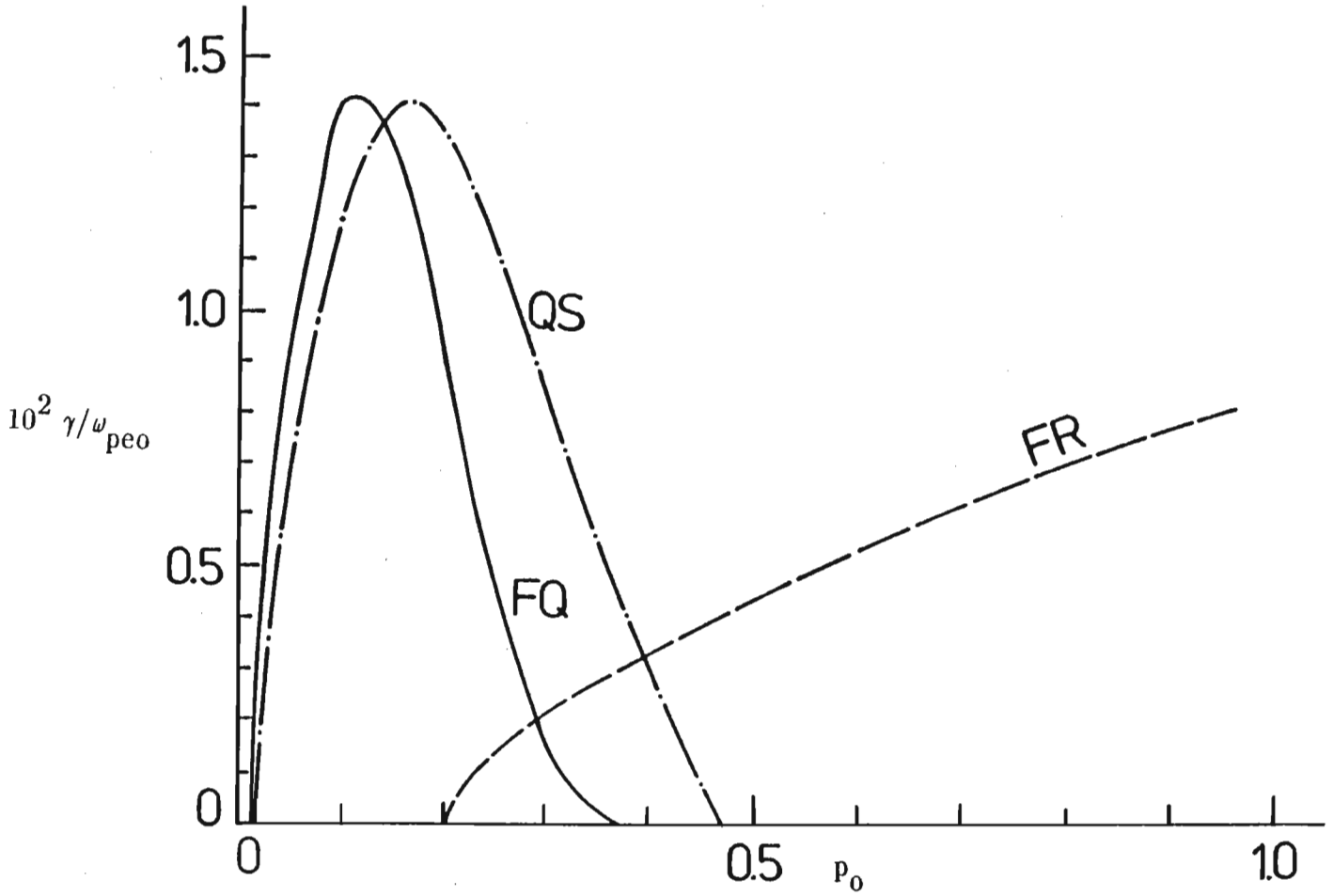

FIG 5.3.2 Normalized growth rate versus p_0. The labelling of the curves is as in fig 5.3.1 . Here $K\lambda_{de} = 0.01$ and other parameters are the same as in fig 5.3.1 . Note that p_0 is related with the ratio of the electron quiver velocity V_0 $(= eE_0/m_{eo}\omega_0)$ and the speed of light. For a given value of the laser wavelength λ, a and p_0, the intensity I is computed using the formula [25] $V_0/c = 8.5 \times 10^{-10} \sqrt{I}\,\lambda = p_0 + ap_0/(1+p_0^2)^{1/2}$, where I is in W/cm^2 and λ in microns.

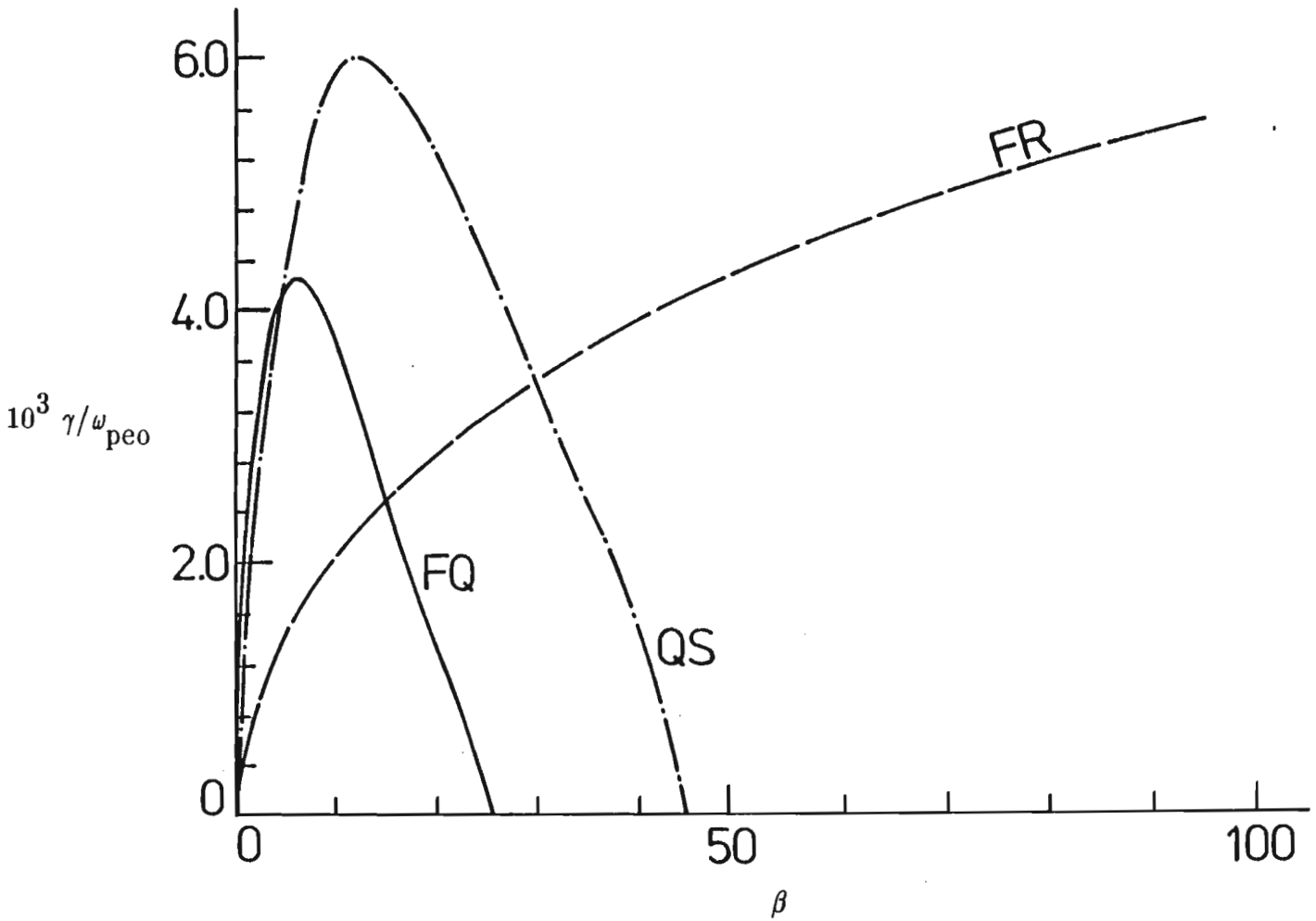

FIG 5.3.3 Normalized growth rate versus β with $I = 1.4 \times 10^{16}$ W/cm^2. The labelling of the curves is as in fig 5.3.1 . Other plasma parameters are the same as in fig 5.3.2 . For a given value of β, the electron temperature is determined by means of the formula T_e (eV) = $(c/4.19)^2\ 10^{-14}/\beta$.

CHAPTER SIX

SUMMARY AND CONCLUSION

Using linear theory we have derived the dispersion relation for electrostatic instabilities propagating in an ion–beam plasma system. We have considered both the electrons and the ions to be magnetized. The dispersion relation was solved fully using no approximations and analysis was restricted to low frequency waves. Both drifts perpendicular and parallel to the external magnetic field $\vec{B}_0$ were considered. The effect of an anisotropic velocity distribution of the beam ions on the instability growth rates was examined. Calculations were performed for two typical wavelengths, corresponding to normalized wavenumber k = 1 ($k\rho_i = 0.32$) and k = 5 ($k\rho_i = 1.6$), were ρ_i is the ion gyroradius.

For k = 1 at perpendicular beam drift, the instability spectrum is dominated by the ion acoustic and ion–ion streaming instabilities. The latter propagates for angles much more oblique to $\vec{B}_0$ and in a manner similar to its counterpart in an unmagnetized plasma which propagates in a cone about the beam direction. The transition from the one mode to the other is dependent on the beam velocity. Differentiation between the modes was made possible by comparing with the ion acoustic dispersion relation as well as their sensitivity to the ion beam temperature T_b. The ion acoustic instability, being dependent on resonance in velocity space, reacts sharply to changes in T_b and damps for $T_b \sim 0.3$. The ion–ion streaming instability, on the other hand, is less sensitive to temperature changes. These modes decay more slowly, damping around $T_b \sim 0.7$.

The effect of anisotropy ($T_\perp \neq T_\parallel$) in ion beam velocity distribution was found to enhance the instability growth rates. Since $T_\perp/T_\parallel$ of the beam was increased by keeping $T_\perp$ fixed

and reducing $T_{||}$, this enhancement was associated with reduction in parallel (to $\vec{B}_0$) ion Landau damping for the ion acoustic instability. While for the ion–ion streaming instability a reduction in overall beam temperature narrows the thermal spread. This could allow for a sharper beam resonance and consequent larger wave growth. This behaviour is consistent with earlier findings [5,6,7]. The anisotropy also lowers the threshold drift velocity for the excitation of the ion acoustic instability.

For the case k = 5 (perpendicular drift) the instability is purely two–stream in nature, as the modes do not satisfy the ion acoustic dispersion relation. In addition they exhibit growth for relatively large ion beam temperatures. However, the exact behaviour of the instability is found to change at a drift speed of $V_{oy} = 1.6$. For speeds below this value, its behaviour is typical of its associated instability in an unmagnetized plasma. However, for $V_{oy} > 1.6$ it is found that at maximum growth ω_r and $\vec{k}.\vec{V}_0$ assume constant values. This is typical of the modified two–stream instability as found by Papadopoulos et al. [9], McBride et al. [10] and Bharuthram and Johnstone [12].

For parallel drift with k = 1 the isotropic situation gets more complex. For a beam speed $V_{oz} = 1.25$ the wave satisfies the ion acoustic dispersion relation (4.2.1) and damps rapidly (due to increasing ion Landau damping) with increasing T_b. In the range $1.5 < V_{oz} < 2$ it is far less sensitive to changes in T_b and does not satisfy the ion acoustic dispersion relation. The modes have maximum growth for $\vec{k} \parallel \vec{V}_0 \parallel \vec{B}_0$, and are associated with the ion–ion streaming instability since its features are similar to the two–stream instability in an unmagnetized plasma. For speeds in the range $2.5 < V_{oz} < 4$ there is a dramatic shift in propagation angles of the waves, with γ_{max} moving away from parallel (to $\vec{B}_0$) propagation. In addition, the modes react sharply to changes in T_b, damping rapidly. Although this behaviour is typical of the ion acoustic wave, the phase speeds are below that of the ion acoustic wave. We call these modes ion acoustic–like. They have been shown to exist by

Fried and Gould [23] and were also obtained by Gary and Omidi [7].

For speeds in the range $5 < V_{oz} < 8$ there is yet another shift in propagation angles. At maximum growth the real frequencies satisfy the relation $\omega_r - \vec{k}.\vec{V}_0 \simeq \Omega_i$. The associated modes are thus called ion beam cyclotron waves.

The effect of ion beam anisotropy once again is to enhance wave growth. The reason for increased growth with decreasing $T_{||}$ has been associated with a decrease in ion Landau damping of a negative energy mode for the ion acoustic instability and a narrowing of the beam thermal spread for the ion–ion streaming instability.

The case k = 5 with parallel drift is very similar to perpendicular drift with the same k value. The unstable modes are purely two–stream in nature, changing from one similar to that in an unmagnetized plasma to a modified two–stream type at a drift speed $V_{oz} = 1.6$.

In the previous chapter we have addressed an instability of a completely different nature, the nonlinear modulational instability of an intense electromagnetic wave (pump wave) arising from an interaction with the background plasma slow response. The density variations associated with the latter, coupled to the electron quiver velocity, produces a nonlinear electron current. Three types of slow responses, the forced–Raman (FR), quasistatic (QS) and forced–quasistatic (FQ) were considered. Nonlinearities arising from the relativistic electron mass variation have been included. Analytical expressions for the growth rate for each type of interaction has been derived. Their relative strengths for typical plasma parameters are compared. For low pump amplitudes the FQ and QS interactions are found to dominate, while for a stronger pump mode only the FR interaction contributes to the instability.

Finally, we briefly mention possible extensions to our work. In our work both the beam and background ions have equal mass. The above analysis could be extended to an unequal mass situation, thereby providing an additional variable plasma parameter (ion mass ratio). We have kept the electrons as the hottest component in our work. The case of equal and hotter beam ions ($T_b \geq T_e$) constitute a wide field of study. The kinetic study of an ion–beam plasma system could be extended to study high frequency waves associated with electron motion. In the low frequency regime, higher drift speeds would enable a broader study of ion cyclotron waves.

The study of the modulational instability is restricted to field aligned modulations. An extension to oblique modulation will provide a more general result.

APPENDIX A

The final integral in (3.1.18) after performing the integration over ϕ reduces to

$$-\frac{e\phi_{1k\omega}k_z n_{bo}}{T_{\|}C_{\perp}^2(2\pi C_{\|}^2)^{1/2}}\sum_{p=-\infty}^{\infty}\int_0^{\infty}\left[\int_{-\infty}^{\infty}\frac{\exp[-(V_z-V_{oz})^2/2C_{\|}^2]}{[p\Omega_i+\vec{k}\cdot\vec{V}_o+k_z(V_z-V_{oz})-\omega]}(V_z-V_{oz})\,dV_z\right]\times$$
$$\exp\left[-\frac{V_{\perp}^2}{2C_{\perp}^2}\right]J_p^2(\mu)\,V_{\perp}\,dV_{\perp}\,. \qquad \text{A.1}$$

Consider the integral with respect to dV_z :

$$\int_{-\infty}^{\infty}\frac{\exp[-(V_z-V_{oz})^2/2C_{\|}^2]}{[p\Omega_i+\vec{k}\cdot\vec{V}_o+k_z(V_z-V_{oz})-\omega]}(V_z-V_{oz})\,dV_z\,.$$

We let $x = (V_z-V_{oz})/\sqrt{2}C_{\|}$, to obtain

$$\frac{\sqrt{2}C_{\|}}{k_z}\int_{-\infty}^{\infty}\frac{xe^{-x^2}}{[x-(\omega-\vec{k}\cdot\vec{V}_o-p\Omega_i)/\sqrt{2}k_zC_{\|}]}\,dx\,.$$

Defining $z_b = (\omega-\vec{k}\cdot\vec{V}_o-p\Omega_i)/\sqrt{2}k_zC_{\|}$, this becomes

$$\frac{\sqrt{2}C_{\|}}{k_z}\int_{-\infty}^{\infty}\frac{xe^{-x^2}}{(x-z_b)}\,dx\,. \qquad \text{A.2}$$

Since $x/(x-z_b) = 1 + z_b/(x-z_b)$, (A.2) may be written as

$$\frac{\sqrt{2}C_{\parallel}}{k_z}\left[\int_{-\infty}^{\infty} e^{-x^2}dx + z_b\int_{-\infty}^{\infty}\frac{xe^{-x^2}}{(x-z_b)}\,dx\right] = \frac{\sqrt{2}C_{\parallel}}{k_z}\left[\sqrt{\pi} + \sqrt{\pi}\,z_b\,Z(z_b)\right],$$

A.3

where we have used the well known result $\int_{-\infty}^{\infty} e^{-x^2}dx = \sqrt{\pi}$ and written the second part in terms of the Z – function. Then (A.1) reduces to

$$-\frac{e\phi_{1k}\omega^{n}_{bo}}{T_{\parallel}C_{\perp}^2}\sum_{p=-\infty}^{\infty}\int_0^{\infty}\left[\,1 + z_b\,Z(z_b)\,\right]\exp\left[-\frac{V_{\perp}^2}{2C_{\perp}^2}\right]J_p^2(\mu)\,V_{\perp}\,dV_{\perp}\,.$$

APPENDIX B

Equation (5.2.13) can be written as

$$m_{eo}c\frac{\partial \vec{p}_e}{\partial t} + m_{eo}c^2\Gamma\,(\vec{p}_e\cdot\nabla)\vec{p}_e = m_{eo}c\frac{\partial \vec{A}}{\partial t} + e\nabla\phi - m_{eo}c^2\Gamma\,\vec{p}_e\times(\nabla\times\vec{A}) - m_{eo}c\Omega_{eo}\Gamma\,\vec{p}_e\times\hat{z} - T_e\nabla(\ln n_e)\,, \qquad \text{B.1}$$

where $\Gamma = (1+p^2)^{-1/2}$. Substituting for $\vec{p}_e$ and $\vec{A}$ from (5.2.12) and using (5.2.14), equation (B.1) becomes

$$m_{eo}c\,(\frac{\partial p}{\partial t} - i\omega_o p)\,(\hat{x}-i\hat{y})\,e^{ik_oz}\,e^{-i\omega_o t} + m_{eo}c^2\Gamma\,[p\,(\hat{x}-i\hat{y})\,e^{ik_oz}\cdot\nabla]\,p(\hat{x}-i\hat{y})\times e^{ik_oz}\,e^{-2i\omega_o t} = m_{eo}c\,(\frac{\partial A}{\partial t} - i\omega_o A)\,(\hat{x}-i\hat{y})\,e^{ik_oz}\,e^{-i\omega_o t} + e\nabla\phi - m_{eo}c^2\,\Gamma\,p\,(\hat{x}-i\hat{y})\,e^{ik_oz}\times[\nabla\times A(\hat{x}-i\hat{y})\,e^{ik_oz}]\,e^{-2i\omega_o t} - m_{eo}c\Omega_{eo}\Gamma\,p(\hat{x}-i\hat{y})\,e^{ik_oz}\times\hat{z}\,e^{-i\omega_o t} - T_e\nabla(\ln n_e)\,. \qquad \text{B.2}$$

Equation (B.2) is multiplied by $e^{i\omega_o t}$ and integrated with respect to t over one period, that is from t = 0 to $t = 2\pi/\omega_o$. Since in the interval $\Delta t = 2\pi/\omega_o$, ϕ, p, A and n_e do not change significantly (slowly varying), they can be kept constant and using

$$\int_0^{2\pi/\omega_o} e^{\pm i\omega_o t}\,dt = 0 \quad \text{(real part)}\,,$$

we obtain

$$\frac{\partial p}{\partial t} - i\omega_o p = (\frac{\partial A}{\partial t} - i\omega_o A) + i\Omega_{eo}\frac{p}{(1+p^2)^{1/2}}\,. \qquad \text{B.3}$$

This process is called averaging over the fast time scale [31]. Substituting (B.3) into (B.2) we obtain

$$m_{eo}c^2\Gamma\,(\vec{p}_e\cdot\nabla)\vec{p}_e = e\nabla\phi - m_{eo}c^2\Gamma\,\vec{p}_e\times(\nabla\times\vec{A}) - T_e\nabla(\ln n_e)\,. \qquad \text{B.4}$$

APPENDIX C

CAUCHY ROOTFINDER

To solve $F(\omega) = 0$, we proceed as follows. If $F(\omega)$ has n roots $\omega_1, \omega_2, \cdots, \omega_n$ within a contour Ω_c and is analytic within and on the contour, then we can write

$$F(\omega) = (\omega - \omega_1)(\omega - \omega_2) \cdots (\omega - \omega_n)\, H(\omega) ,$$

where $H(\omega)$ is analytic on and within Ω_c. Consider

$$S_v = \frac{1}{2\pi i} \oint \frac{\omega^v F'(\omega)}{F(\omega)}\, d\omega . \qquad \text{C.1}$$

We note that

$$F'(\omega) = (\omega - \omega_2) \cdots (\omega - \omega_n)\, H(\omega) + (\omega - \omega_1)(\omega - \omega_3) \cdots (\omega - \omega_n)\, H(\omega) + \cdots + (\omega - \omega_1)(\omega - \omega_2) \cdots (\omega - \omega_n)\, H'(\omega) .$$

$$\frac{\omega^v F'(\omega)}{F(\omega)} = \frac{\omega^v}{\omega - \omega_1} + \frac{\omega^v}{\omega - \omega_2} + \cdots + \frac{\omega^v}{\omega - \omega_n} + \frac{\omega^v H'(\omega)}{H(\omega)} . \qquad \text{C.2}$$

Since the last term in (C.2) is analytic, its contribution to the integral in (C.1) is zero. By the Cauchy Integral Theorem

$$\frac{1}{2\pi i} \oint \frac{F(\omega)}{\omega - \omega_0}\, d\omega = f(\omega_0) ,$$

S_0 = n (the number of roots of $F(\omega)$ within Ω_c). The n × n system

$$
\begin{aligned}
S_1 &= \omega_1 + \omega_2 + \omega_3 + \cdots + \omega_n \\
S_2 &= \omega_1^2 + \omega_2^2 + \omega_3^2 + \cdots + \omega_n^2 \\
&\vdots \quad \vdots \quad \vdots \quad \vdots \qquad \vdots \\
S_n &= \omega_1^n + \omega_2^n + \omega_3^n + \cdots + \omega_n^n
\end{aligned}
$$

can be transformed into the complex polynomial

$$\sum_{0}^{n} a_v \omega^v = 0$$

of degree n, with $a_n = 1$ [34]. The following descending recurrence relation yields a_v :

$$a_v = -\frac{1}{n-v} \sum_{v+1}^{n} a_p S_{p-v} .$$

The solution of the polynomial equation yields all the roots of $F(\omega)$ within Ω_c. These roots are refined by using the Newton–Raphson method.

The contour Ω_c, chosen as rectangular, is depicted below.

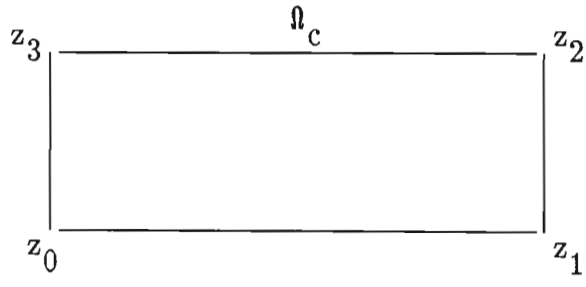

If the first integral $S_0 = n = 0$, then we choose a different contour. If $S_0 < 0$, then the

integrand in (C.1) cannot be analytic at all points besides the zeros of $F(\omega)$. In this case we shrink the contour to exclude such points or choose a new contour. We can select the number of roots that are required by shrinking Ω_c iteratively until n $\leq$ no. of roots required. The integration in (C.1) is performed numerically using the extended Simpson's rule.

REFERENCES

1 D. Gresillon, F. Doveil and J.M. Buzzi, *Phys. Rev. Lett.* **34**, 197 (1975).

2 D.S. Lemons, J.R. Asbridge, S.J. Bame, W.C. Feldman, S.P. Gary and J.T. Gosling, *J. Geophys. Res.* **84**, 2135 (1979).

3 S.A. Fuselier and D.A. Gurnett, *J. Geophys. Res.* **89**, 91 (1984).

4 D.L. Gallagher, *J. Geophys. Res.* **90**, 1435 (1985).

5 K. Akimoto and D. Winske, *J. Geophys. Res.* **90**, 12095 (1985).

6 K. Akimoto and N. Omidi, *Geophys. Res. Lett.* **13**, 97 (1986).

7 S.P. Gary and N. Omidi, *J. Plasma Phys.* **37**, 45 (1987).

8 S.A. Fuselier, S.P. Gary, M.F. Thomsen, S.J. Bame and D.A. Gurnett, *Ion Beams And The Ion/Ion Acoustic Instability Upstream From The Earth's Bow Shock*, Los Alamos National Laboratory, internal report (1988).

9 K. Papadopoulos, R.C. Davidson, J.M. Dawson, I. Haber, D.A. Hammer, N.A. Krall and R. Shanny, *Phys. Fluids* **14**, 849 (1971).

10 J.B. McBride, E. Ott, J.P. Boris and J.H. Orens, *Phys. Fluids* **15**, 2367 (1972).

11 C.S. Wu, Y.M. Zhou, S.T. Tsai, S.C. Guo, D. Winske and K. Papadopoulos, *Phys. Fluids* **26**, 1259 (1983).

12 R. Bharuthram and D.B. Johnstone, *Modified Two–Stream Instability in the presence of Counter–Streaming Anisotropic Ion Beams*, submitted to S.A. Journal of Physics.

13 S.P. Gary and J.J. Sanderson, *J. Plasma Phys.* **4**, 739 (1970).

14 R. Bharuthram, University of Natal, *M.Sc. Thesis* (1974).

15 G. Watson, *A Treatise on the Theory of Bessel Functions*, Cambridge University Press, 2nd Edition (1944).

16 B.D. Fried and S.D. Conte, *The Plasma Dispersion Function*, Academic Press, New York (1961).

17 J.M. Kindel and C.F. Kennel, *J. Geophys. Res.* **76**, 3055 (1971).

18 V.E. Zakharov and E.A. Kuznetsov, *Sov. Phys. JETP* **39**, 285 (1974).

19 B.D. Fried and A.Y. Wong, *Phys. Fluids* **9**, 1084 (1966).

20 D. Winske, M. Tanaka, C.S. Wu and K.B. Quest, *J. Geophys. Res.* **90**, 123 (1985).

21 N. Sato, H. Sugai and R. Hatakeyama, *Phys. Rev. Lett.* **34**, 931 (1975).

22 F.F. Chen, *Introduction to Plasma Physics and Controlled Fusion*, page 97, Plenum, New York (1984).

23 B.D. Fried and R.W. Gould, *Phys. Fluids* **4**, 139 (1961).

24 M.V. Goldman and D. Newman, *Phys. Rev. Lett.* **58**, 1849 (1987).

25 P.K. Shukla, N.N. Rao, M.Y. Yu and N.L. Tsintsadze, *Phys. Rep.* **138**, nos. 1 & 2 (1986).

26 M.Y. Yu, P.K. Shukla and K.H. Spatschek, *Phys. Rev. A* **18**, no. 4, 1591 (1978).

27 M.Y. Yu, P.K. Shukla and N.L. Tsintsadze, *Phys. Fluids* **25**, no.6, 1049 (1982).

28 N.N. Rao, P.K. Shukla and M.Y. Yu, *Phys. Fluids* **27**, no. 11, 2664 (1984).

29 P.K. Shukla, R. Bharuthram and N.L. Tsintsadze, *Physica Scripta* **38**, 578 (1988)

30 P.K. Shukla, R. Bharuthram and N.L. Tsintsadze, *Phys. Rev. A* **35**, no. 11, 4889 (1987).

31 D.W. Nicholson, *Introduction to Plasma Theory*, John Wiley & Sons, New York (1983).

32 V.I. Karpman, *Nonlinear Waves in Dispersive Media*, Pergamon, New York (1975).

33 R. Bharuthram, P. Singh and P.K. Shukla, *Phys. Rev. A* **37**, 1017 (1988).

34 H. Maasberg and M.A. Hellberg, *Ion Cyclotron Instabilities Driven By The Nearly Perpendicular Neutral Beam Injection In The Wendelstein VII–A Stellerator*, Max–Planck–Institut Fur Plasmaphysik, IPP 2/282 (1986).